



REPUBLIQUE DU CAMEROUN
Paix - Travail - Patrie

UNIVERSITE DE DOUALA

ECOLE DOCTORALE DES SCIENCES
FONDAMENTALES ET APPLIQUEES

Unité de Formation Doctorale
des Sciences de l'Ingénieur

Laboratoire Energie Modélisation Matériau et
Méthodes



REPUBLIC OF CAMEROON
Peace - Work - Fatherland

THE UNIVERSITY OF DOUALA

POSTGRADUATE SCHOOL FOR
PURE AND APPLIED SCIENCES

Postgraduate Training Unit
for Engineering Sciences

Laboratory of Energy Modeling Materials
and Methods

École Doctorale
DOCTORAL SCHOOL
SPIM
(Sciences Pour l'Ingénieur et
Microtechniques)

**PHD THESIS OF THE ESTABLISHMENTS OF BURGUNDY FRANCHE-COMTE UNIVERSITY
AND DOUALA UNIVERSITY**

**PREPARED AT THE BURGUNDY FRANCHE-COMTEUNIVERSITY DIJON FRANCE AND
UNIVERSITY OF DOUALA CAMEROON**

Doctorate School n°37

ED SPIM BURGUNDY ET EDOSFA DOUALA

PhD Instrumentation Electronics Computers and Image (IEII)

By

MATANGA JACQUES

**STUDY AND REALIZATION OF A MULTISPECTRAL DETECTOR (FILTER) BY
NON-DESTRUCTIVE SPECTRAL DISPERSION THROUGH THE
NANOSTRUCTURE FILMS.**

Thesis presented and defended in Douala Cameroon, the 2020/06/13

Composition of the Jury:

Pr. MOUKENGUE IMANO ADOLPHE
Pr. ORIA VINCENT
Pr. NYOBE YOME JEAN MAURICE
Pr. TIEDEU ALAIN BERTIN
Pr. SABIR JACQUIR
Pr. GOUTON PIERRE
Pr. BOURILLOT ERIC
Pr. ELE PIERRE

Teacher Researcher EDOSFA
Teacher Researcher NJIT NJ USA
Teacher Researcher EDOSFA
Teacher Researcher ENSP Yde
Teacher Researcher U PARIS SUD
Teacher Researcher UB Fr
Teacher Researcher UB Fr
Teacher Researcher EDOSFA

President
Thesis Reporter
Thesis Reporter
Thesis Reporter
Thesis Examiner
Thesis Director
Thesis Co-Director
Thesis Co-Director

Titre : Etude et réalisation d'un détecteur (filtre) multispectral par dispersion non-destructive spectrale à travers des films à nanostructure.

Mots clés : nanostructures, Nanoscience, Nanotechnologie, films à couches minces, réseaux de diffraction, filtre optique, imagerie multispectrale. Lithographie, photonique, réseau de filtres optiques.

Résumé : Le développement des techniques d'imagerie multispectral, d'holographie et de lithographie permet d'exploiter les propriétés des réseaux diffractants dans une grande variété de composants photoniques. Ils sont incorporés dans des diodes laser comme réflecteurs de Bragg distribués, dans différentes fonctions d'optique intégrée pour le multiplexage en longueur d'onde ou les interconnexions optiques, ou inscrits au sein même des fibres, conduisant à une grande variété de capteurs pour la détection d'éléments chimiques, la mesure des températures, des pressions, des accélérations d'acquisition et ou de restitution d'images multispectrales etc... [Lee et al. 2007] [Pagnoux et al. 2005].

Parmi ces dispositifs, les réseaux résonnants suscitent un très vif intérêt car ils permettent d'obtenir des filtres ultra-sélectifs à partir d'une structure relativement simple. Cette structure est constituée par un guide diélectrique sur lequel est gravé un réseau sub-longueur d'onde de faible profondeur et ou épaisseur. Hors résonance, la structure réfléchit et transmet la lumière selon les propriétés de réflectivité et transmission très proches de celles du dioptre constitué par l'empilement de couches diélectriques.

Ce travail présente les études expérimentales et théoriques menées pour surmonter les verrous technologiques inhérents à la réalisation de filtres optiques multispectaux à couches minces. L'objet de cette thèse est d'étudier et concevoir à partir de films minces nanométriques des filtres optiques ultra-sélectifs, en exploitant une structure de réseau résonnant conçue par dépôt de multicouches de nanofilms de métamatériaux pour surpasser les performances des filtres actuels, en particulier dans le domaine de leurs caractéristiques spectrales et de leur sensibilité à la polarisation. Un enjeu de l'étude est de développer le procédé de fabrication associé, de dégager les limitations technologiques imposées par l'état de l'art, de proposer un procédé reproductible et si possible compatible avec un développement technologique collectif et à faible coût.

Le second en jeu était d'utiliser les échantillons issus de la fabrication des réseaux de diffraction pour l'associer à un capteur

L'analyse des performances expérimentales, confrontées aux prévisions théoriques et aux limitations technologiques, doit conduire à une estimation réaliste des potentialités des filtres proposés. Pour se faire nous avons commencé notre étude par une revue de littérature sur l'ensemble des éléments clés du sujet, la Nanotechnologie, la nanoscience ces avantages ces inconvénients, ces possibilités. Une revue de la littérature sur l'imagerie multispectrale et ces ascendants.

Ensuite nous avons présente les différentes méthodes de fabrication des nanostructures à couches minces, des nanostructures multicouches, et nous avons fait un choix de fabrication selon les moyens disponibles au laboratoire ICB. Cette démarche nous a conduit à la caractérisation par microscopie électronique des échantillons obtenus par Lithographie.

Enfin une étude théorique a été faite, celle-ci permettant par simulation sur Matlab, et Python de vérifier les résultats obtenue (propriétés de résonance des réseaux de diffraction) par observations microscopique. Une étude poussée de ces propriétés a été faite, et les paramètres de réalisation et des nanostructures ont été définie. De nouveaux échantillons réalisés et observé nous permet de conclure que le choix de des méthodes est la bonne eu égard aux réseaux spectraux obtenus par simulation de transmission et de réflexion.

Ces filtres sont particulièrement avantageux pour un fonctionnement en réflexion, car la réalisation nécessite un faible nombre de couches pour assurer la transmission large bande hors résonance. Du point de vue de l'utilisateur, ils sont complémentaires des filtres Fabry-Perot, utilisés essentiellement en transmission, le fonctionnement en réflexion sous incidence oblique permettant un montage simplifié sans lame séparatrice. Cependant, l'utilisation pratique de ces filtres est limitée par une très forte sélectivité angulaire, d'autant plus contraignante pour les filtres ultra-sélectifs car la divergence du faisceau est plus grande que la tolérance angulaire du filtre, cette limitation devenant plus importante sous incidence oblique. La sensibilité de la réponse du filtre à la polarisation constitue une autre limitation.

Mais la confirmation de ces résultats probant et

fabriqué à base de transistor tri-CCD au laboratoire LE2I, afin de concevoir un dispositif d'acquisition pointu en imagerie multispectral et de vision.

remplis d'espoir par observation visionique n'a pas été possible du fait du manque de matériel adapté à la caractérisation expérimental spectral de nanostructures réalisées.

Title: Study and realization of a multispectral detector (filter) by non-destructive spectral dispersion through the nanostructure films.

Keywords: nanostructures, nanoscience, nanotechnology, thin film, diffraction gratings, optical filter, multispectral imaging. Lithography, photonics, optical filters array

Abstract: The development of multispectral imaging, holography and lithography techniques exploits the properties of diffracting arrays in a wide variety of photonic components. They are incorporated in laser diodes as distributed Bragg reflectors, in various integrated optical functions for wavelength division multiplexing or optical interconnections, or inscribed within the fibers themselves, leading to a wide variety of sensors for detection of chemical elements, measurement of temperatures, pressures, accelerations of acquisition and or restitution of multispectral images, etc. [Lee et al. 2007] [Pagnoux et al. 2005].

Among these devices, the resonant networks arouse a great interest because they allow to obtain ultra-selective filters from a relatively simple structure. This structure consists of a dielectric guide on which is etched a subwavelength network of shallow depth and thickness. Except resonance, the structure reflects and transmits the light according to the properties of reflectivity and transmission very close to those of the dioptr constituted by the stack of dielectric layers.

This work presents the experimental and theoretical studies carried out to overcome the technological obstacles inherent to the realization of thin-film multispectral optical filters.

The aim of this thesis is to study and design ultra-selective optical filters based on nanoscale thin films, by exploiting a resonant network structure conceived by depositing multilayer nanowires of metamaterials to surpass the performances of the current filters. Particular in the field of their spectral characteristics and their sensitivity to polarization. An issue of the study is to develop the associated manufacturing process, to identify the technological limitations imposed by the state of the art, to propose a reproducible process and if possible compatible with a

The analysis of experimental performances, confronted with theoretical predictions and technological limitations, must lead to a realistic estimate of the potentialities of the proposed filters. To do this we began our study with a literature review on all the key elements of the subject, Nanotechnology, nanoscience these advantages these disadvantages, these possibilities. A review of the literature on multispectral imaging and these ascendants.

Then we presented the different methods of manufacturing thin film nanostructures, multilayer nanostructures, and we made a manufacturing choice according to the means available at the ICB laboratory. This approach led us to the characterization by electron microscopy of the samples obtained by lithography.

Finally a theoretical study was made, this one allowing by simulation on Matlab, and Python to check the obtained results (resonance properties of the diffraction gratings) by microscopic observations. A thorough study of these properties was made, and the parameters of realization and nanostructures were defined. New samples made and observed allowed us to conclude that the choice of methods is the right one considering the spectral networks obtained by simulation of transmission and reflection.

These filters are particularly advantageous for operation in reflection, because the realization requires a small number of layers to ensure broadband transmission off resonance. From the point of view of the user, they are complementary to Fabry-Perot filters, mainly used in transmission, the operation in oblique incident reflection allowing a simplified assembly without separating blade. However, the practical use of these filters is limited by a very high angular selectivity, all the more constraining for ultra-selective filters because the divergence of the beam is greater than the angular tolerance of the filter, this limitation becoming more important under oblique

collective technological development and low cost.

The second was to use the samples from the fabrication of the diffraction gratings to associate it with a tri-CCD transistor-based sensor in the IMVIA laboratory, in order to design a sharp acquisition device in multispectral imaging and of vision.

incidence. The sensitivity of the filter response to polarization is another limitation.

But the confirmation of these convincing and hopeful results by visual observation was not possible because of the lack of material adapted to the spectral experimental characterization of nanostructures realized.



Dedication

*« If all life inevitably comes to end,
we must, during ours, color it with our
colors of love and hope”*

*In memory of my parents and my older
brother, His Majesty Chief of Boumkwa*

Mr. MBELLA MATANGA François

Acknowledgements

I thank the President of the Jury and its members for participating in this exchange and for their contribution to improving the rendering of these thesis works.

I express my gratitude to Professor Pierre GOUTON, former member of the Computer Electronics and Image Laboratory (ImVIA) of the University of Burgundy Franche Comté in Dijon France, for codirecting my thesis. The existence and the new knowledge of the Laboratory owe a lot to its dynamism and its commitment which have little equal. His conception of human relationships helps to create a very pleasant and friendly working atmosphere.

I express my unconditional admiration for Doctor Eric BOURILLOT, head of the laboratory or the Burgundy Carnot Institute in Dijon (ICB), codirector of this thesis. Thanks to his kindness, he made my stay in Dijon possible and unforgettable. Without him, this thesis would never have been. I do not forget his efforts throughout my research. May he find here the sign of my gratitude.

I would like to thank Professor Pierre ELE, Assistant Coordinator of the ED of Douala University for welcoming me to his laboratory and agreeing to codirect this these. I am pleased that he has agreed to continue this work despite his heavy responsibilities and his new orientation.

I wish to express my sincere gratitude to Mr. Yvon LACROUTE, technical manager of experimental devices and equipment at the ICB laboratory at the University Of Burgundy Franche Comté Of Dijon, as well as to the entire technical team of this laboratory for their availability, assistance and my experimental technical initiation and the mastery of electron microscopy.

To all, gentlemen, President, reporter, and jury members who have agreed to take their time to cover this work and to honor their presence with the jury; I say a warm thank you.

I would also like to thank Professor Adolphe MOUKENGUE IMANO from the University of Douala who trusted me by proposing and agreeing to supervise my work of DEA. I am extremely grateful to him for giving me time

This work owes much to the valuable help of Professor Jean NYOBE YOME who followed me during this thesis work. I thank him for introducing me to research; for mentoring me by sharing joys and difficulties.

I had the chance to work with Professor Jean MBIHI who taught me a lot on the experimental level. His knowledge in the field of electronics and signal processing helped me

throughout my thesis, not to mention our scientific discussions that have always been successful in writing my DIPET2.

I would like to greet and thank all the members of the IMVIA laboratory, in particular Samuel CHEF who supervised me during my thesis internship (his good humor contributes largely to the good atmosphere of the team), AMADOU DIARA, and MAMADOU. T., for their communicative scientific dynamism, and Roland ALIMA for his kindness and efficiency.

To my teachers at ENSET at Douala University, I extend my sincere thanks, especially to the teachers: Professors; Jean François ESSIBEN and Léandre NNEME NNEME for their widely appreciated scientific and social discussions.

Many apologies to everyone I have forgotten. I thank my parents from the bottom of my heart for always allowing me to follow the path of studies. Thank you for their support, their encouragement and especially their love which has always been a motivating source.

To my deceased parents: sir MATANGA Jacques and madam NGUENG Helene.

To my elder brother Emile SENDJI MATANGA and his wife Valerie SENDJI MATANGA, my Elder Louise YAMBA MATANGA, Catherine LOMBI MATANGA and Little Jacqueline NGASSE MATANGA Sisters for their unwavering and unwavering support.

Special thanks to my younger Noé-Oscar MATANGA, to Mr YOMB Jacques Moise and all my nephews

To all my friends and acquaintances.

Finally, I cannot forget to thank my wife Ruth Fidèle BEBE and daughters: KATHLEEN, CHRYSTALLE PAGUIELE and BELITZE ALLEGRA, for their great love and moral support during all these years. She taught me that after the rain, there is always a good weather. ..

Table of contents

Dedication.....	i
Acknowledgements.....	ii
Table of contents.....	iii
List of tables.....	vii
List of figures.....	x
List of symbols and abbreviations.....	xiv
Abstract.....	xv
Resume.....	xvi
INTRODUCTION.....	1
CHAPTER I: BIBLIOGRAPHIC SYNTHESIS OF NANOTECHNOLOGY AND MULTISPECTRAL SYSTEMS.....	4
I.1. The importance of the multispectral in Artificial Vision.....	4
I.1.1. Objectives and relevance.....	4
I.1.2. History and development.....	5
I.2. State of the art on existing systems.....	6
I.2.1. The systems based on interference filters.....	6
I.2.2. Systems based on liquid crystal filters.....	7
I.2.3. Dichroic filters to the nanostructures filters.....	8
I.3. Contribution of nanoscience: introduction to nanotechnology.....	8
I.3.1 Basic concepts - Definitions and Emergences.....	8
I.3.1.1. Nanosciences.....	10
I.3.1.2. Nanotechnology.....	10
I.3.1.3. Emergences.....	10
I.4. Impact factors of nanoscience and nanotechnology in multispectral imaging.....	11
I.4.1. Implications of nanoscience and nanotechnology in Biology and Medicine domain.....	12
I.4.2. Implications in electronic – engineering sciences – and research literature.....	12
I.4.3. Societal implication and ethical sensitivity.....	15
I.5. Overview on multispectral systems.....	19
I.5.1. Historical back ground of multispectral systems: What is Multispectral Image?.....	20
I.5.2. Brief systems overview.....	22
I.5.2.1. Fundamental Basis for multispectral systems.....	22
I.5.2.2 Multispectral System View and Its Interdisciplinary Nature.....	23
I.5.3. Spectral data operating strategies.....	24
I.5.4. Generalities about electromagnetic spectrum.....	25
I.5.4.1 Electromagnetic spectrum composition.....	25
I.5.4.2. Measuring electromagnetic radiation.....	26
I.6. Conclusion.....	27
Chapter II: APPLICATIONS OF MULTISPECTRALRE CONSTRUCTION METHOD FOR THE OPTIMAL APPROXIMATION OF THE SPECTRAL RESPONSE OF A MULTICOMPONENT IMAGE.....	30

II.1. reconstruction of the spectral response of an image using exponential functions.....	32
II.1.1. Overview of this method	32
II.1.2. Gaussian function.....	34
II.3. setting up of an equation of the multi-component image acquisition system.....	36
II.3.1. Proposal.....	36
II.3.2. Identification of H via the matrix method	38
II.3.2.1. Pseudo-inverse matrix	38
II.3.2.2. Wiener inverse.....	40
II.4. approximation of the spectral response by neural learning	41
II.4.1. Introduction	41
II.4.2. Perceptron.....	41
II.4.3. Multi-layer perceptron.....	42
II.4.4. Supervised learning	43
II.4.5. Gradient backpropagation algorithm.....	44
II.4.6. Second order optimization method.....	44
II.4.7. Optimisation by the Levenberg-Marquardt method	45
II.4.8. Methodology	45
II.5. global results analysis.....	47
II.5.1. Comparison of the various methods.....	47
II.6. Conclusion.....	51
CHAPTER III: DESCRIPTION OF ANALYTICAL DEVICES AND THE METHODS FOR THE GROWTH AND SYNTHESIS OF NANOSTRUCTURED THIN FILMS.....	52
III.1. How to work the matter on the nanometric scale?	52
III.2. Manufacturing processes of nano-objects and nanomaterials.....	53
III.2.1. Physical channel processes	56
Physical Vapor Deposition Methods: PVD (Physical Vapor Deposition).....	56
III.2.2. Chemical channel processes.....	57
III.2.5.2. Charged-Particle-Beam Approaches:.....	63
III.2.5.3. Other Lithographic Approaches.....	64
III.3.1. OL Series 750.....	66
III.3.2. CS-2000 spectroradiometer.....	67
III.4. Choice of nanostructures manufacturing technique	68
III.5. Conclusion	71
CHAPTER IV: THEORY, DESIGN AND SYNTHESIS OF THE NANOFILMS FILTER: METHODOLOGIES	72
IV.1. analytical and computational method: Basic theory	73
IV.1.1. Maxwell's Equations and Plane Electromagnetic Waves.....	73
IV.1.2. Background.....	76
IV.1.3.3 Fourier Transform in x and y Only	78
IV.1.3.4. Wave Vector Components	79
IV.1.4. Matrix form of Maxwell's equations	80

IV.1.5. Matrix wave equation	82
IV.1.5.1 Block Matrix Form	83
IV.1.5.3. Solution to the matrix wave equation	83
IV.1.6 Multilayer framework: scattering matrices	86
IV.1.7. Calculating transmission and reflection.....	91
IV.2. experimental methods	94
IV.2.1. Thin film deposition methods	95
IV.2.2. Experimental process: Lithography's Key Role in the Process	97
IV.2.2.1. Principles and methods	97
IV.2.2.2. The general sequence of processing steps	98
IV.3. Application of RCWA, and experimental study of silver, gold, germanium nanofilms filters.	99
CHAPTER V: THEORICAL SIMULATION, EXPERIMENTAL SETUP: RESULTS AND DISCUSSION	103
V.1 global results	104
V.2. 3D Electromagnetic wave simulation using RCWA	106
V.3. Transmittance, Reflectance and Absorbance of each material.....	108
V.3.1 case of germanium thickness 350 nm	109
V.3.2. Case of gold.....	109
V.3.3. Case of silver.....	110
V.4. Transmittance, Reflectance and Absorbance of multilayer system.....	110
V.4.1. Case of multilayer combination of material: Ge-Au-Ag.....	111
V.4.2. Case of multilayer combination of material: Au-Ge-Ag.....	111
V.4.3. Case of multilayer combination of material: Ag, Au, Ge.	112
V.5. Analyze and discussion	112
GENERAL CONCLUSION AND PERSPECTIVES.....	120

list of tables

Table 1.a: Colour representation of the first part of Macbeth colour chart	[45]
Table 1.b: Colour representation of the second part of Macbeth colour chart	[46]
Table 2-a: Comparison between 5 spectral reconstruction methods applied to colour database	[46]
Table 2.b: Comparison between 5 spectral reconstruction methods applied to colour database	[46]
Table 3: Mean spectral reconstruction error for previous methods	[47]
Table 4.a: Spectral reconstruction using the LM Neural Network	[47]
Table 4.b: Spectral reconstruction using the LM Neural Network	[47]
Table 4.c: Spectral reconstruction using the LM Neural Network	[47]
Table 4.d: Spectral reconstruction using the LM Neural Network	[47]
Table 4.e: Spectral reconstruction using the LM Neural Network	[47]
Table 4.f: Spectral reconstruction using the LM Neural Network	[48]
Table 5: Neural implementation and computer specification	[48]
Table 6: Methods of manufacturing nano-objects or nanostructured thin films	[52]
Table 7: Process conditions and NSTF structures for NSTF fabrication or synthesis	[53]
Table 8: Capabilities and summary of various lithography methods	[57]
Table 9: general approaches of nanomaterials and nanostructures fabrication	[67]

list of figures

- Figure 1 : multispectral artificial vision. (McClure, 1994) [6]
- Figure 2: Overview of artificial vision system (Robert et al., 1991) [6]
- Figure 3: **principle of a multispectral camera based on the wheel filters principles** [7]
- Figure 4: functional principle of a Tri - CCD camera [10]
- Figure 5: Prototypes of nanomachines designed by Professor k. [11]
Eric Drexler © 1991-2007 Institute for Molecular Manufacturing.
- Figure 6: Representation of a nano robot. © Oliver Burston, [11]
Wellcome Images Digital artwork/Computer graphic 2005.
- Figure 7: country comparison time trend (number of articles vs. time) [14].
- Figure 8: country auto-correlation map (fifty most prolific countries) [15].
- Figure 9: Schematic illustration of the world of nanotechnology and nanoscience [18]
- Figure 10: General conceptual view of multispectral systems. [22]
- Figure 11: Multispectral system view and its interdisciplinary nature [23]
- Figure 12: The electromagnetic spectrum shown with familiar sources [26]
- Figure 13: Illustration showing comparison between wavelength, frequency and energy [27]
- Figure 14: Block diagram of the physical phenomena allowing an object to be seen [30]
- Figure 15: Primary colour defined by: $R=173$ $G=197$ $B=78$; $N^{\circ} 11$ [32]
- Figure 16: Spectral reconstruction using Gaussian functions [34]
- Figure 17: Multi spectral image acquisition system [34]
- Figure 18: Modelling of the acquisition system and the illumination [37]
(Each primary is represented by its colour)
- Figure 19: Spectral density rebuilt from the Penrose inverse. [37]
The initial spectrum is a dotted line; the rebuilt spectrum is a solid line.
- Figure 20: Spectral density rebuilt from the inverse of Wiener [39]
- Figure 21: Example of a layer of formal neurone [40]
N is the number of examples or observables.
- Figure 22: Multi-layer neural network (Multi-Layer Perceptron) [41]
- Figure 23: Skeleton diagram of the weight learning rule [42]
- Figure 24: The MLP architecture of the proposed method [43]
- Figure 25: Rebuilt spectral density through learning of a two-layer network. [44]
A dotted line shows the initial spectrum; a solid line shows the rebuilt spectrum.
- Figure 26: The two approaches of development of nano-objects and the nanostructures [51]

Figure 27: schematics illustrating the general steps and	[53]
Figure 28: Three major processes for PVD: (a) thermal evaporation,	[54]
(b) Sputtering growth, and (c) pulsed laser deposition	
Physical mechanism for a PVD process	
Figure 29: schematic of a conventional CVD reactor	[54]
Figure 30: A schematic of spin coating process	[55]
Figure 31: (a) Schematic diagram explaining the principle	[56]
of high pressure torsion. (b) Schematic diagram explaining the principle of SPD.	
Figure 32: Schematic diagram explaining the principles of glancing angle deposition.	[57]
Figure 33: Overview of the characterization bench with OL Series 750 in white room	[64]
Figure 34: illustration of CS-2000	[65]
Figure 35: Geometry of RCWA	[74]
Figure 36: The 2D Unit Cell for Single Layer	[74]
Figure 37: z- uniform media	[75]
Figure 38: visualization of solution and different modes	[83]
Figure 39: Sample of an infinitely periodic lattice	[84]
Figure 40: sample of multilayer's with finite thickness, and different modes	[84]
Figure 41: multilayer structure showing optical phenomena	[85]
Figure 42: multilayer structure highlighting scattering phenomena	[86]
free between two free space separated by a material medium (layer 1).	
Figure 43: modes and scattering phenomena in all layers	[87]
Figure 44: scattering phenomena when $\lim L=0$	[87]
Figure 45: scattering phenomena explained transmission. When $L=0$.	[88]
Figure 46: structure emphasizing reflection and transmission each in their plane	[89]
Figure 47: Differential Grating Diffraction Analysis Hierarchy	[90]
Figure 48: Highlighting the evolution of the thicknesses of thin film	[92]
Figure 49: Principe of (PVD) and (CVD)	[93]
Figure 50: simplified mechanism of The PVD method	[93]
Figure 51: simplified mechanism of the PCVD method	[93]
Figure 52: Schematic illustration of Lithography	[95]
Figure 53: Schematic diagram of a Lithographic,	[95]
Process to transfer a positive or negative image onto a substrate.	
Figure 54: General sequence of processing steps for a typical photolithography process	[96]
Figure 55: Plane wave front incident on a single surface.	[96]
Figure 56: orientation of the components of the	[97]
electromagnetic fields of the incident wave: case of normal incidents.	

Figure 57: (a) Convention defining the positive directions of the electric and magnetic vectors for p-polarized light (TM waves); (b) Convention defining the positive directions of the electric and magnetic vectors for s-polarized light (TE waves).	[97]
Figure 58: (a) Process conditions and NSTF structures for NSTF manufacturing case of Gold; (b) 100 μ m gold NSTF coated with germanium from multilayered aggregates at the air glass interface, (c) Optical microscope observation of NSTF.	[98]
Figure 59: Light path in a laminate material	[101]
Figure 60: (a) Cartoon illustration of nanoshell fabrication; (b) Electron microscope observation noted intensities vivid colors; (c) SEM image of nanoshell arrays; (d) Electron microscope observation; (e) Reflectance of the thin layers of Ag, Au, and Ge; (f) Transmittance of the thin layers of Ag, Au, and Ge, (g) transmittance of Ag, and Al with R, G, B	[102]
Figure 61: 3D simulation of electric and magnetic field for the 3 materials; (a) E_{ψ} field intensity of Ge; (b) E_{θ} : field intensity of Ge; (c) H_{ψ} field intensity of Ge; (d) H_{θ} field intensity of Ge; (e) E_{ψ} field intensity of Ag; (f) E_{θ} field intensity of Ag; (g) H_{ψ} field intensity of Ag; (h) H_{θ} field intensity of Ag; (i) E_{ψ} field intensity of Au; (j) E_{θ} field intensity of Au; (k) H_{ψ} field intensity of Au; (l) H_{θ} field intensity of Au.	[103]
Figure 62: spatial distribution of $[E_x]^2$ calculated for non-discretized Sinusoidal profile in TM polarization (a) the entire groove, and (b) the same region as multilayer.	[105]
Figure 63: diagram-showing variation on transmittance, reflectance and absorbance Germanium in different illumination angle (a) 10° (b) 15° (c) 25°.	[106]
Figure 64: diagram-showing variation on transmittance, reflectance and Absorbance Germanium in different illumination angle (a) 10° (b) 15° (c) 25°	[107]
Figure 65: diagram-showing variation on transmittance, reflectance and Absorbance Germanium in different illumination angle (a) 10° (b) 15°.	[108]
Figure 66: diagram-showing variation on transmittance, reflectance and Absorbance of a multilayer sample Ge-Au-Ag with different thickness (a), and absorbance of the sample (b).	[108]
Figure 67: Diagrams showing the manufacturing mechanisms of the samples	[110]
Figure 68: (a) Diffusion of a light beam by spherical particle . (b) Optical phenomena of diffusion	[111]
Figure 69: observation at the AFM of the networks realized	[111]
Figure 70: diagrams showing the different structures made	[113]
Figure 71: diagram showing the dispersion (a), the variation of	[116]

The intensity of the electric field (b), the absorbance of germanium (c).

Money case: (d), (e), (f); gold case: (g), (h), (i); highlighting,

the colours of the reflected or transmitted radiation

Figure 72: diagram highlighting the problem of manufacturing nanostructures.

[118]

LIST OF SYMBOLS AND ABBREVIATIONS

$A \equiv$ Arbitrary matrix (full rank).

μCP : Micro Contact Printing

ϵ : permittivity of the space

AFM: Atomic Force Microscope

Ag: Silver

AOTF: Acousto-optic Tunable Filter

Au: Gold

CVD: Chemical Vapor Deposition

DNA: Deoxyribonucleic Acid

E: vector represented electric field

EBL: Electron Beam Lithography

EBPL: Electron Beam Projection Lithography

EM: Electromagnetic

EQE: External Quantum Efficiency

GaN: Gallium Nitride

Ge: Germanium

GLAD: Glancing Angle Deposition

H: vector represented magnetic field

HD: High Definition

IBL: Ion Beam Lithography

IBM: Ion Beam Microscope

ICB : Institute Carnot de Bourgogne

IQE: Internal Quantum Efficiency

MEB: Scanning Electron Microscopy

MIMIC: Materialize Interactive Medical Image Control System

MSI: Multispectral Systems

NIL: NanoImprint Lithography

NIR: Near Infrared

NSTFs: Nanostructured Thin Films

PCVD: Plasma Chemical Vapor Deposition

PMMA: PolymethylMethacrylate

PVD: Physical Vapor Deposition

R: Reflectance Modulus
RCWA: Rigorous Coupled Analysis
RGB: Red Green Blue
S: Longitudinal Magnetic field Component
SAMIM: Solvent Assisted MicroMolding
SEM: Scanning Electron Microscopy
SFIL: Step and Flash Imprint Lithography
SP: Surface Plasmons
SPL: Scanning Probe Lithography
SPR: Surface Plasmon Resonant
STM: Scanning Tunneling Microscope
T: Transmittance Modulus
TFTs: Thin Firm Transistors
U: Longitudinal field Component Electric
W \equiv Eigen vector matrix calculated from **A**

Abstract

The development of multispectral imaging, holography and lithography techniques exploits the properties of diffracting arrays in a wide variety of photonic components. They are incorporated in laser diodes as distributed Bragg reflectors, in various integrated optical functions for wavelength division multiplexing or optical interconnections, or inscribed with in the fibers themselves, leading to a wide variety of sensors for detection of chemical elements, measurement of temperatures, pressures, accelerations of acquisition and or restitution of multispectral images, etc. [Lee et al. 2007] [Pagnoux et al.2005].

Among these devices, the resonant networks arouse a great interest because they allow to obtain ultra-selective filters from a relatively simple structure. This structure consists of a dielectric guide on which is etched a subwavelength network of shallow depth and thickness. Except resonance, the structure reflects and transmits the light according to the properties of reflectivity and transmission very close to those of the dioptr constituted by the stack of dielectric layers.

This work presents the experimental and theoretical studies carried out to overcome the technological obstacles inherent to the realization of thin-film multispectral optical filters.

The aim of this thesis is to study and design ultra-selective optical filters based on nanoscale thin films, by exploiting a resonant network structure conceived by depositing multilayer nanowires of metamaterials to surpass the performances of the current filters. Particular in the field of their spectral characteristics and their sensitivity to polarization. An issue of the study is to develop the associated manufacturing process, to identify the technological limitations imposed by the state of the art, to propose are producible process and if possible compatible with a collective technological development and low cost.

The second was to use the samples from the fabrication of the diffraction gratings to associate it with a tri-CCD transistor based sensor in the IMVIA laboratory, in order to design a sharp acquisition device in multispectral imaging and of vision.

The analysis of experimental performances, confronted with theoretical predictions and technological limitations, must lead to a realistic estimate of the potentialities of the proposed filters. To do this we began our study with a literature review on all the key elements of the subject, Nanotechnology, nanoscience these advantages these disadvantages, these possibilities. A review of the literature on multispectral imaging and these ascendants.

Then we presented the different methods of manufacturing thin film nanostructures, multilayer nanostructures, and we made a manufacturing choice according to the means available at the ICB laboratory. This approach led us to the characterization by electron microscopy of the samples obtained by lithography.

Finally a theoretical study was made, this one allowing by simulation on Matlab, and Python to check the obtained results (resonance properties of the diffraction gratings) by microscopic observations. A thorough study of these properties was made and the parameters of realization of nanostructures were defined. New samples made and observed allowed us to conclude that the choice of methods is the right one considering the spectral networks obtained by simulation of transmission and reflection.

These filters are particularly advantageous for operation in reflection, because the realization requires a small number of layers to ensure broad band transmission off resonance. From the point of view of the user, they are complementary to Fabry-Perot filters, mainly used in transmission, the operation in oblique incident reflection allowing a simplified assembly without separating blade. However, the practical use of these filters is limited by a very high angular selectivity, all the more constraining for ultra-selective filters because the divergence of the beam is greater than the angular tolerance of the filter, this limitation becoming more important under oblique incidence. The sensitivity of the filter response to polarization is another limitation.

But the confirmation of these convincing and hopeful results by visual observation was not possible because of the lack of material adapted to the spectral experimental characterization of nanostructures realized.

Keywords: nanostructures, nanoscience, nanotechnology, thin film, diffraction gratings, optical filter, multispectral imaging. Lithography, photonics, optical filters array

Résumé

Le développement des techniques d'imagerie multispectral, d'holographie et de lithographie permet d'exploiter les propriétés des réseaux diffractants dans une grande variété de composants photoniques. Ils sont incorporés dans des diodes laser comme réflecteurs de Bragg distribués, dans différentes fonctions d'optique intégrée pour le multiplexage en longueur d'onde ou les interconnexions optiques, ou inscrits au sein même des fibres, conduisant à une grande variété de capteurs pour la détection d'éléments chimiques, la mesure des températures, des pressions, des accélérations d'acquisition et ou de restitution d'images multispectrales etc. [Lee et al. 2007] [Pagnoux et al. 2005].

Parmi ces dispositifs, les réseaux résonnants suscitent un très vif intérêt car ils permettent d'obtenir des filtres ultra-sélectifs à partir d'une structure relativement simple. Cette structure est constituée par un guide diélectrique sur lequel est gravé un réseau sub-longueur d'onde de faible profondeur et ou épaisseur. Hors résonance, la structure réfléchit et transmet la lumière selon les propriétés de réflectivité et transmission très proches de celles du dioptré constitué par l'empilement de couches diélectriques.

Ce travail présente les études expérimentales et théoriques menées pour surmonter les verrous technologiques inhérents à la réalisation de filtres optiques multispectaux à couches minces.

L'objet de cette thèse est d'étudier et concevoir à partir de films minces nanométriques des filtres optiques ultra-sélectifs, en exploitant une structure de réseau résonnant conçue par dépôt de multicouches de nanofilms de métamatériaux pour surpasser les performances des filtres actuels, en particulier dans le domaine de leurs caractéristiques spectrales et de leur sensibilité à la polarisation. Un enjeu de l'étude est de développer le procédé de fabrication associé, de dégager les limitations technologiques imposées par l'état de l'art, de proposer un procédé reproductible et si possible compatible avec un développement technologique collectif et à faible coût.

Le second en jeu était d'utiliser les échantillons issus de la fabrication des réseaux de diffraction pour l'associer à un capteur fabriqué à base de transistor tri-CCD au laboratoire IMVIA, afin de concevoir un dispositif d'acquisition pointu en imagerie multispectral et de vision.

L'analyse des performances expérimentales, confrontées aux prévisions théoriques et aux limitations technologiques, doit conduire à une estimation réaliste des potentialités des filtres proposés. Pour se faire nous avons commencé notre étude par une revue de littérature sur l'ensemble des éléments clés du sujet, la Nanotechnologie, la nanoscience ces avantages ces inconvénients, ces possibilités. Une revue de la littérature sur l'imagerie multispectrale et ces ascendants.

Ensuite nous avons présente les différentes méthodes de fabrication des nanostructures à couches minces, des nanostructures multicouches, et nous avons fait un choix de fabrication selon le moyens disponibles au laboratoire ICB. Cette démarche nous a conduite à la caractérisation par

microscopie électronique des échantillons obtenus par Lithographie.

Enfin une étude théorique a été faite, celle-ci permettant par simulation sur Matlab, et Python de vérifier les résultats obtenue (propriétés de résonance des réseaux de diffraction) par observations microscopique Une étude poussée de ces propriétés a été faite, et les paramètres de réalisation et des nanostructures ont été définie. De nouveaux échantillons réalisés et observé nous permet de conclure que le choix de des méthodes est la bonne eu égard aux réseaux spectraux obtenus par simulation de transmission et de réflexion.

Ces filtres sont particulièrement avantageux pour un fonctionnement en réflexion, car la réalisation nécessite un faible nombre de couches pour assurer la transmission large bande hors résonance. Du point de vue de l'utilisateur, ils sont complémentaires des filtres Fabry-Perot, utilisés essentiellement en transmission, le fonctionnement en réflexion sous incidence oblique permettant un montage simplifié sans lame séparatrice. Cependant, l'utilisation pratique de ces filtres est limitée par une très forte sélectivité angulaire, d'autant plus contraignante pour les filtres ultra- sélectifs car la divergence du faisceau est plus grande que la tolérance angulaire du filtre, cette limitation devenant plus importante sous incidence oblique. La sensibilité de la réponse du filtre à la polarisation constitue une autre limitation.

Mais la confirmation de ces résultats probant et remplis d'espoir par observation visionique n'a pas été possible du fait du manque de matériel adapté à la caractérisation expérimental spectral de nanostructures réalisées.

Mots clés : nanostructures, Nanoscience, Nanotechnologie, films à couches minces, réseaux de diffraction, filtre optique, imagerie multispectrale. Lithographie, photonique, réseau de filtres optiques.

INTRODUCTION

The Developments made in recent years in image processing techniques in nanoscience and / or nanotechnology can exploit plasmonics properties of structured nonmaterials in the design, production of a wide variety of photonic and electronic components. They are integrated in the achievement of the laser diode as Bragg grating; indifferent optical functions or visionics (basic structure of dichroic lenses), and the realization of systems or devices of multispectral acquisition (sensors, camera) ... etc.

Among these devices, the existing multispectral systems (MSI) until then are based on two mains types of technology (scan and snapshot): those based on interference filters (filter wheel system), those based on liquid crystal filters, and those based single or multiple sensor. These devices although powerful have numerous drawbacks on technological, economic.

The problems we face in general in these models are: the clutter, the vibration of the wheels producing an images flicker, the destructive dispersion of filters, the diffraction related to the indices and their different thickness of a filter to another; the impossibility of real time, the very large absorption in the short wavelength, vignetting introduced by the size of these filters for some models. These problems are major technological challenges posed by the existing. The optical filtering is based on techniques of thin layers; as well as nano-layers thickness much less than the wavelength. A suitable multilayer system deposited on a substrate allows to reach the transmittance and reflectance desired. Thus from theoretical models, and technological developments we can define a filter template and carry it out from the nano-films for applications in the field of multispectral. For this purpose, the firstfruits of research in the field have already been undertaken and carried out:

- The Fabry-Perot interferometer,
- The 1D resonant filters arrays,
- The photonics sieve for spectral analysis,
- The 2D and 3D resonant networks

The Fabry-Perot interferometer is optical device consisting of two partially reflective surfaces to high reflectance of interference without diffraction.

In the 1990s, the 1D resonant filters arrays have emerged as an alternative to the Fabry- Perot filters for use in free space [1]. These filters have a clear advantage for reflection operation, because the realization requires a low number of layers to ensure the off resonance wide-band transmission. But in practice many limitations: angular selectivity, sensitivity of the polarization filter are notable.

The photonic sieve for spectral analysis, of fairly simple principle, consisting of opaque metallic film drilled with one or more sub-wavelength apertures (150 nm) can transmit light with an efficiency one hundred fold higher than that theory predicts for simple holes. This efficiency may be

even greater than the area occupied by holes, meaning that even the light which falls next to the holes will emerge from the other side of the sample. This special transmission is due to the coupling of the incident light with surface plasmons. The transmission spectra contain peaks corresponding to surface plasmon modes which depend on the symmetry of the periodic surface lattice parameter.

More recently, the 2D and 3D resonant networks have been proposed to improve the angular tolerance and achieve the insensitivity to polarization filters under oblique incidence Fehrembach et al. [98]. This early work demonstrated interesting theoretical potentialities, but whose experimental verification must be provided.

Many results indicate that another problem of sub-wavelength apertures, as the optical diffraction can be controlled by the issue of surface plasmons. These findings raise fundamental questions and suggest many applications. They also highlight the important scientific and technological potential of controlling the properties of surface plasmons by the use of modern nano fabrication techniques. Surface plasmons (SP) have since renewed interest in various fields. In 2000 a new discipline appears: plasmonics, seeking to take advantage of the resonant interaction obtained under certain conditions between electromagnetic radiation (light) and the free electrons at the interface between a metal and a dielectric material (air or glass). This interaction generates electron density waves, behaving like waves and called plasmons or surfaces plasmons.

The Plasmonic is credited with many potential applications. By giving a new way to control the behavior of light, it could improve the resolution of microscopes, increase the yield of components, electronic systems, and lead to effective couplings devices between optical and electrical signals or even pick up and improves the technological challenge posed by multispectral devices.

The purpose of this thesis is to study and design optical filters in nanostructures by exploiting plasmonics materials theories to exceed current performance, if necessary improve some aspect and technological disadvantages inherent in the filters currently present on the market. A stake of the study is to develop an application that is compatible with a collective technological development real time system. Experimental performance analysis, face the theoretical predictions and technological limitations, should lead to a realistic estimate of the potential of the proposed filter, and its feasibility. To do so, an ambitious tender specification not accessible by current filters has been established:

- operation in transmittance under any incidence
- wavelength centered around 550nm
- width spectral field of the visible (380 nm to 780 nm) – more to NIR
- rejection rate above 100
- Independence to polarization
- Possibility of spectral tunability over several nanometers.

The interest of using a single filter centered at 550 nm to develop multispectral lies in the use of the illuminant: white light, and the fact that one can study several spectral discrimination band; 350 nm (blue) to 1100 nm (NIR). It is actually a high performance alternative to standard color cameras because the amount of crosstalk between the bands is much lower, especially between the NIR channel and the color channels. Subsequently the filter may be useful for a variety of applications where color and NIR imaging should be performed simultaneously.

To satisfy the requirements of the specification, we articulated our work on five chapters:

- the first chapter, deals with the review of literature and the State of the art inherent in the subject, Bibliographic synthesis of Nanotechnology and Multispectral systems,
- the second chapter, deals with applications of multispectral reconstruction spectral response .
- the third chapter deals with the description of the methods and realization of devices in nanofilms, this chapter specifies the materials, the structure of the filters, and the method used to produce samples of nanofilms on a substrate. A critical analysis of the accuracy and reproducibility of different manufacturing steps of the chosen method is made.
- the fourth chapter presents the theories, optical and electromagnetic properties necessary and sufficient for the design and synthesis of nanostructure multispectral filter array,
- the fifth chapter is devoted to the simulation study of the types of filters, the design methodology, simulations, results discussion and experimental setup.

This study was conducted as part of a supervision of thesis between the University of Douala in Cameroon and the University of Burgundy in France. The conduct of the thesis has relied on cooperation between two laboratories of the University of Burgundy: the IMVIA and the Nanotechnology Team (ICB).

CHAPTER I: BIBLIOGRAPHIC SYNTHESIS OF NANOTECHNOLOGY AND MULTISPECTRAL SYSTEMS

At the end of the 1950s, Richard Feynman held a visionary conference, remained unnoticed for decades, but famous today [1]. Indeed, this conference laid the foundations of nanoscience and nanotechnology in imagining, well before the advent of the atomic force microscope, the possibility to manipulate and control objects at the atomic level. This perspective allows today to rethink the electronics as Assembly of nanoscale components [2]. This chapter has no claim to cover the whole of this vast area, but by a few examples, to give the reader an idea of the contribution of nanoscience to a renewed approach to image processing, and design more advanced multispectral systems and more accurate.

I.1. The importance of the multispectral in Artificial Vision

During recent years, the multispectral developed in significant ways. The applications are vast from astronomy (lenses interference, astronomical telescopes...), which was precursor to common applications such as the control and security (sensors, detectors...), cell biology (chips, systems of DNA sequencing...), agronomy (image acquisition systems, filters, cameras...), health (biochips), etc. The development of artificial vision systems capable of recording image sequences in the visible, the near-infrared or mid-infrared is a research topic growing. According to dictionary, a multispectral image is one that captures image data at specific frequencies across the electromagnetic spectrum. The wavelengths may be separated by filters or by the use of instruments that are sensitive to particular wavelengths, including light from frequencies beyond the visible light range, such as infrared.

In artificial vision spectral imaging can allow extraction of additional information that human eye fails to capture with its receptors for red, green and blue. It was originally developed for space-based imaging. Multispectral imagings are the main type of images acquired by remote sensing (RS) radiometers. Dividing the spectrum in to many bands, multispectral is the opposite of panchromatic, which records only the total intensity of radiation falling on each pixel.

I.1.1. Objectives and relevance

The artificial multispectral visional, lows to analyze samples at each point of the visible surface. It allows to characterize the heterogeneity of the objects and to detect local defects on the surface of the samples to study. In an artificial vision system, each image associated with spectral condition is scanned and put in the form of a matrix. Each element of this matrix, called gray level is a number proportional to the light intensity of the point (or pixel) corresponding. On usual artificial vision systems, these matrices include several hundreds of lines and columns. They are typically of size 1024*1024 or 2048*2048. The gray levels are often encoded 0, 12 bit, which provides 256 levels

of brightness. Black is often coded with the value 0, white by 255. The development of artificial vision is currently limited by several factors. First of all spectral sensitivity range of the ordinary CCD camera does not cover the entire region of the PIR, and extends only from 400 to 1100 nm [3]. The increasingly digitization is often done on 8 bits, giving only 256 levels of gray. More sophisticated cameras have a higher resolution with encoding on 12 or even 16-bit gray scale. The noise of the spectral measure is considerably higher than that of the usual NIR spectrometers. He reached (with non-cooled cameras) 500×10^{-6} to 1000×10^{-6} optical density units, while an ordinary spectrometer has a noise of only 20×10^{-6} units. To process images, it is necessary to have powerful computers and algorithms adapted to multispectral images still the domain of research.

I.1.2. History and development

The early works in the field of the multispectral applied to artificial vision have been conducted by Taylor and Mac Clure (1989) in the near infrared (NIR) [3]. A device used by these authors is presented in figure 1. The samples are illuminated by tungsten filament lamps. The interferential filters placed in front of the camera allow to select the reflected light wavelengths. Thus, it is possible to acquire image sequences of the same sample, corresponding to different spectral conditions.

Robert et al. (1991) [103] have also built a system of artificial vision NIR (figure2). The light source is a tungsten filament lamp whose spectrum extends from 340 to 2000 nm. A grating monochromator allows the wavelengths selection of light. The NIR camera is here equipped with a Vidicon tube and is sensitive up to 2000 nm. The system is set in a way to record image sequences between 900 to 1900 nm, with a step of 50 nm. The Basic statistics of discrimination applied to multispectral images have been described by Bertrand et al. (1996).

Park et al. (1995) [104] have developed a multispectral image analysis system designed to automate the inspection of poultry carcasses in slaughterhouses. The CCD camera is equipped with 6 Interferential filters at 542, 571, 641, 700, 720 and 847 nm. The images include 752 lines and 480 columns, and the gray scale is coded on 8 bits.

Treado et al. (1992) [105] have combined device AOTF (Acoustico-optic tunable filter, or modular photo-acoustic filters) with an image analysis system. In their tests, the light selected by the AOTF device is directed on the sample, placed below the eyepiece of a microscope. A cooled CCD camera allows to record sequences of images with 128×128 pixels. The useful field of the camera is close to $100 \mu\text{m}$. The authors use the system for the study of human epithelial cells.

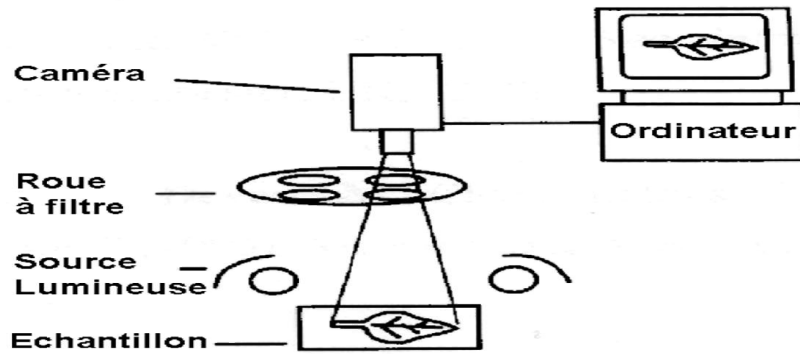


Figure 1 : multispectral artificial vision. (McClure, 1994)

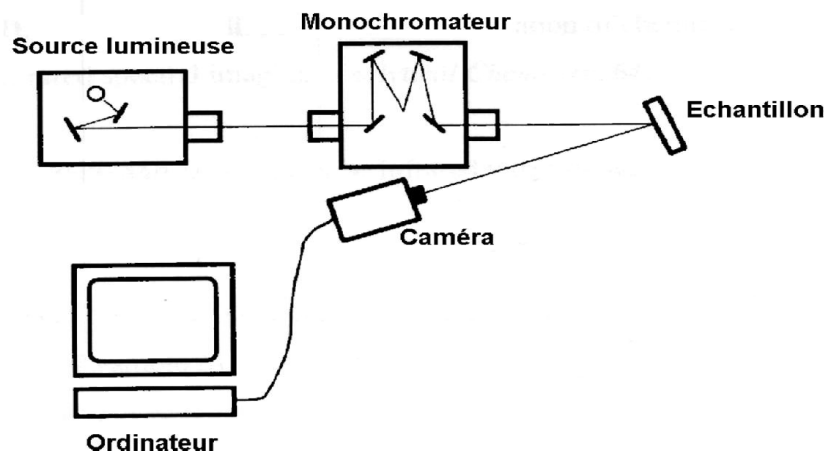


Figure 2: Overview of artificial vision system (Robert et al., 1991)

I.2. State of the art on existing systems

Several multispectral systems have been developed in the laboratories and the first cameras hitting the market offering of HD images with a dozen of spectral bands. The processing of multispectral images remains a scientific issue due the vector nature information attached to each pixel, and the complex nature of interactions between light and object. The multiplication of information channels pushes the limits of conventional image analysis methods around the generic problematic of segmentation, selection of attributes, classification, filtering, dimensionality reduction, etc... These existing multispectral devices are based on two types of technology:

I.2.1. The systems based on interference filters

These are filter wheels systems having advantages of course but many disadvantages, such as clutter, the vibration of the wheels producing images flickering, the destructive dispersion of filters, the diffraction problem with indices of filters, the varying thicknesses of one filter to another. Finally another drawback not less major is the impossibility of make real time with this type of system related

to the inertia of the wheel and prohibiting any possibility to analyze moving objects.

I.2.2. Systems based on liquid crystal filters

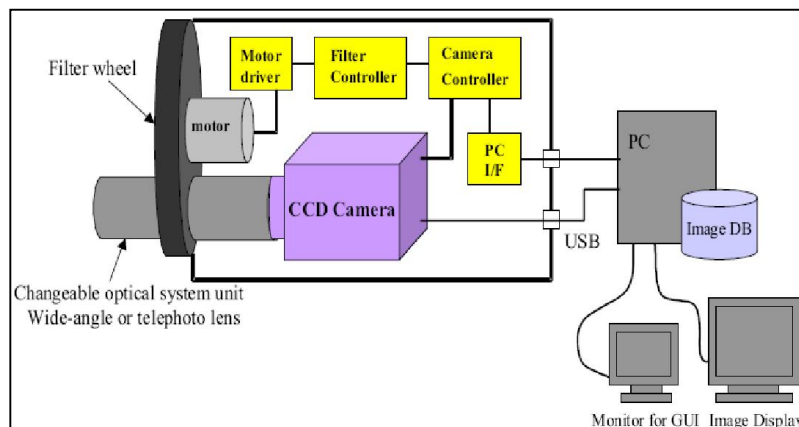


Figure 3: principle of a multispectral camera based on the wheel filters principles

These systems are well fast (each filter response time is in the order of ms). They have meanwhile several flaws including: significant absorption in wavelengths and the problem of vignetting (reduction of useful image part) introduced by the size of these filters. Thus, only the optical center can be used.

The introduction of filters using the principle of thin film interference caused a jump in the design and implementation of multispectral systems. Dichroic filters made their appearance. The most successful use to date of this filter is the tri-CCD camera whose operating principle is shown in Figure 4. The source of the incident light is decomposed into three secondary sources, what constitutes the 3 shots of the RGB color image. This use was a great success thanks to the quality of images obtained colors compared to images from Bayer filters. An application not less widespread concerns videos projectors.

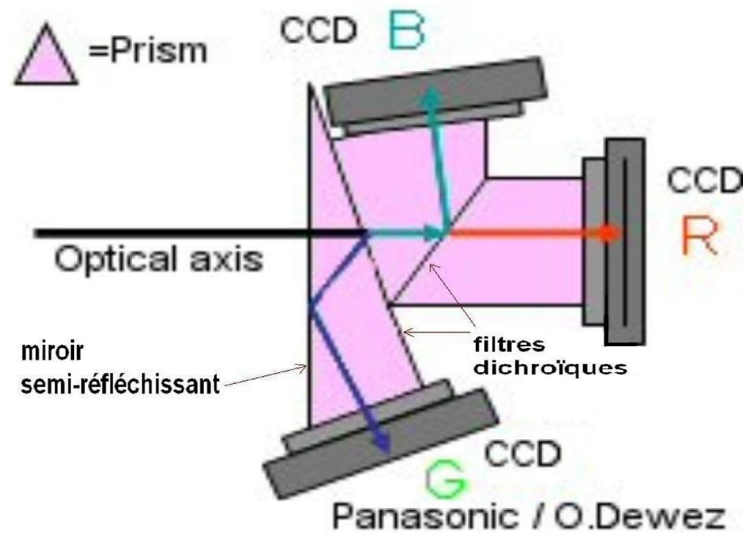


Figure 4: functional principle of a Tri - CCD camera

I.2.3. Dichroic filters to the nanostructures filters

A dichroic filter is an optical system having undergone several deposits of materials giving the power splitter. Some filters made in the field of the video-projectors and Tri - CCD cameras show efficient systems in terms of non-destructive reflectance and transmittance in the spectral bands of the visible. More such a device allows obtaining a very quick response. In order to go further and at the level of accuracy of the response, and the ergonomics of the device, one explores in recent years and at present time another science and another technology: nanoscience or nanotechnology.

I.3. Contribution of nanoscience: introduction to nanotechnology

The optical filtering is based on thin-film techniques. A suitable multilayer system deposited on a substrate to achieve the desired transmittance and reflectance. Thus from theoretical models we can define a filter template and make it for applications in the field of multispectral.

I.3.1 Basic concepts - Definitions and Emergences

The terms of nanomaterials and nanotechnology grouped in nanosciences cover a domain of achievements whose pitch is less than one micron. They are obtained either by technologies that allow a reduction in the size of the components, or the production of nano-objects that are self-organizing. Be come in recent years a common use, the term nanomaterial is to some extent ambiguous; and need to be specified because it does not necessarily refer, as its name both to suggest, at the nanometer, distance little greater than the distance between neighboring atoms in a crystalline or molecular structure. To do this we need to take into account developments that have occurred in the field of science and technology.

First of all draw attention to developments in terms of organization. The intramolecular organization was known or at least suspected since the beginning of the previous century, but beyond that, the organization of atomic, ionic, or molecular species in condensed phases, the random or non-random distribution character, was ignored [11]. With regard to the crystalline material, knowledge was bounded by the power of investigation of research tools available. The conventional optical microscopy whose theoretical limit was the order of wavelengths of visible, i.e. the micrometer, allowed to recognize crystal grains and grain boundaries, without provided access to their internal organization [11].

The appearance of electron microscopy allowed to won several orders of magnitude in resolution; it favors the development of microscopy methods in the near field, local analysis methods on the submicron scale. In addition, she gave the basics of high-resolution electron microscopy and atomic force microscopy (AFM) or field-effect, with images on the scale of interatomic distances. These allowed where it was limited due to lack of better to the idea of a random distribution of species in a solid solution, to recognize effects order long-distance, local partial order or fragmentation at a lower scale of crystal structures, though, the order effects.

All these effects fall within the 1-100 nm scale, and allow us to highlight two discriminating characters: one scientific and the other technique:

- We consider that we are dealing with a nanomaterial when its constitution scale is below a limit below which its properties are different from those of the usual solid material. For example, if one is interested in the mechanical properties, the threshold appears to grain size lower than few microns. Similarly, for optical properties, specific phenomena occur to scales that are superior to the nanometer by orders of greatness from 1 to 3. A further threshold appears for all materials when a dimension at least particles are low enough to induce quantum effects. It is well this time of nanoscale dimensions [12].
- The developments and advances in technology have allowed over the years to achieve materials or structures which the definition pitch is increasingly weaker without reaching the point where their properties are affected [11], [13]. This is achieved in a top-down process, by are firemen etching techniques. The most obvious example is the miniaturization of the components of electronic microchips. The current point technology allows to reach a definition pitch of the order of 50 nm. We'll see that we are still significantly above the threshold of occurrence of quantum phenomena [12]. Symmetrically (bottom-up), it is possible to directly achieve very small objects, or to recognize their existence and to manipulate them (for example, presence in some soot of carbon nanotubes) [13].

All these effects and these scientific and technical developments are causing the birth of a new science and technology whose bases, the ramifications are more complex, extended, multidimensional and multidisciplinary: Nanosciences and Nanotechnologies.

I.3.1.1. Nanosciences

According to the encyclopedia, nanosciences and nanotechnologies (from Greek *vávoç* dwarf) can be defined for minima as the set of the studies and processes of manufacture and manipulation of structures (electronic, chemical, etc...), devices and hardware systems to the nanometer scale (nm). In this context, nanoscience is the study of phenomena, methods for control and manipulation of matter at the Atomic, molecular and macromolecular scales where properties differ significantly from those that prevail at a larger scale.

I.3.1.2. Nanotechnology

Nanotechnology is defined as the study, design, characterization, production, and application of structures, devices and hardware systems by controlling shape and size at the nanoscale [14]. Despite the relative simplicity and precision of these definitions, the NTS have several acceptances related to the cross-cutting nature of this young discipline. Indeed, they use, while allowing new possibilities, disciplines such as optics, biology, mechanics, micro-technology, etc...

I.3.1.3. Emergences

Behind the daydreams, the announcement effects, several studies have been conducted to understand the evolution of nanosciences and nanotechnologies. Thus considering the fact that the definitions are not stabilized, the common component of the different methods used is to measure the nanotechnological activity in three ways: scientific publications (instead for fundamental knowledge), patents (instead for the technological aspects), and possibly institutions and companies concerned or even capital invested (to measure the economic and industrial activity actual). With regard to numerous articles, patents, published applications and industries that flare up this sector, a strong evolution is substantial since the first use of the prefix 'nano' in 1911 by a scientist, through the speech from Richard Feynman in 1959 until the present day. The current development of nanosciences and nanotechnologies mobilizes and covers a broad spectrum of domains and scientific disciplines.

From the point of view of mobilized scientific knowledge, several sub-disciplines are particularly useful in the development of fundamental knowledge of the NST. Indeed, detailed analyses [15] in the manner which are published and built, scientific papers on nanotechnology and nanoscience, show the emergence of three specific subfields:

- Nanobiology which concerns, bioscience, pharmaceutical and biotechnologies;
- the field of nanomaterials and chemical synthesis;

- the field of nanoelectronics, superconductivity, microelectronics and quantum computer

All these three fields are articulated with each other with more less intensity and distance. The correlation and cross-correlation relationships generate new disciplines which have a significant impact on the modalities of organization and structuring of industrial activity that they mobilize in the area concerned. Essentially the fields of application are varied. Molecular Engineering made possible by the invention of the scanning tunneling microscope to build and develop molecules according to his will; to the medical by exploiting the properties of nanomaterials for various applications (contrasting agents for imaging cells, therapeutic for cancer control and targeted therapy), or to diagnosis tools or drug delivery, as shown in figures 5 and 6.

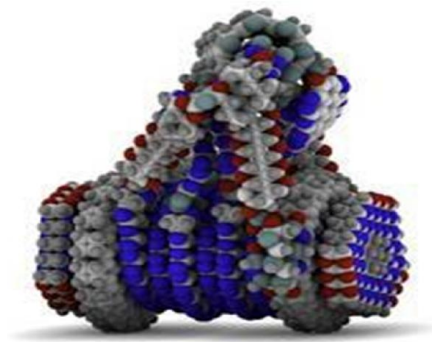


Figure 5: Prototypes of nanomachines designed by Professor k. Eric Drexler © 1991-2007 Institute for Molecular Manufacturing.



Figure 6: Representation of a nano robot. © Oliver Burston, Wellcome Images Digital artwork/Computer graphic 2005.

I.4. Impact factors of nanoscience and nanotechnology in multispectral imaging

Advances in nanoscience and nanotechnology promise to have major impact factors for health, wealth, and peace in the upcoming decades. Knowledge in this field is growing worldwide leading to fundamental scientific advances. In turn, this will lead to dramatic changes in the ways that materials, devices, and systems are understood and created.

The coincident expansion of “nanoscale science” or nanoscience and nanotechnology already will play a fundamental role not only in molecular imaging, but also in sensors, biosensors, biomarkers, electronic, spectroscopy, telecommunications and drug delivery over the next decade. The US National Nanotechnology Initiative (see the statement by M.C.Roco, available at http://www.nano.gov/roco_vision.html) recognizes that “the relative arrangement of the elementary blocks of matter into their assemblies leads to new properties and functions even for the same chemical composition.” Ironically, as devices and agents become smaller, they will require bigger and more multidisciplinary teams to realize the anticipated revolution.

I.4.1. Implications of nanoscience and nanotechnology in Biology and Medicine domain

Nanotechnologies are also complex to address because they are cross-cutting technologies which can find applications in most economic sectors. It is an area with little specific and multidisciplinary outlines by nature (physics, chemistry, biology, etc.)

In the Biology and Medicine domain, the recent emergence of molecular imaging as an integrated discipline in academic medical centers has set the stage for an evolutionary leap in diagnostic imaging and the raspy see figure 6. Molecular imaging is not a substitute for the traditional process of image formation and interpretation, but is intended to improve diagnostic accuracy and sensitivity by providing an in vivo analog of immunocyto-chemistry or in situ hybridization [16]. It is less concerned with nature image contrast or resolutions, which are keys for depicting the effects of the disease on surrounding normal tissues, but rather, it seeks to enhance the conspicuity of microscopic pathologies by targeting the molecular components or processes that represent actual mechanisms of disease [16]. The diagnosis and treatment of cancer have been greatly improved with the recent developments in nanotechnology. One of the promising nanoscale tools for cancer diagnosis is fluorescent nanoparticles (NPs), such as organic dye-doped NPs, quantum dots and up conversion NPs that enable highly sensitive optical imaging of cancer at cellular and animal level, etc...Ultimately the development of nanotechnologies is bearer of progress in medical field: new miniaturized medical diagnostic tools; better targeted drugs in the form of nanovectors.

I.4.2. Implications in electronic – engineering sciences – and research literature

A revolution is occurring in science and technology, based on the recently developed ability to measure, manipulate and organize matter on the nanoscale 1to100 billions of a meter. At the nanoscale, physics, chemistry, biology, materials science, and engineering converge toward the same principles and tools. As a result, progress in nanoscience will have very far-reaching impact. In electronic and engineering sciences, the nanoscale is not just another step toward miniaturization, but a qualitatively new scale. The new behavior is dominated by quantum mechanics, material confinement in small structures, larges interfacial volume fraction, and other unique properties, phenomena and processes. Many current theories of matter at the microscale have critical lengths of nanometer dimensions (electronic components technology theory). These theories will be inadequate to describe the new phenomena at the nanoscale. Various characteristics such as wide bandgap, strong polarization field, and high electron velocity make GaN one of the attractive materials in advanced electronics in recent times. Nanowire-structured GaN can be applicable to various transistors for enhanced electrical performances by its geometrical feature. Similarly metal-oxide thin-film transistors (TFTs) using silver nanowire, or gold nanowire have been achieve in electronic domain. Therefore, the involvement of nanoscience or nanotechnology is inevitable and large in the creation of multispectral systems, such as sensors, detectors, processing and image analysis systems, in improving spectroscopy, imaging systems, Photonics in General, etc... Transportation: Nanomaterials and nanoelectronics will yield lighter, faster, and safer vehicles and more durable, reliable, and cost-effective roads, bridges, runways, pipelines, and rail systems. Nanotechnology-enabled aerospace products alone are projected to have an annual market value of about \$70 billion in ten years (Hitachi Research Institute, personal communication, 2001).

As knowledge in nanoscience increases worldwide, there will likely be fundamental scientific advances. In turn, this will lead to dramatic changes in the ways materials, devices, and systems are understood and created. Innovative nanoscale properties and functions will be achieved through the control of matter at its building blocks: atom-by-atom, molecule-by-molecule, and nanostructure-by-nanostructure. Nanotechnology will include the integration of these nanoscale structures into larger material components, systems, and architectures. However, within these larger scale systems the control and construction will remain at the nanoscale.

Today, nanotechnology or nanoscience is still in its infancy, because only rudimentary nanostructures can be created with some control. However, among the envisioned breakthroughs are orders-of-magnitude increases in computer efficiency, human organ restoration using engineered tissue, “designer” materials created from directed assembly of atoms and molecules, as well as

emergence of entirely new phenomena in chemistry and physics.

Nanotechnology or nanoscience is booming! In the global fundamental nanotechnology and nanoscience research literature as represented by the Science Citation Index/Social Science Citation Index (SCI/SSCI, 2006), global nanoscience or nanotechnology publications grew dramatically in the last two decades [17] as shown in figure 7.

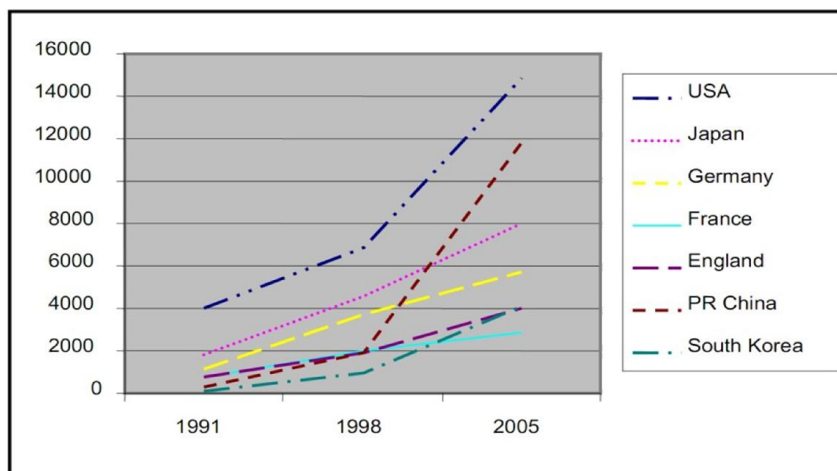


Figure 7: country comparison time trend (number of articles vs. time) [17].

The craze, the importance and the impact of nanoscience or nanotechnology are shown by the large mass of writings, publications, and literary articles on the subject or using composite words or derivatives as shown in figure 7 below.

Nanotechnology or nanoscience has captured the imaginations of scientists, engineers and economists not only because of the explosion of discoveries at the nanoscale, but also because of the potential societal implications as figure 8 shows.

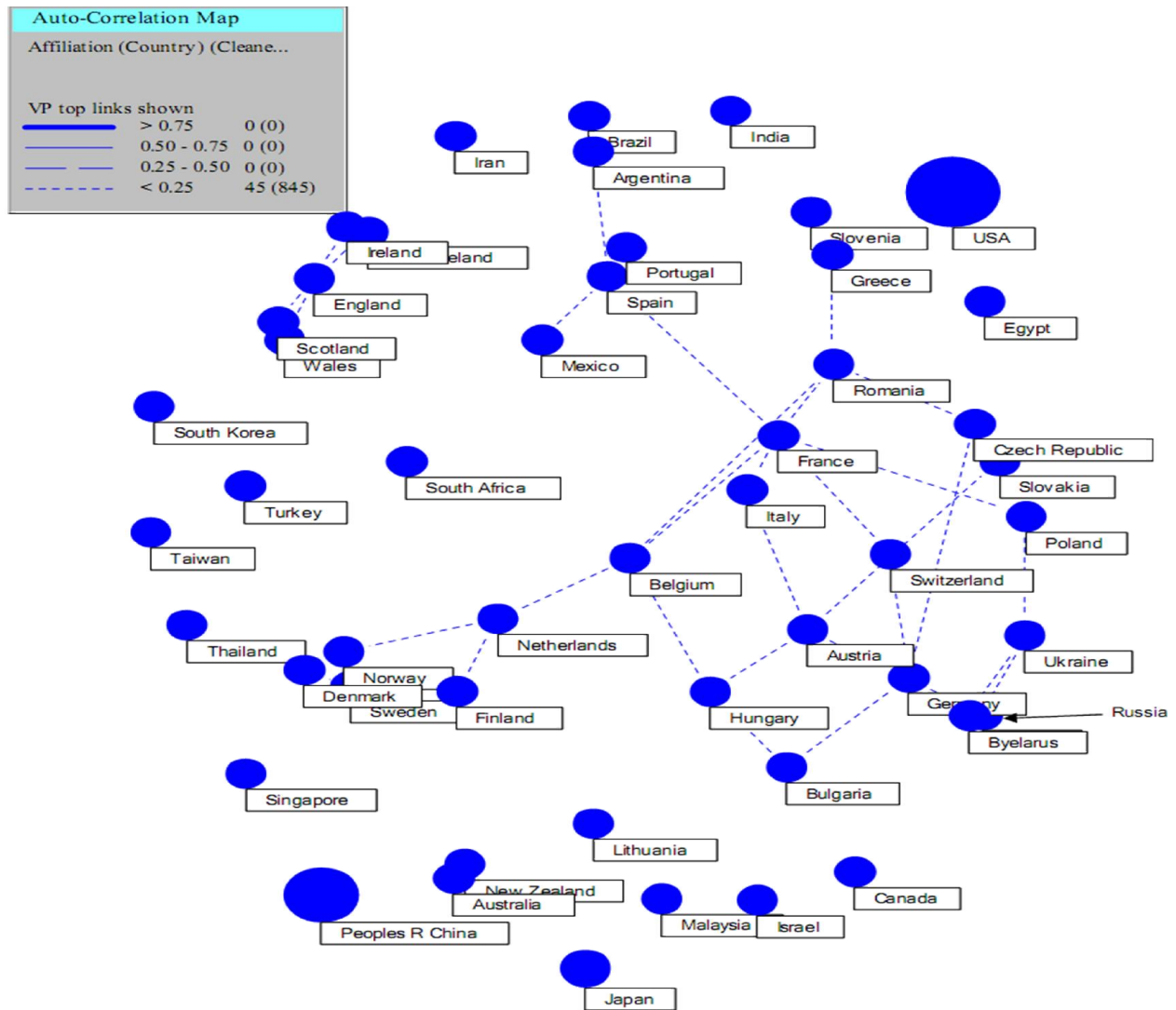


Figure 8: country auto-correlation map (fifty most prolific countries) [17].

Nanotechnology's relevance is underlined by the importance of controlling matter at the nanoscale for healthcare, the environment, sustainability, and almost every industry. There is little doubt that the broader implications of this nanoscience and nanotechnology revolution for society at large will be profound.

I.4.3. Societal implication and ethical sensitivity

New technologies come into being through a complex interplay of technical and social factors. The process of innovation that will produce a nanotechnology and diffuse its benefits into society is complex and only partially understood. Economists, as well as scholars in other fields, have long studied the generation, diffusion, and impact of scientific and technological innovation [18]. These studies outline the variables likely to determine the rate and direction of these impacts, and to identify relevant research questions. They provide a foundation on which to build studies of societal implications of nanotechnology or nanoscience. Societal implication of this young discipline lies partly in the

interactive process of innovation and diffusion and also in unintended consequences and second orders. Scientific discoveries do not generally change society directly; they can set the stage for the change that comes about through the confluence of old and new technologies in a context of evolving economic and social needs.

Nanotechnologies or Nanosciences are so diverse that their manifold effects will likely take decades to work their way through the socio-economic system. While market factors will determine ultimately the rate at which advances in nanotechnology get commercialized, sustained support for nanoscience research is necessary in this early stage of development so as not to become a rate-limiting factor.

Perhaps the greatest difficulty in predicting the societal impacts of new technologies has to do with the fact that once the technical and commercial feasibility of an innovation is demonstrated, subsequent development may be as much in the hands of users as in those of the innovators and other development industrial sectors. Thus the harmonious diffusion and impact of technological innovations of Nanoscience or Nanotechnology often depends on the development of complementary technologies and of the user network. As a result, new technologies can affect society in ways that were not intended by those who initiated them. But the impact of innovation and technology diffusion will be modest unless they are part of a broader reform process in the area of product, capital and labor markets. Often these unintended consequences are beneficial, such as spinoffs with valuable applications in fields remote from the original innovation. To assess a nanotechnology (or any technology) in terms of its unintended consequences, researchers must examine the entire system of which the technology is a part through its entire life cycle. One concern nanotechnology unintended consequences raises the question of the uncontrolled development of self-replicating nanoscale machines. A new form of life different from that known (i.e., carbon-based) would be a dramatic change that is not foreseen in the near future. Because a number of very serious technical challenges would have to be overcome before it would be possible to create nanoscale machines that could reproduce themselves in the natural environment. Finally, an important aim of a societal impact investigation of nanotechnology is to identify harms, conflicts over justice and fairness, and issues concerning respect for persons. For example, changes in workforce needs and human resources are likely to bring benefits to some and harm to others. Other examples of potential issues include safeguards for workers engaged with hazardous production processes, equity disputes raised by intellectual property protection, and questions about relationships between government, industry, and universities.

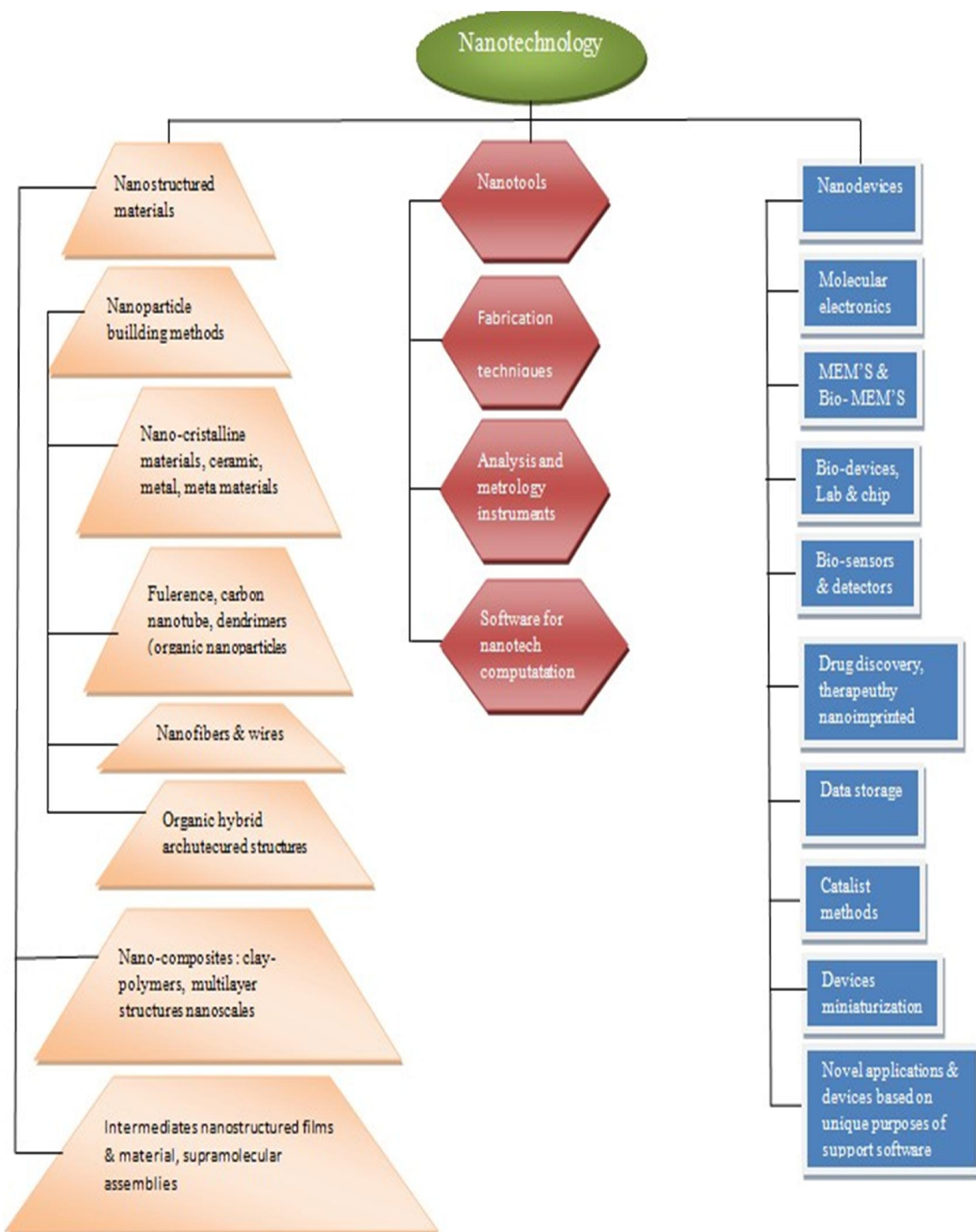
It allows to exclude all nanosized objects as simple molecules that have the same properties regardless of the number of molecules present. The polymer molecules whose degree of

polymerization does not change of ownership are not nano-objects: thus the DNA is not a nano-object. However, it is often difficult to restrict to this strict definition. Indeed the terms "nano" or "nanotechnology" are sometimes used for reasons of communication belonging to nanotechnology is not really clear. Other hand, belonging to the nanotechnology techniques may not be identified as such because this visibility could be detrimental because of the fears of these new technologies. Finally, the borders of this definition can be sometimes blurred. For example the micelles, structures that occur naturally to minimize repulsions hydrophobic and hydrophilic, are cited as belonging to the nanobiotechnology.

Thus, this study is based on this definition of nanotechnology, but it can include applications for which there is not necessarily consensus on their belonging to nanotechnology, and instead not to mention existing applications for which there is currently no visibility on the fact that they use nanotechnology.

On tracking the nano evolution, it has been stated that no matter what the market outcomes in the near or long term, nanoscience will never be an industry unto itself but a science of many avenues of application, and possibility that could redefine the direction of several industries This insight allows one to recognize that nanotechnology is not "a technology" but "a set of technologies," yielding a set of technical breakthroughs that will seep into many different markets. Within such a framework, the world of nanotechnology may be divided into three broad categories: nanostructured materials, nanotools, and nanodevices. The various components of these categories are schematically illustrated in Table 1.

Table 1: Schematic illustration of the world of nanotechnology and nanoscience.



I.5. Overview on multispectral systems

Generally, multispectral systems designate one and/or shooting devices allowing for simultaneously recording in different bands of the spectrum visible or invisible. In image processing, multispectral systems are the collection and analysis of reflected, emitted, or back-scattered energy from an object or an area of interest in multiple bands of regions of the electromagnetic spectrum (Jensen, 2005). Subcategories of multispectral systems include hyperspectral, in which hundreds of bands are collected and analyzed, and ultraspectral systems where many hundreds of bands are used (Logicon, 1997). In the same way according to Dictionary of Earth Sciences (Ailsa Allaby and Michael Allaby, 1999), is the simultaneous use of several different sensors to obtain images or spectral information from various portions of the electromagnetic spectrum. An example was the multispectral scanner on the Landsat Earth-orbiting satellites, which simultaneously recorded green, red, and two infrared spectral bands. Since different materials (e.g. soil, rock and vegetation) reflect differing amounts of light at different wavelengths, they can be identified by their characteristic spectral ‘signatures’. Spectral imaging can allow extraction of additional information the human eye fails to capture with its receptors for red, green and blue. It started originally in field for space-based imaging.

To meet the needs and requirements of applications such as the colorimetric measurement and the research of spectral signatures, for example, with more than three channels acquisition systems have been proposed [x,y,z]. Several multispectral systems have been developed in the laboratories and the first cameras hitting the market offering of HD images with a dozen of spectral bands. Such systems provide richer data than do traditional RGB camera, generally known under the name of multispectral data. Processing these multispectral images remains a scientific issue of share vector nature information attached to each pixel, and the complex nature of interactions between light and matter. The multiplication of information channels pushes the limits of analytical methods of classic images around the generic problems of segmentation, selection of attributes, classification, dimensionality reduction, etc. Methods and appropriate means must then be implemented to exploit all the information conveyed. Often, it is not a simple extension of the color approaches classic but many dedicated tools.

We present here some tools and/or systems widely used in the processing of multispectral images. This chapter begins with a brief historical background, intended to provide a scenes as to how multispectral land began and what are its chief motivations. This is followed by a brief systems overview, fundamentals that control how information might be conveyed from the scenes surface to sensor devices and spectral data operating strategies. Next is presented information about the electromagnetic spectrum and the multispectral concept for economically sensing and analyzing

measurements. The chapter is concluded with examples of MSFA'S showing how data analysis may be carried out using pattern recognition concepts and illustrating one of the less intuitive aspects of the process of information extraction.

I.5.1. Historical back ground of multispectral systems: What is Multispectral Image?

Spectral imaging is a combination of imaging and spectroscopy, where a complete spectrum is collected at every location of an image plane. This powerful technique is sometimes called hyperspectral or multispectral imaging. Spectral imaging is not restricted to visible light, but works from ultraviolet to infrared.

According to the Oxford Dictionary, a spectrometer is an apparatus used for recording and measuring spectra, especially as a method of analysis. Spectroscopy captures the entire spectrum, light intensity as a function of wavelength. Spectral response curve, that gives spectral imaging the ability to discriminate specific chemicals and elements. The unique reflections and absorbances are the signature of the compound. Humans interest in spectroscopy dates far back, and we can notice in 1869 the use of a spectrohelioscope to view the solar corona by the astronomer P.J.C. Janssen [19]. The observation of the Earth from 'heaven' does not date from the launch of the first satellites. As early as 1840, F. Arago advocated the application of photography to the establishment of topographic maps. In 1858, Nadar, first aeronaut photographer, rises to 80 m in a balloon above the Petit-Bicêtre (near Paris) and realizes a view regarded as the first aerial history. Very quickly, such observations aroused the interest of all and in particular the military: from the First World War, the aircraft and photography gave a new dimension to recognition operations. For nearly a century, the chemical image of photography will be the support of multispectral systems (remote sensing). The first satellite was launched in 1957. Scientific and economic of multispectral systems applications will start to grow in the early 1970s.

A brief history of multispectral systems as a governmental activity, a commercial industry, and an academic field provides the student with a perspective on development of the technology and emergence of multispectral systems applications. Accounts of multispectral systems history generally begin in the 1800's, following the development of photography. Many of the early advancements of multispectral systems can be tied to military applications which continue to drive most of multispectral systems as remote sensing technology development even today. However, after World War II, the use of multispectral systems in science and infrastructure extended its reach into many areas of academia and civilian life. The recent revolution of geospatial technology and applications, linked to the explosion of computing and internet access, brings multispectral systems (remote sensing, cameras, sensors) technology and applications into the everyday lives of most people on the

planet. One could argue that there are very few aspects of life that are not touched in some way by this powerful and enabling way of viewing, understanding, and managing our world.

So far, man-made image sensors have not been able to acquire spectral information of incident radiation, but only an estimate of spatially-sampled and spectrally-weighted intensity values. Common linear and area image sensors are designed to sample a one- or two-dimensional optical image and convert it to an electronic image by means of optoelectronic conversion. As result, a scanning process, namely a series of exposures in the spectral and/or spatial domain, is very often necessary to acquire multiple images with different spectral domains.

As we continue on in this history paragraph, we must bear in mind that the early innovators of multispectral systems and photogrammetry did not have access to the sophisticated electronics and computing devices that we take for granted today! In fact, until very recently, it was often difficult to convince decision makers and managers that imagery could produce information as accurate (or even more accurate) than data collected on the ground. Today, almost everyone with a computer, a television, or a cell phone is familiar with the common products of color and digital mapping. The challenge today is not seeking acceptance for these technologies as much as it is making end users and decision makers aware of certain limitations and uncertainties inherent in these products. Whereas production of an image base map used to require an expert and very specialized equipment, today it can be done with in expensive software on a standard computer. It's quite easy to make a very accurate, useful product; it is just as easy to make a very inaccurate one.

Although, multispectral systems techniques had been in use for many years. The beginning of the space age greatly stimulated the development of multispectral systems technology both for space and for aircraft systems. The space age is generally acknowledged to have begun with the launch of sputnik by the Soviet Union in October 1957. This event had a fundamental effect on society in general. Among other things, it turned thinking to considerations of how satellites might be useful. In addition to the launching of several meteorology satellites, early research had already begun on land surface sensing by the time of NRC study. The central question being pursued was could aerospace technology be used to better manage the Earth's natural and man-made resources. The operation related to land remote sensing were expected to have the highest economic impact, because it is on land were the people live that the majority of the economic and resource activity takes place. Thus potential for the usefulness of multispectral systems through land remote sensing technology was thought to be very high.

Professional expertise and experience is still needed to ensure that multispectral systems and elevation models meet target specifications and that they can be used appropriately in a broad range of applications.

I.5.2. Brief systems overview

I.5.2.1. Fundamental Basis for multispectral systems

Generally, to begin the discussion for multispectral systems methods for gathering information remotely, consider the fundamental basis for the technology. Information theoretic principles provide that information is potentially available at altitude or at any region from the energy fields arising from the Earth's surface, and in particular from the spectral, spatial and temporal variations of those fields. Both the electromagnetic and the gravitational energy fields (Remote sensing) are of potential interest. To capture the information, one must measure the variation of those fields, and relate them to the information desired. The main purpose of multispectral imaging systems is the potential to classify the image using multispectral classification. This is a much faster method of image analysis than is possible by human interpretation. A conceptual view of multispectral systems is illustrated in figure 9 below. As the figure shows, the system may be divided into three basic parts: the scene, the sensor, and the processing system.

The scene is that part of the system that lies in front of the sensor pupil. It consists of the object (Earth's surface, image, etc.) and the intervening atmosphere. For systems in the optical portion of the spectrum that rely on solar illumination, the sun is included. This portion of the system is characterized by not being under human control, not during system design nor operation.

The sensor is that part of the system that collects the main body of the data to be used. It can be passive optical systems, active microwave (radar) and optical (lidar) systems. The sensor is ultimately the one that measures the information (CCD, or recorder).

The processing system is that part of the system over which the data analyst is able to exercise the most control and have the most choice. There are some limited circumstances where complete automation is both possible and desirable; this is not the case for most uses.

The sensor system is usually characterized by being under human control during the system design phase, but less so or not at all during system operation.

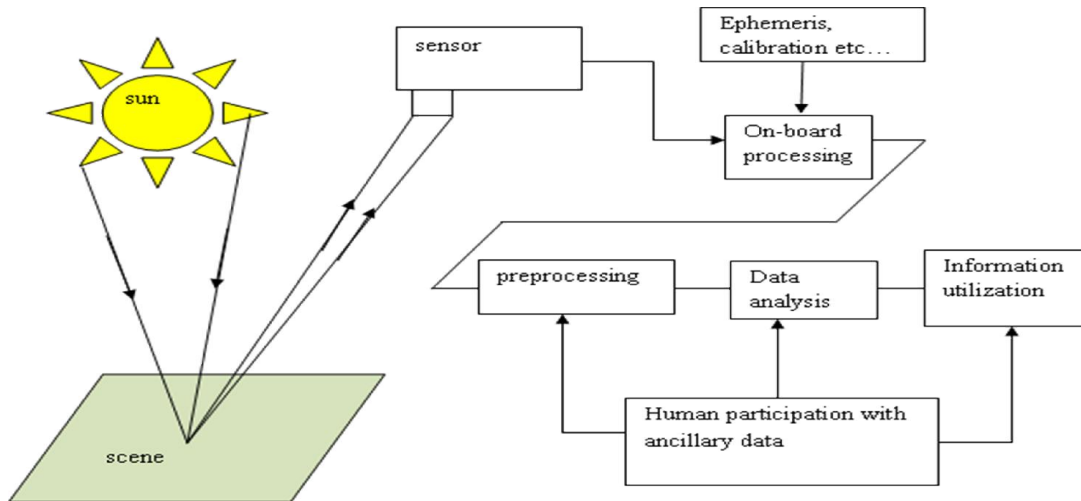


Figure 9: General conceptual view of multispectral systems.

I.5.2.2. Multispectral Systems View and Its Interdisciplinary Nature

This section presents and discusses the different multispectral acquisition systems in the first part. Then, it focuses specifically on MSFAs. First, a classification of all of these systems is presented in Figure 10. We distinguish MSI systems by their ability to produce snapshot images, to use a single sensor or not and by the technology used to split the light. Many imaging applications such as air-borne reconnaissance and tracking systems demand detection in both visible and infra-red spectrums. Typically, separate objectives must be used because no single objective lens system can accommodate multi-spectral images at both visible and infra-red wavelengths with adequate resolution. In particular, conventional refractive IR objectives disperse visible light, thereby, degrading image quality. Increasingly industry has been forced to less desirable reflective-type IR objectives.

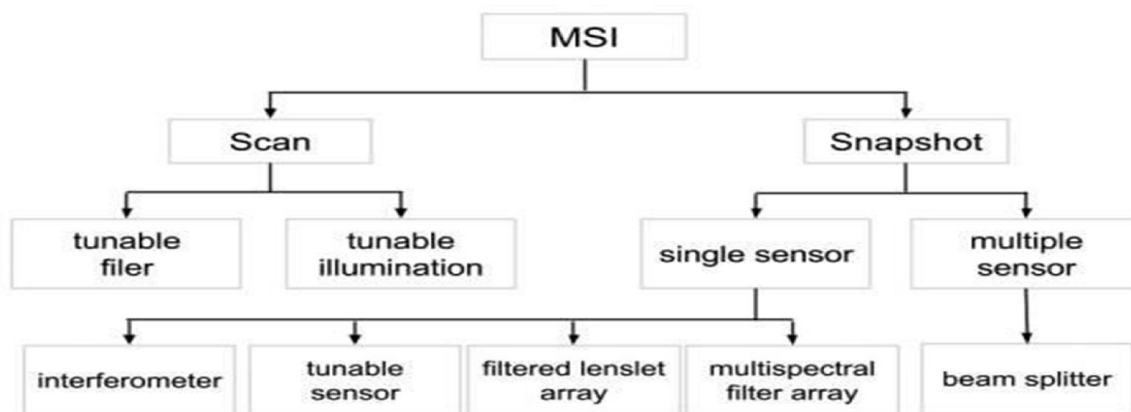


Figure 10: Multispectral system view and its interdisciplinary nature.

According to the literature, a multispectral image can be defined by an array of X rows, Y columns and P spectral channels. The multispectral values can be represented by several spectral components (c_p) at each spatial location (x, y). The image is such that it would have been acquired through multiple sensors with different spectral sensitivities. We can define the system by:

$$c_p(x, y) = \int I(x, y, \lambda) \Phi_p(\lambda) d\lambda \quad (1)$$

Where p indexes over channels, λ is the wavelength, $I(x, y, \lambda)$ is the spectrally-dependent irradiance at each location and $\Phi_p(\lambda)$ is the spectral sensitivity function for a given sensor response. Spectral imaging sensors sample the spectral irradiance $I(x, y, \lambda)$ of a scene and thus collect a three-dimensional (3-D) dataset typically called a data cube. Since data cubes are of a higher dimensionality than the two dimensional (2-D) detector arrays currently available, system designers must resort to either measuring time-sequential 2-D slices of the cube or simultaneously measuring all elements of the data cube by dividing it into multiple 2-D elements that can be recombined into a cube in postprocessing. These two techniques are described see (figure 10) as scanning and snapshot.

1.5.3. Spectral data operating strategies

The use of imaging spectrometers was rare before the arrival of 2-D CCD arrays in the 1980s, but steadily grew as detector technology advanced. Over the following 30 years, better optical designs, improved electronics, and advanced manufacturing have all contributed to improving performance by over an order of magnitude since that time. But the underlying optical technology has not really changed. Modified forms of the classic Czerny- Turner, Offner, and Michelson spectrometer layouts remain standard. Snapshot spectral imagers, on the other hand, use optical designs that differ greatly from these standard forms in order to provide a boost in light collection capacity by up to three orders of magnitude. In the discussion below, we provide what we believe is the first overview of snapshot spectral imaging implementations. After providing background and definitions of terms, we present a historical survey of the field and summarize each individual measurement technique.

The field of spectral imaging is plagued with inconsistent use of terminology, beginning with the field's name itself. One often finds spectral imaging, imaging spectrometry (or imaging spectroscopy), hyperspectral imaging, and multispectral imaging used almost interchangeably. Some authors make a distinction between systems with few versus many spectral bands (spectral imaging versus imaging spectrometry), or with contiguous versus spaced spectral bands (hyperspectral versus multispectral imaging). In the discussion below, we use spectral imaging to refer simply to any

measurement attempting to obtain an $I(x, y, \lambda)$ datacube of a scene, in which the spectral dimension is sampled by more than three elements. In addition, we use the term snapshot as a synonym for nonscanning, systems in which the entire dataset is obtained during a single detector integration period. Thus, while snapshot systems can often offer much higher light collection efficiency than equivalent scanning instruments, snapshot by itself does not mean high throughput if the system architecture includes spatial and/or spectral filters. When describing a scene as dynamic or static, rather than specifying the rate of change in absolute units for each case, we simply mean to say that a dynamic scene is one that shows significant spatial and/or spectral change during the measurement period of the instrument, whether that period is a microsecond or an hour.

When describing the various instrument architectures, pixel can be used to describe an element of the 2-D detector array or a single spatial location in the datacube (i.e., a vector describing the spectrum at that location). While some authors have tried introducing “spaxel” (spatial element) to describe the latter, this terminology has not caught on, so we simply use “pixel” when describing a spatial location whose spectrum is not of interest, and “point spectrum” when it is.

While many authors refer to the spectral elements of a datacube as bands, we use “channel” to refer to individual spectral elements and reserve the use of bands for broad spectral regions [such as the visible band or the longwave IR (LWIR) band]. It is useful to have a terminology for a single horizontal plane of the datacube (the image taken over a single spectral channel), so we refer to this as a “channel image”. A single element of the datacube is referred to as a “voxel” (volume element). When describing the dimensions of the datacube, we use N_x , N_y , and N_w as the number of sample elements along the $(x; y)$ spatial and λ spectral axes, respectively, so that the total number of data cube elements is given by $N_x N_y N_w$. We try to avoid describing the data cube in terms of resolution, since many authors use this to refer to the number of sampling elements, while others refer to it as the number of resolvable elements. At the Nyquist sampling rate, these two differ by a factor of two, but if one always refers to the number of samples, then the meaning is clear. One can also note that it is problematic to talk about a single value for resolution when discussing computational sensors, since the number of resolvable elements for these systems varies with the scene. Some scenes are easier to resolve than others.

Also, many authors make a distinction between spectrometer, spectrograph, and spectroscope, with distinctions varying among researchers. We make no distinction here and generally stick to using spectrometer, except where this clashes with a given field’s nomenclature.

I.5.4. Generalities about electromagnetic spectrum

I.5.4.1 Electromagnetic spectrum composition

The electromagnetic (EM) spectrum is the range of all types of EM radiation. Radiation is energy that travels and spreads out as it goes – the visible light that comes from a lamp in your house and the radio waves that come from a radio station are two types of electromagnetic radiation. The other types of EM radiation that make up the electromagnetic spectrum are microwaves, infrared light, ultraviolet light, X-rays and gamma-rays.

We know more about the electromagnetic spectrum than we may think. The image below shows where we might encounter each portion of the EM spectrum in our day-to-day life.

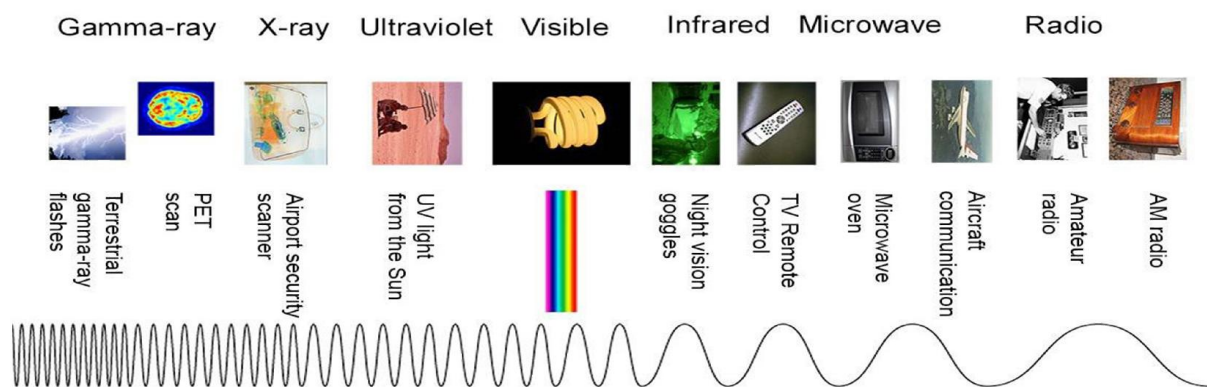


Figure 11: The electromagnetic spectrum shown with familiar sources

The electromagnetic spectrum from lowest energy/longest wavelength (at the right) to highest energy/shortest wavelength (at the left), (Credit: NASA's Imagine the Universe).

- **Radio:** Your radio captures radio waves emitted by radio stations, bringing your favorite tunes. Radio waves are also emitted by stars and gases in space.
- **Microwave:** Microwave radiation will cook your popcorn in just a few minutes, but is also used by astronomers to learn about the structure of nearby galaxies.
- **Infrared:** Night vision goggles pick up the infrared light emitted by our skin and objects with heat. In space, infrared light helps us map the dust between stars.
- **Visible:** Our eyes detect visible light. Fireflies, light bulbs, and stars all emit visible light.
- **Ultraviolet:** Ultraviolet radiations are emitted by the Sun and are the reason skin tans and burns. "Hot" objects in space emit UV radiation as well.
- **X-ray:** A dentist uses X-rays to image your teeth, and airport security uses them to see through your bag. Hot gases in the Universe also emit X-rays.
- **Gamma ray:** Doctors use gamma-ray imaging to see inside your body. The biggest gamma-ray generator of all is the Universe.

Electromagnetic radiation can be described in terms of a stream of mass-less particles, called photons, each traveling in a wave-like pattern at the speed of light. Each photon contains a certain amount of energy. The different types of radiation are defined by the amount of energy found in the photons. Radio waves have photons with low energies, microwave photons have a little more energy than radio waves, infrared photons have still more, then visible, ultraviolet, X-rays, and, the most energetic of all, gamma-rays.

I.5.4.2. Measuring electromagnetic radiation

Electromagnetic radiation can be expressed in terms of energy, wavelength, or frequency. Frequency is measured in cycles per second, or Hertz. Wavelength is measured in meters.

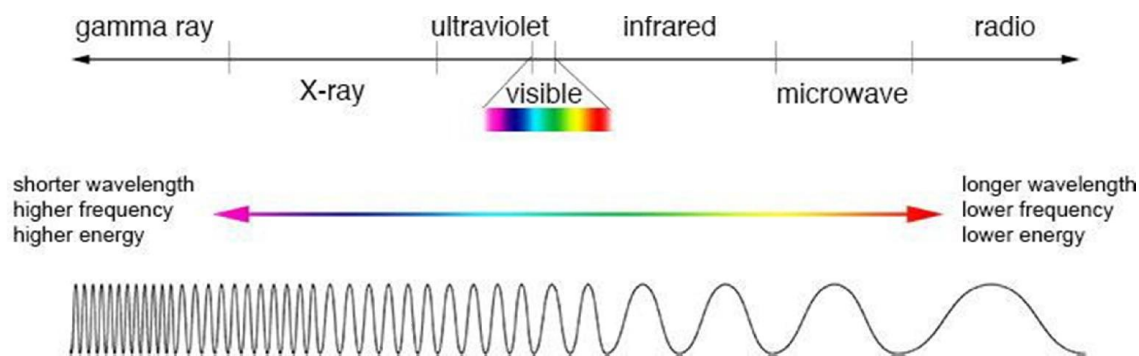


Figure 12: Illustration showing comparison between wavelength, frequency and energy

Energy is measured in electron volts. Each of these three quantities for describing EM radiation is related to each other in a precise mathematical way. But why have three ways of describing things.

Each, with a different set of physical units. Comparison of wavelength frequency and energy for the electromagnetic spectrum. The short answer is that scientists don't like to use numbers any bigger or smaller than they have to. It is much easier to say or write "two kilometers "than" two thousand meters. Generally, scientists use whatever units a readiest for the type of EM radiation they work with.

Astronomers who study radio waves tend to use wavelengths or frequencies. Most of the radio part of the EM spectrum falls in the range from about 1 cm to 1 km, which is 30 gigahertz (GHz) to 300 kilohertz (kHz) in frequencies. The radio is a very broad part of the EM spectrum.

Infrared and optical astronomers generally use wavelength. Infrared astronomers use microns (millionths of a meter) for wavelengths, so their part of the EM spectrum falls in the range of 1 to 100 microns. Optical astronomers use both angstroms (0.00000001 cm, or 10^{-8} cm) and nanometers (0.0000001cm, or 10^{-7} cm). Using nanometers, violet, blue, green, yellow, orange, and red light have wavelengths between 400 and 700 nanometers. (This range is just tiny part of the entire EM spectrum, so the light our eyes can see is just a little fraction of all the EM radiation around us.)

The wavelengths of ultraviolet, X-ray, and gamma-ray regions of the EM spectrum are very small. Instead of using wavelengths, astronomers that study these portions of the EM spectrum usually refer to these photons by their energies, measured in electron volts (eV). Ultraviolet radiation falls in the range from a few electron volts to about 100 eV. X-ray photons have energies in the range 100 eV to 100,000 eV (or 100 keV). Gamma-ray then is all the photons with energies greater than 100 keV.

I.6. Conclusion

The present chapter highlights various factors, state of art, implications, evolution, correlations and autocorrelations of nanoscience or nanotechnology with achievement of multispectral imaging processing. Nanotechnologies are based on knowledge and mastery of the infinitely small. They constitute a field research and multidisciplinary development involving the manufacture of new materials and new devices from tools or techniques for structuring matter at the Atomic, molecular and supramolecular level. The development of nanotechnology was initiated in the early 1980s with the invention of the Scanning Tunneling Microscope (STM) which was the first tool to allow the observation of objects at this scale. Nanotechnologies are cross-cutting nature and using disciplines such as physics, chemistry and biology while making it more permeable borders between traditional scientific and technological disciplines. The areas of application of nanotechnologies are mainly the information technology (increasing power and decreasing size of electronic components, increasing storage possibilities...), image processing, multispectral imaging, health (new medical diagnostic tools, targeted treatment of diseased cells...), new materials and energy (energy savings in transport, new cells photovoltaic...).

Nanoscience efforts will require that investigators learn each other's languages in some depth and form partnerships that integrate individual intellectual components into a cohesive team approach. The complexity of the new nanotechnologies and the scope of their clinical and commercial applications require direct and immediate access to diverse "in-house" expertise, which may dramatically impact the traditional academic paradigm for doing science with respect to conceiving new models for team organization and resource allocation. Among the expected breakthroughs are orders-of-magnitude increases in computer efficiency, human organ restoration using engineered tissue, "designer" materials created from directed assembly of atoms and molecules, and the emergence of entirely new phenomena in chemistry and physics. It explicitly seeks to create new opportunities for interdisciplinary work. It is balanced across five broad activities: fundamental research; grand challenges; centers and networks of excellence; research infrastructure; and, the ethical, legal, and social implications, including educational and workforce programs. Moreover, sober, technically competent research on the interactions between nanotechnology and society will

help mute speculative hype and dispel some of the unfounded fears that sometimes accompany dramatic advances in scientific understanding. The problematics of safety in the use of nanotechnology is a major issue but it does not concern in the same way the different application areas: the electronics sector is not affected, and the health sector is already highly regulated. On the other hand, problematics related to the safety of production and the use of nanoparticles and nanomaterials appear very clearly.

In summary to meet the needs and requirements applications as far color where looking for signatures spectral for example, the acquisition systems with more than three channels have been proposed. Such systems provide data richest that do the traditional cameras RGB, data generally known as image multispectral. Methods and appropriate means must then be implemented to exploit the best any information conveyed. Often, it is a question not a simple extension approaches color classic but many tools dedicated. We have presented here some tools widely used in the image processing multispectral. Strategies exploitation of spectral data, their characteristics and features are put forward and illustrated in chapter II, which highlights some of these applications, and an optimal method of reconstructing the spectral color response of Macbeth chart based on neural networks.

Chapter II: APPLICATIONS OF MULTISPECTRALRE CONSTRUCTION METHOD FOR THE OPTIMAL APPROXIMATION OF THE SPECTRAL RESPONSE OF A MULTICOMPONENT IMAGE

The images used have three components, which cover generally the visible spectrum of the visible light. In most cases, this type of image is sufficient to resolve the problems met. But there are specific cases in which more than three components are required. It is necessary to have a good command of the acquisition system in the following cases:

- when images are acquired outdoors. Thus aerial images under a clear sky are different from those taken under a cloudy sky.
- when the object of study presents spectral information beyond the visible (example of certain plants that emit in infrared).
- when it is necessary to acquire an image with greater precision so as to avoid any confusion between the different colour hues.
- when the Lab or Luv space is to be used, it is essential to know the composition of the reference white.
- Finally, when it is necessary to calibrate the acquisition system.

To bring some solutions of the above-mentioned problems, we propose to tackle in this chapter the complex question linked with the colour image acquisition system.

Two types of media are often used for storing images: the analogue medium, in the form of paper or magnetic tape, and the digital medium, which is the most recent form. The latter has known a lightening development with the arrival of large hard disks. This development has caused the multiplication of the image recording formats. Despite the diversity of methods, most of the formats code the pixel according to 3 components. When the formats are compressed, the quantity of information can be reduced while preserving a semantic content.

A colour image in digital format may come from two sources:

- by digital synthesis, the use of a 2D or 3D software package,
- a color image acquisition software package.

The second case is the one we are focussing on; we can mention the digital camera, digital camcorder, scanner, and finally the colour camera, which is the one we usually use for the acquisition of colour images.

In practice, four solutions are used in the making of colour digital images:

- the colour pixel is obtained by grouping 3 pixels and each photo element is sensitive to red, green and blue (method leading to reduce the spatial resolution).

- using a prism, the three RGB planes are then recomposed. This technique is known as "three-CCD", and has a good spatial resolution.
- Another less common technology consists in designing the semiconductor junction (multi-layer CMOS sensor) so as to be able to provide the three RGB data by the photo element. This technique is in full evolution.
- The last method, the most often used, consists in using a set of three filters with a black and white camera. Each filter is a band-pass filter focussed on the red, green and blue wavelengths.
- The fourth acquisition system is more delicate to set up. A complicated protocol has to be used to achieve the colour image. Among the component field we find several types of filters: manual or automatic piloting filters or liquid crystal filters.

This acquisition system using the set of filters (fourth point) can be extended for the assessment of the spectral response of a multi-component image. Although devices dedicated to multispectral exist, method point number 4 is used because it does not require enormous investments. To acquire a multispectral image, several different pass-band filters are necessary. The set of filters should cover the spectral field chosen, but there are a number of difficulties. In the scientific literature, solutions are proposed for the implementation of such a system. Depending on the applications, these solutions can be split into two parts:

The solutions used in the field of image synthesis. Most works explore the visible field. The multispectral approach is used here to alter lighting conditions. This allows far more relevant colour rendering. An image acquisition system is not necessary. A transformation is sought that will allow the passage from the colour space to the spectral space so as to make the effect of light play on the colour or the orientation of objects, etc.

The second method is that used by those who wish to work in fields other than the visible or simply by those who wish to improve the colorimetric quality so as to minimise the metamerism phenomenon.

In the first part of this chapter, we will describe the multispectral reconstruction methods using circular and exponential functions. These techniques are already used in the image synthesis field. Although, the field of application of those methods are dedicated to virtual reality, and try to translate a natural physical phenomenon.

In the second part, we will describe the method that is now used for the reconstruction of the spectral response of a multi-component image. This technique can be extended to the calibration of any other digitization system.

Finally, the last part will be dedicated to our spectral response reconstruction method based on neural networks. A comparative and objective analysis will lead us towards the best method

depending on the colour problem to be solved. The content of this chapter was the subject of an article which was published in the journal of Electronic Imagine [97].

II.1. reconstruction of the spectral response of an image using exponential functions

II.1.1. Overview of this method

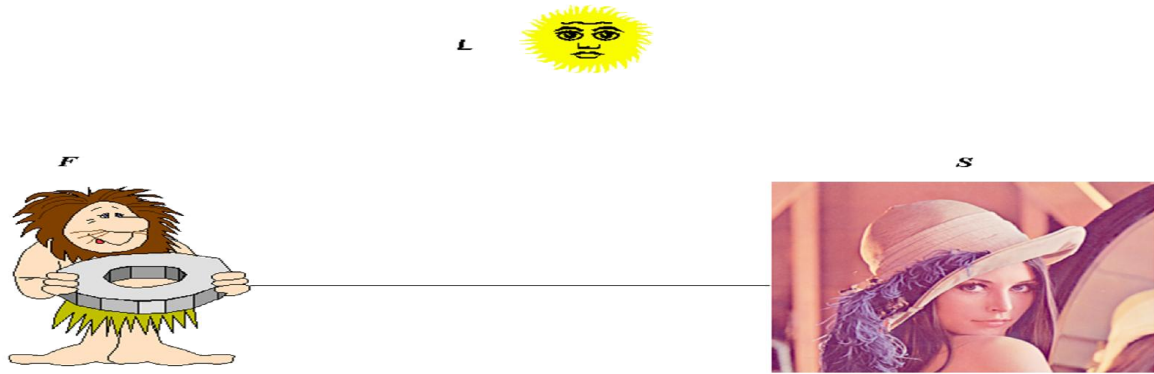


Figure 13: Block diagram of the physical phenomena allowing an object to be seen

The integral relation described in equation (1) is a simplification of the physical phenomena involved in the lighting of an object. This observation is an established fact since the light interference phenomena have been discovered but often neglected. The work carried out by Smits and Meyer [20] was a precursor in the field. They tried to simulate the interference phenomena so as to take them into account the colour rendering.

Figure 12 sums up quite well all the phenomena of perception or acquisition of objects. This block diagram is composed of the object we wish to see. This object is characterised by its spectral reflectance s_λ . It is illuminated by a light L_λ coming from a point source. Consider any observer; if a monochromatic light produces the illumination, all these parameters are constant. On the other hand, for a polychromatic light, these parameters will depend on the wavelength λ . This phenomenon has been formed in equation by the relation (2):

$$v_i = k \int_{\lambda_{\min}}^{\lambda_{\max}} L(\lambda) s(\lambda) f_i(\lambda) d\lambda \quad (2)$$

s is the spectral reflectance of the object observed and f_i represents one of the basic functions of the CIE ("Commission Internationale à l'Eclairage").

If \bar{x} , \bar{y} , \bar{z} are the basic functions, the CIE proposes an XYZ colorimetric base that connects the spectral response of the object with the observer response according to equations (3), (4), (5) :

$$X = k \int_{\lambda_{\min}}^{\lambda_{\max}} L(\lambda) s(\lambda) \bar{x}(\lambda) d\lambda \quad (3)$$

$$Y = k \int_{\lambda_{\min}}^{\lambda_{\max}} L(\lambda) s(\lambda) \bar{y}(\lambda) d\lambda \quad (4)$$

$$Z = k \int_{\lambda_{\min}}^{\lambda_{\max}} L(\lambda) s(\lambda) \bar{z}(\lambda) d\lambda \quad (5)$$

k is a constant, which is obtained by using a white reference.

In 1989, A.S. Glassner [21] proposed a solution that allows the transformation of a colour image into a spectral image. The aim of this work was to have a tool capable of generating a spectral correspondence from drawings. It forms the foundation of the spectral reconstruction of colour images.

We were trying to match a triad (R, G, B) with its spectral distribution. In order to succeed, we started with a transformation that allows the passage from the RGB space to the XYZ space of the CIE. Given L_λ and s_λ which respectively symbolise the illumination and the reflectance of the object to be visualised and depend on the wavelength. If we are only interested in the visible range, the colour v is defined by the fundamental relation (see equation 2).

The colour is defined in a three-dimensional space (3D). To obtain a bijective relation between the colour and its spectrum, three basic functions g_j are determined that could fully describe this spectrum. Consequently, any spectral density can then be described through the knowledge of these basic functions g_i and coordinates a_i so that (6):

$$s^* = \sum_{j=1}^3 a_j g_j \quad (6)$$

with : $s_\pi^* = s_\lambda \cdot L_\lambda$

By replacing s^* with its value in the equation (2), we achieve the relation (7):

$$v_i = k \int_{\lambda_{\min}}^{\lambda_{\max}} \sum_{j=1}^3 a_j g_j(\lambda) f_i(\lambda) d\lambda \quad (7)$$

If we render λ discrete, we arrive at the following relation (8):

$$v_i^* = k \sum_{\lambda_{\min}}^{\lambda_{\max}} \sum_{j=1}^3 a_j g_j(\lambda) f_i(\lambda) \Delta\lambda \quad (8)$$

A matrix version is given below (8):

$$\begin{pmatrix} v_1 \\ v_2 \\ v_3 \end{pmatrix} = \begin{bmatrix} h_{11} & h_{12} & h_{13} \\ h_{21} & h_{22} & h_{23} \\ h_{31} & h_{32} & h_{33} \end{bmatrix} \begin{pmatrix} a_1 \\ a_2 \\ a_3 \end{pmatrix} \quad (9)$$

$v = H.a$

with:

$$h_{ij} = k \sum_{\lambda_{\min}}^{\lambda_{\max}} g_j(\lambda) f_i(\lambda) \Delta\lambda \quad (10)$$

Where $\Delta\lambda$ represents the spectral resolution. It can be admitted that these basic functions meet two constraints:

- They should be linearly independent.
- They should be maximum for the red, the green and the blue wavelengths, which are defined by: $\lambda_r, \lambda_g, \lambda_b$.

We calculate the error committed in rebuilding the reference colour coming from Macbeth colour chart (called also "Macbeth ColorChecker") as well as the spectral relation by the relation (11, 12) below:

$$\Delta v = \frac{1}{3} \sum_i \sqrt{\frac{(v_i - v_i^*)^2}{v_i^2}} \quad \text{with } i=1,2,3 \quad (11)$$

$$\Delta s = \frac{1}{J} \sum_{i=1}^J |s_i - s_i^*| \quad (12)$$

J represents the total number of spectral data:

$$J \approx \frac{\lambda_{\max} - \lambda_{\min}}{\Delta\lambda} \quad (\text{the approached integer value}) \quad (13)$$

v_i is the initial colour and s its spectral reflectance. s^* is the reflectance calculated with the relation (6) and v_i^* is obtained by using the relation (8).

To have a basis for comparison, we used the Macbeth colour chart. The Macbeth colour chart is less rich than that of Munsell. It is composed of 24 colours numbered from 1 to 24. Each colour is characterised by its three components RGB and its spectral response. The spectral response of each colour was carried out by a spectroradiometer. These data are standard and more especially used for calibration.

Figure (13) shows the colour corresponding to number 11 in the Macbeth colour chart.



Figure 14 : Primary colour defined by :
R= 173 G=197 B=78 ; N° 11

II.1.2. Gaussian function

Although the introduction of circular functions has brought in certain richness at spectral resolution level, this representation is still far from the real color spectrum. The faithful reproduction of the color is difficult to reach. Maloney and al [22], Peercy [23], propose a solution using Gaussian functions. A comparison between circular and Gaussian function has done by Peercy and a deep analysis shows that these methods seem to be similar. Here, we propose to summarize the Gaussian method.

The main reason was to approximate the spectral reflectance by simulating the spectral response of the photosensitive sensors so as to make their model adhere to physical reality. Peercy proposes to use Gaussian functions as basic functions focussed on the primary colours RGB. This choice is not unimportant because the spectral responses of the red, green and blue filters used in cameras have allure close to the Gaussian and are focussed. The equations (14) characterise these basic functions.

$$\begin{cases} g_1 = e^{-\ln 2 \left(2 \frac{\lambda - \lambda_r}{\sigma_1} \right)^2} \\ g_2 = e^{-\ln 2 \left(2 \frac{\lambda - \lambda_g}{\sigma_2} \right)^2} \\ g_3 = e^{-\ln 2 \left(2 \frac{\lambda - \lambda_b}{\sigma_3} \right)^2} \end{cases} \quad (14)$$

The parameters σ_i allow the colour effect to be taken into account, whether or not it is saturated. They are calculated by the relation (15):

$$\begin{cases} \sigma_1 = \xi_{12} \omega_{\min} + (1 - \xi_{12}) \omega_{\max} \\ \sigma_2 = \xi_{23} \omega_{\min} + (1 - \xi_{23}) \omega_{\max} \\ \sigma_3 = \min(\sigma_1, \sigma_2) \end{cases} \quad (15)$$

$$\text{With: } \xi_{12} = \frac{|v_r - v_g|}{v_r + v_g} \quad \text{and: } \xi_{23} = \frac{|v_g - v_b|}{v_g + v_b}$$

The constants ω_{\min} and ω_{\max} (respectively 10 nm and 150 nm) are obtained empirically. v_r , v_g , v_b are red, green and blue primary colours. The figure 15 shows an example of spectral reconstruction starting from basic Gaussian functions. We used the colour number 11 in the Macbeth colour chart base defined in figure 14.

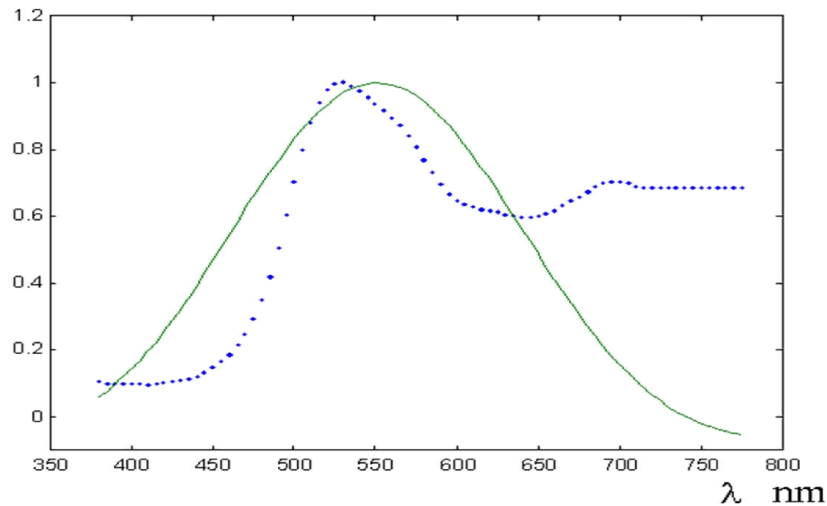


Figure 15: Spectral reconstruction using Gaussian functions

A dotted line shows the initial spectrum; A solid line shows the rebuilt spectrum ($R=173$, $G=187$, $B=78$, $N^{\circ} 11$, $\Delta s = 27.06\%$).

Results are better for the wave lengths near the blue and diverge toward the red. Although the global result is satisfactory, it can be seen that the error on the rebuilt spectrum remains high. These errors can be the cause of the metamerism phenomena met in colorimetry. That is why, in the rest of this paper, we shall propose works based on physical reality [97].

It is difficult to make a judgement on just one colour so, in the last part; we shall be presenting a study on a wider palette of colours.

II.3. setting up of an equation of the multi-component image acquisition system

II.3.1. Proposal

Compared to the previous method, the image is obtained by an electronic acquisition system. The acquisition system is composed of: the object to be observed, an illumination, a set of filters, the optics, the camera and finally a PC equipped with an acquisition card. All this is schematized in figure 16.

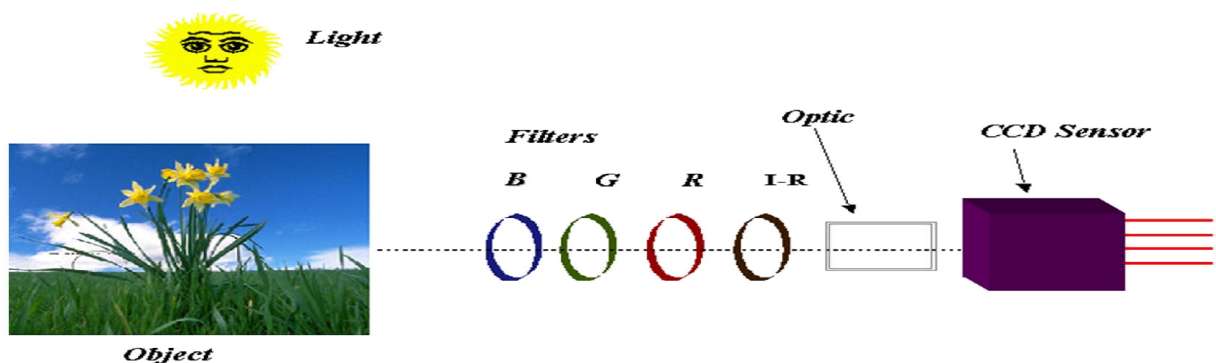


Figure 16: Multispectral image acquisition system

We consider that the acquisition system is characterized by optical properties Γ_λ , Φ_i , the spectral filter blocked on the wavelength of the primary i (or any other frequency of the studied spectrum) and photosensitive properties W_λ . The object is illuminated by a polychromatic light [24], [25], [26]. By generalizing the relation defined by the equation (2), we obtain the discrete relation (15):

$$v_i = k \sum_{\lambda_{\min}}^{\lambda_{\max}} L(\lambda) s(\lambda) \Gamma(\lambda) W \Phi_i(\lambda) \Delta \lambda \quad (16)$$

The number of filters may vary from 1 (monochrome image) to N . The larger N is the better is the spectral or colorimetric resolution. For a standard colour image $N=3$.

If we take $H=[L, \Gamma, W, \Phi, \dots]$ then the relation (16) leads to the matrix equation (17) for one colour:

$$v = H \cdot s \quad (17)$$

H is often unknown, which represents the acquisition system with which the illumination is associated. $V=[v_1, v_2, \dots, v_N]^T$ represents the colour vector for a space with N dimension. $s=[s_1, s_2, \dots, s_J]^T$ is the spectral density of the studied object. As the object is composed of just one colour, it is impossible to identify H . We generally use the Munsell colour atlas [24] or the Macbeth colour chart. For this work, we arbitrarily use the Macbeth colour chart. This chart is composed of 24 colours, we obtain a system of 24 equations with x unknowns (x is equal generally 80 for a best spectral resolution from 400 to 800 nm).

Equation (17), which is true for one objet, can be rewrite as equation (18) below for K objects (colour nuances):

$$V = H \cdot S \quad (18)$$

V is a matrix which has the dimension $N \times K$ (K = total number of different colours).

S is a matrix which has the dimension $J \times K$ (J defined by the relation 12), represents all the spectral reflectances of the chart.

H has the dimension $N \times J$.

The advantage of using the Macbeth colour chart is that we know the spectral response s of each colour in the data base; therefore, from the colour vectors v obtained via the acquisition system, we resolve our system to find H . Consequently, we can identify our acquisition system if the light is properly defined. This results in the relation (19):

$$H = V \cdot S^\circ \quad (19)$$

The matrix S° is the generalised inverse of the matrix S . If S is a square and non-singular then:

$$S^\circ = S^{-1}.$$

To find H in most cases, we shall analyse two types of approach: either through an approached inverse matrix or by a neural approach.

II.3.2. Identification of H via the matrix method

II.3.2.1. Pseudo-inverse matrix

Matrix S (composed of all the spectral responses of the colour contained in the Macbeth colour chart) is not simply non-singular. Such as defined, our system does not allow any solution or an infinity of solutions. Most of the methods proposed tend towards the optimal solution. Thus, the singular decomposition values are one of them.

We recall here that the notion of inverse applies to square matrices if the columns (rows) of this matrix are linearly independent. When it exists, this inverse is unique for a given matrix. Thus, Moore (1920) proposes to extend this notion of inverse to the matrices not included in the above category [27], [24]. Later, Penrose when resuming Moore's work proposed the generalized inverse matrix called Penrose inverse or pseudo-inverse matrix.

- **Decomposition in singular value or Penrose inverse**

For any matrix S, it accepts decomposition into a product of three matrices that are U, W and Σ (20)

$$S = U \cdot \Sigma \cdot W^T \quad (20)$$

U is the matrix of the Eigen vectors of the matrix $S \cdot S^T$

W is the matrix of the Eigen vectors of the matrix $S^T \cdot S$

$$\Sigma = \begin{bmatrix} \delta^{\frac{1}{2}} & O_1 \\ O_2 & O_3 \end{bmatrix} \quad \text{where } \delta \text{ is } K \times K \text{ diagonal matrix containing the nonzero Eigen values of the}$$

matrix $S S^T$ or matrix $S^T S$. O_1, O_2, O_3 are proper size zero matrices.

We can then calculate the pseudo-inverse S° matrix of matrix S (20):

$$S^\circ = W \cdot \Sigma^\circ \cdot U^T \quad (21)$$

The generalised inverse matrix of Σ is given (22):

$$\Sigma^\circ = \begin{bmatrix} \delta^{-\frac{1}{2}} & O_1^T \\ O_2^T & O_3 \end{bmatrix} \quad (22)$$

In fact this pseudo-inverse S° matrix is the best matrix of all the matrices approaching the inverse of S. The relation (22) is equivalent to the relation (23):

$$H = V \cdot W \cdot \Sigma^\circ \cdot U^T \quad (23)$$

From relationships (18) and (23) the spectral density of a colour x becomes (24):

$$s_x^* = H^\circ \cdot y_x \quad (24)$$

The error on the calculation of Δs is defined in the relation (12).

We employed this method to rebuild the whole system used to acquire data from the Macbeth colour chart. Figure 17 shows the appearance of the system represented by H . The three components RGB lead to three functions $H_i(\lambda)$. The curves H show the spectral response of the whole formed by the spectral acquisition system (spectroradiometer) and the illuminating light. Figure 18 gives the standardized spectral density and its approximation for the colour defined in figure 14.

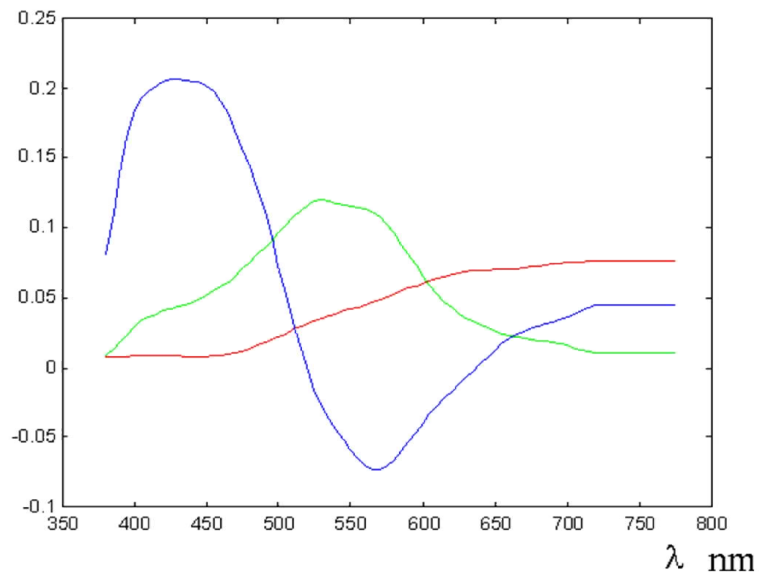


Figure 17: Modelling of the acquisition system and the illumination
(Each primary is represented by its colour)

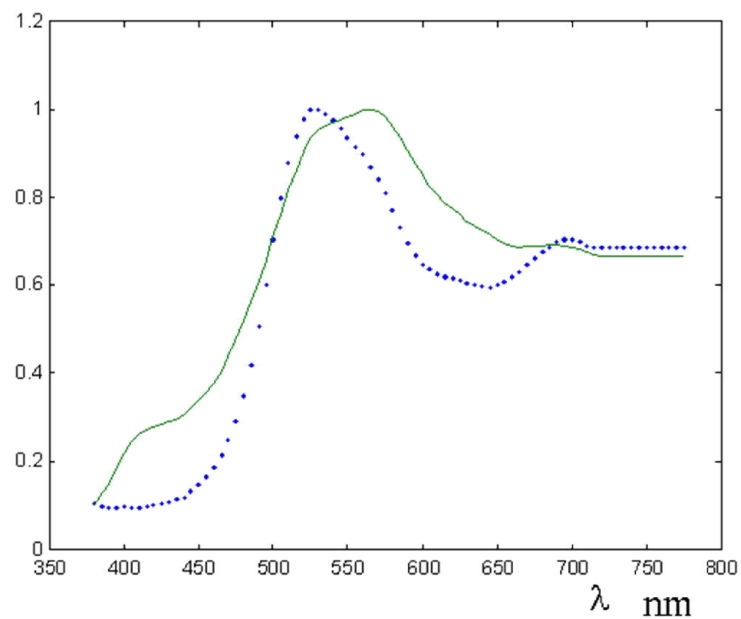


Figure 18: Spectral density rebuilt from the Penrose inverse.

The initial spectrum is a dotted line; the rebuilt spectrum is a solid line.

The Penrose inverse introduces noise that increases the difference between the real spectrum and the calculated spectrum. There are solutions to limit the noise. The first one consists in limiting the number of Eigen vectors. This increases the gap between the real spectrum and that sought for. The solution used here is based on the principle of linear hetero-associative memories. The hetero-associative memory is a neural network that uses the Penrose inverse to calculate the real response knowing the theoretical response. This method is very interesting since it allows the gap between the real spectrum and the rebuilt spectrum to be reduced. This method was preferred to the first solution that consists in drastically reducing the number of Eigen values. Nevertheless it does not converge towards a global minimum

II.3.2.2. Wiener inverse

The method we have just seen gives some good results, but it is noisy. Other methods are often used to reduce this noise. Research workers such as PG Herzog and his team [28] use the smooth inverse called of the Wiener inverse.

Let us note that S^L , the smooth inverse or the Wiener inverse of matrix S, S^L is calculated by the relation (25):

$$S^L = (M^{W2})^{-1} \cdot S^T \cdot (S \cdot (M^{W2})^{-1} \cdot S^T)^{-1} \quad (25)$$

with: $M^{W2} = M^{W1} + \epsilon I$

M^{W1} , a matrix introduced by Mancill [29] is equal to the relation (25) and this matrix is singular. So as to be able to inverse it, it is altered by ϵI where I is the identity matrix and ϵ a very small value.

$$M^{W1} = \begin{bmatrix} 1 & -2 & 1 & 0 & \dots & \dots & \dots & \dots & \dots \\ -2 & 5 & -4 & 1 & 0 & \dots & \dots & \dots & \dots \\ 1 & -4 & 6 & -4 & 1 & 0 & \dots & \dots & \dots \\ 0 & 1 & -4 & 6 & -4 & 1 & 0 & \dots & \dots \\ \dots & \vdots \\ \dots & \dots & 0 & 1 & -4 & 6 & -4 & 1 & 0 \\ \dots & \dots & \dots & 0 & 1 & -4 & 6 & -4 & 1 \\ \dots & \dots & \dots & \dots & 0 & 1 & -4 & 5 & -2 \\ \dots & \dots & \dots & \dots & \dots & 0 & 1 & -2 & 1 \end{bmatrix} \quad (26)$$

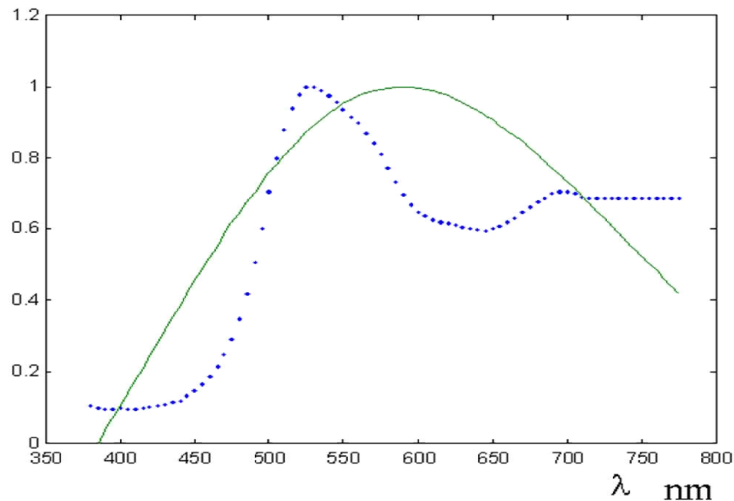


Figure 19: Spectral density rebuilt from the inverse of Wiener.

The initial spectrum is a dotted line; the rebuilt spectrum is a solid line (R=173 G=187 B=78; N° 11; $\Delta s = 17.93\%$).

For the chosen colour, the reconstruction error is higher seeing figure 19 than the pseudo-inverse method. But nevertheless, this difference is smaller than the methods using basic Gaussian functions.

It can be noted that the Wiener inverse method is suitable for the reconstruction of very monotonous spectra. Consequently, it is more suitable for colours situated on the achromatic axis.

II.4. approximation of the spectral response by neural learning

II.4.1. Introduction

All the solutions we have just seen are interesting. But there is still a difference between the initial spectrum and the calculated spectrum. Over recent years, very powerful methods have been developed in the field of pattern recognition. These methods, inspired by neuroscience, are highly efficient mathematical tools. Referring to previous works [30], we propose an extension to the identification of the system represented by matrix H. Indeed, the neural networks are powerful, parsimonious, and universal approximators, for the interpolation of digital data.

Many works exist in the scientific literature which treats the problem of the peripheral calibration (screen, scanner, etc.) [31], [32]. In this part of this article we describe some part of their methods.

Firstly, we will present a brief survey of the neural techniques.

II.4.2. Perceptron

A neural network [33], [34] is composed of elementary integrators or formal neurones and is a succession of two elementary mathematics operators:

- a summation of the input vector x_i or stimulus ($i=1 \dots I$ where I is the dimension of the input vector) weighted by coefficients called weights $w_{j,i}$. This sum evaluates the activation potential a_j of the neurone (26):

$$a_j = \sum_{i=0}^I w_{j,i} x_i \quad \text{With } x_0 = 1 \quad (27)$$

A non-linear thresholding operation, by activation function F which evaluates the output of the neurone.

This can be schematised by Figure (8) below:

$$o_k = F(a_k) \quad (28)$$

The association of several formal neurones will form a layer of neurones (Figure 21). The generalised form of the potential activation vector becomes $A_k = WX_k$ with $w_{j,i}$ the intensity of the connection between the i^{th} input vector and j^{th} neurone. The number of formal neurones varies from 1 to P .

$$\text{And } X_k = [x_0, x_1 \dots x_I]^T \quad W = \begin{bmatrix} w_{1,0} & w_{1,1} & \dots & w_{1,I} \\ w_{2,0} & w_{2,1} & \dots & w_{2,I} \\ \vdots & \vdots & \ddots & \vdots \\ w_{P,0} & w_{P,1} & \dots & w_{P,I} \end{bmatrix} \quad (29)$$

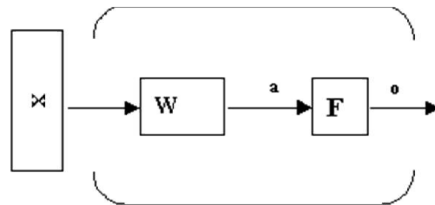


Figure 20: Example of a layer of formal neurone

N is the number of examples or observables.

II.4.3. Multi-layer perceptron

The most frequently used supervised learning network is the MLP (Multi-Layer Perceptron). It is used in a number of industrial applications [35] for signal and image processing such as form recognition [36].

The architecture of a MLP is composed of the assembly of formal neurones in two or more layers (figure 9).

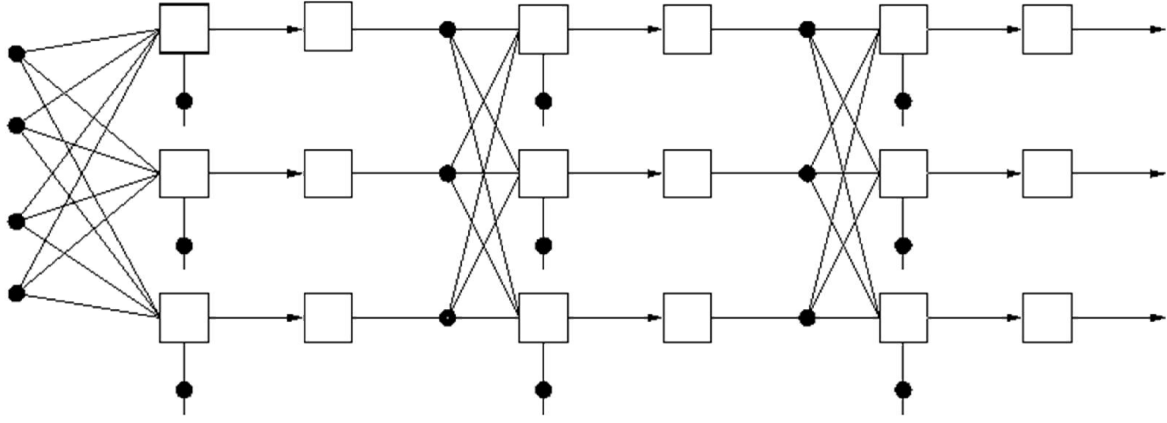


Figure 21: Multi-layer neural network (Multi Layer Perceptron)

The complexity of the network, i.e. the number of layers and the number of neurones per layer, will influence the performance of the interpolation [30].

The network response at output will be evaluated (30) for each example (subscripted k):

$$O_k = F_i(W_i \dots F_2(W_2(F_1(W_1 X_k)))) \quad (30)$$

with W_i connection matrix of layer i and F_i activation function of layer i , x_k the k^{th} observable.

II.4.4. Supervised learning

The supervised learning procedure will require:

A learning and test set that will form the data base with dimension N . The network parameters are calculated from the $N-N_0$ examples formed by the couples $\{\text{input } x_k, \text{ theoretical output } t_k\}$ of the learning basis. Many authors have underlined the importance of the learning basis which should be representative of each class and in sufficient number [37], [101].

The performances of the network are established from the N_0 examples of the test basis. The measurement of performance is established by the comparison between the mean square errors of the learning set and the mean square errors of the test set [101]. When the database is very small the validation of the network parameters uses the leave-one-out cross validation method [101], [102].

The definition of a cost function that measures the difference between the required theoretical output, and the output estimated by the network [38].

The most frequently used cost function is the total cost function (equation 31) of the mean squares or root mean square error, insensitive to its number N of examples [39].

$$J = \frac{1}{2N} \sum_{k=1}^N e_k^T e_k \quad \text{equivalent to} \quad J = \frac{1}{2N} \sum_{k=1}^N (t_k - o_k)^T (t_k - o_k) \quad (31)$$

Where e_k is the instant error vector at network output between the theoretical response vector

t_k and the calculated response vector o_k of the k^{th} stimulus.

The learning of a network is realised by iteration or epoch. An epoch therefore corresponds with the presentation of all the examples for learning.

A minimisation algorithm, of this cost function in relation to the weight W of the network. The choice of the optimisation method will mainly depend on the complexity of the network, i.e. the size of the connection matrices and input vector [40].

II.4.5. Gradient backpropagation algorithm

We cannot speak of supervised learning multi-layer networks without mentioning the most famous one: the MLP error backpropagation network. This algorithm [41], [42] is a generalisation of the Widrow-Hoff rule (or general delta rule) [34].

The correction of the network weights is defined by the following equation (figure 22, equation 32).

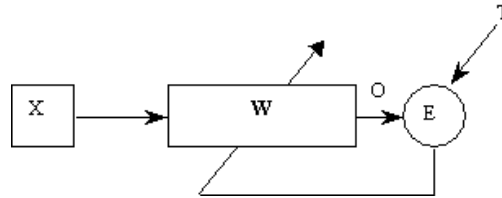


Figure 22: Skeleton diagram of the weight learning rule

$$W_{i+1} = W_i + \Delta W_i \quad \text{with} \quad \Delta W = \sum_{k=1}^N \Delta W_k \quad \text{and} \quad \Delta W_k = -\eta \nabla_w J_k \quad (32)$$

with (η) constant learning rate gradient.

Furthermore, this first order optimisation method does not guarantee the convergence to a minimum of the cost function. The best improvements for minimising the root mean square error for the networks of multi-layer neurones come from the classical optimisation methods for functions with several variables, in particular the digital optimisation methods with no second order constraints such as backpropagation by conjugated gradient, the quasi-Newton algorithm.

II.4.6. Second order optimization method

The second order optimisation methods are descending iterative of the gradient which consists in replacing the cost function with its quadratic approximation to the neighbourhood of the current point (33):

$$Q(S_k) = J_k(W_k) + g(W_k)^T S_k + \frac{1}{2} S_k^T G(W_k) S_k \quad (33)$$

$$\text{with: } \begin{cases} W_{k+1} - W_k = S_k \\ g(W_k) = \nabla_w J \quad ; \text{gradient} \\ G(W_k) = \nabla_w^2 J \quad ; \text{Hessian} \\ J(W_k) = \frac{e(W_k)^T e(W_k)}{2N} \end{cases} \quad (34)$$

e is the error vector, $e = t - o$. W designates the matrix of all the weights of the network layers and the variable k designates the k^{th} iteration.

II.4.7. Optimisation by the Levenberg-Marquardt method

Among the algorithms of the quasi-Newton family, the Levenberg-Marquardt (LM) method [43] is a standard for the optimisation of the root square mean error due to its quick convergence and robust qualities. It is based on the non-linear mean square techniques and the limited neighbourhood Gauss-Newton algorithm.

The main reason for choosing the Levenberg-Marquardt algorithm (LM) is the size of the Hessian matrix depending on the quantity of data in the learning basis, the lesser cost of the calculations and the quick guarantee of the convergence to a minimum (35):

$$\Delta W_k = -[G_k]^{-1} \nabla J_k \quad (35)$$

Among the limited neighbourhood methods, the Fletcher method [44], [45], [101] was chosen and developed. The Hessian is always positive definite, which ensures the convergence to a minimum of the solution.

II.4.8. Methodology

We used a two-layer network, which is largely sufficient, for the problem considered. The first layer (called hidden layer) is composed of a layer of 15 neurons. The number of points in our spectral response fixes the output layer. With a chosen resolution of $\Delta\lambda=5$ nm. With a chosen resolution of $\Delta\lambda$ nm, we actually have 81 points to rebuild. Consequently 81 neurons are necessary on the output layer. This can be schematized by Figure 24 below.

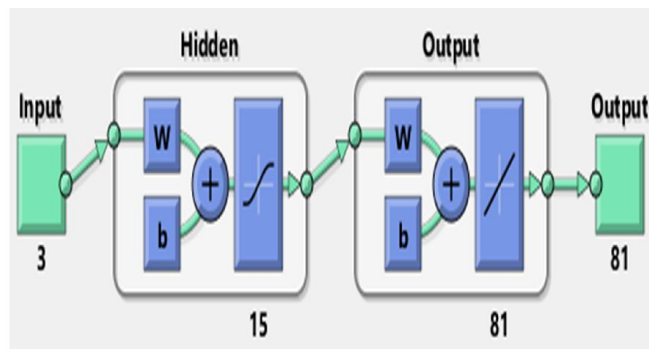


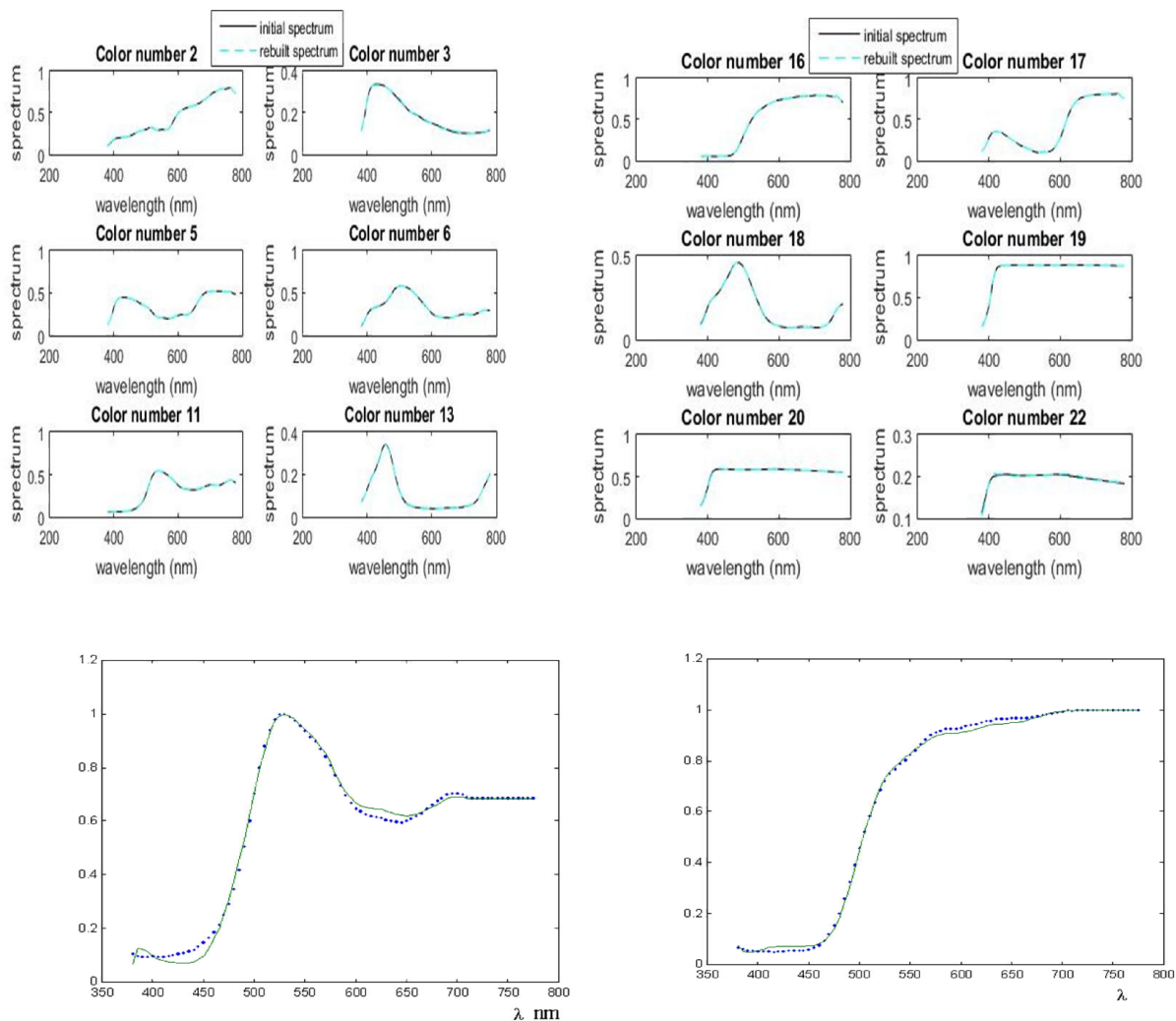
Figure 23: The MLP architecture of the proposed method

Moreover, due to the small database of example, the leave one out cross validation method has been applied [101].

For the learning, we have 24 samples to present to the network. Each input datum puts in a vector of 3 components.

The activation function of the input layer is the activation function of the input layer is a sigmoid function whereas we have a linear activation on the output layer.

After the learning stage, we keep the weight matrices W_1 , W_2 and the activation thresholds B_1 and B_2 . These 2 matrices and the 2 associated vectors represent the system to be identified. Therefore, starting from any triplet, whether or not it is in the Macbeth colour chart, we can deduce its spectral response. Considering the very few filters used, (here red, green and blue) it will always contain approximation errors. The solution we suggest is to increase the number of filters. This solution is conditioned by the place required for storing such an image. The results are shown in the figure 24.



(R=173 V=187 B=78 ; N° 11 ; $\Delta S = 1.5\%$)

N° 16 ; $\Delta S = 0.99\%$

Figure 24 : Rebuilt spectral density through learning of a two-layer network.

A dotted line shows the initial spectrum; A solid line shows the rebuilt spectrum.

For colour N° 11 chosen an N° 16 (N° 16 is one of the best approximation within the meaning of Least Mean Squares) in the Macbeth colour checker, the reconstruction is better as are the visual results. The method converges very quickly, after 20 iterations. The spectral reconstruction error is 1.5% and therefore supplants the Penrose inverse method, which until then, was the reference method. For sample n°16 this error is less than 1%..

II.5.global results analysis

II.5.1. Comparison of the various methods

For one colour, it is difficult to have a proper idea. So as to bring in a deep analysis of the various spectral image reconstruction methods, the comparison is done on the whole colour of the Macbeth colour chart.

In this analyse, table 1-a, table 1-b show the whole chart colour of our database and one can see for each colour the RGB components. Table 2-a, table 2-b, give different errors produced by each reconstruction method for each colour in the database and table 3 gives the mean error. Table 4-a to table 4-f gives for each colour the initial spectral reflectance in dotted line and the reconstruction spectral using a multi-layer LM (Levenberg-Marquardt) optimisation in solid line. Table 5 resumes the technical specification using to implement the neuronal learning. The new method we proposed is the best approximation, since it permits to perfectly rebuild the spectral reflectance.

The method uses the Penrose inverse remains acceptable, because it is very fast in time of calculation and permits fast verifications. In our application, to avoid the noise due to this inversion method we preferred a hetero-associative memory with learning rate constant.

For the whole samples which composed the basis for our study, the neural method gives the best results for all samples.

This comparative survey spread to the set of the 24 colours gives satisfaction on the proposed scientific approach. Neuronal aspect is not the only element to take in consideration since it has been done by various authors, but here we have brought a deep analyse in the method of optimisation and results show that LM approximation is well adapted in this case. Only 24 colours (in our database) is used to rebuild the spectral reflectance, for each colour, it produces the best spectral reconstruction. So the mean error is less than 0.6%. Thanks to the present power computer we can easily implement a 3 layers network neuronal configuration. The learning process takes less than 1 hour CPU times which seems reasonable. Although in the scientific literature no indication is given on the number of neurones for hidden layers, best results have been obtained with 6 neurones for the layer 1 and 20 neurones for the layer 2. The output layer is constructed with 80 neurones.

We observe that the Penrose inverse is second in relation to the other remaining methods. This survey shows that the 3rd position is attributed to the Gaussian basic function approach. Finally the

Wiener inverse is worst. This is in contradiction with the author who based their affirmation only on a few chosen colours [97].

The neuronal network method we proposed requires a long time of learning. In many applications the identification of the system acquisition or visualization is done once. Therefore the 3 layers are necessary for best identification. Otherwise 2 layers can be used in order to reduce the learning time.

Number	1	2	3	4	5	6	7	8	9	10	11	12
Red	129	205	112	103	146	120	223	91	203	107	173	233
Green	96	163	135	121	142	198	141	106	106	74	197	175
Blue	82	144	169	81	188	182	57	178	114	122	78	61
Colour												

Table 2.a: Colour representation of the first part of Macbeth colour chart

Number	13	14	15	16	17	18	19	20	21	22	23	24
Red	65	88	186	240	197	0	249	211	173	136	99	65
Green	75	160	70	208	103	146	248	209	172	135	99	65
Blue	163	87	73	47	162	178	248	210	173	135	99	65
Colour												

Table 2.b: Colour representation of the second part of Macbeth colour chart

Number	1	2	3	4	5	6	7	8	9	10	11	12
Δs Exponential function (%)	53.60	41.32	13.18	49.18	30.34	23.30	23.01	18.40	22.62	42.84	27.06	25.37
Δs Penrose inverse (%)	23.70	9.32	24.05	31.83	13.79	9.70	4.28	18.27	6.03	27.65	11.55	3.61
Δs Wiener inverse (%)	56.99	48.24	10.57	55.54	31.61	20.83	49.80	13.34	53.93	43.88	36.03	46.68
Δs LM Neural Network (%)	0.61	0.14	0.55	1.08	0.17	0.12	0.23	0.41	0.08	0.23	0.28	0.15

Table 3-a: Comparison between 5 spectral reconstruction methods applied to colour database

Number	13	14	15	16	17	18	19	20	21	22	23	24
Δs Exponential function (%)	23.61	31.09	20.75	26.08	22.32	32.57	19.80	19.91	18.89	18.82	20.00	19.34
Δs Penrose inverse (%)	18.77	15.01	6.87	1.89	4.02	27.24	15.26	17.02	17.90	17.92	17.28	14.18
Δs Wiener inverse (%)	12.77	39.42	58.42	41.99	47.18	17.47	45.79	44.11	42.82	42.03	42.54	40.47
Δs LM Neural Network (%)	0.35	0.39	0.16	0.09	0.22	0.14	0.06	0.12	0.47	0.54	0.85	5.79

Table 3.b: Comparison between 5 spectral reconstruction methods applied to colour database

Reconstruction method	Mean spectral estimation error
Δs Exponential function (%)	26,81
Δs Penrose inverse (%)	14,88
Δs Wiener inverse (%)	39,26
Δs LM Neural Network (%)	0.55

Table 4: Mean spectral reconstruction error for previous methods

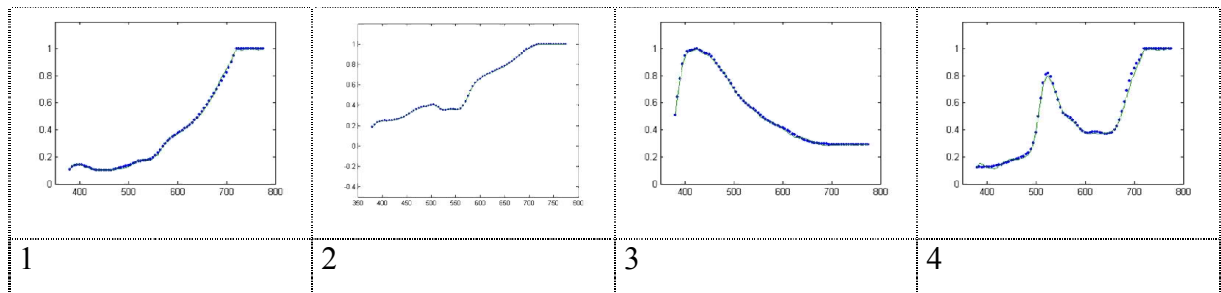


Table 5.a: Spectral reconstruction using the LM Neural Network

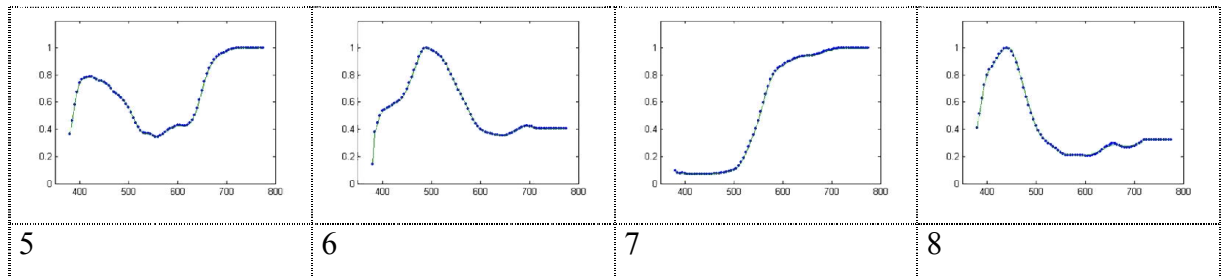


Table 5.b: Spectral reconstruction using the LM Neural Network

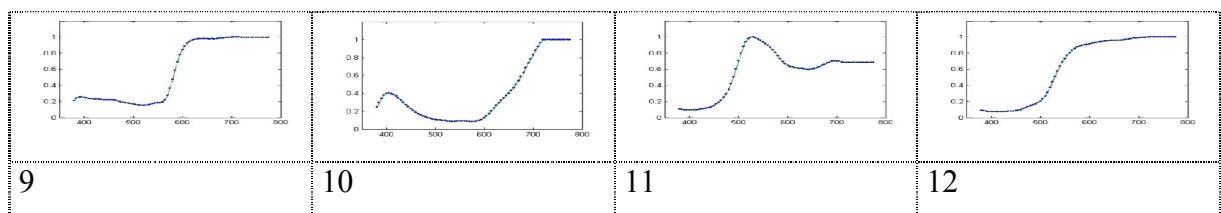


Table 5.c: Spectral reconstruction using the LM Neural Network

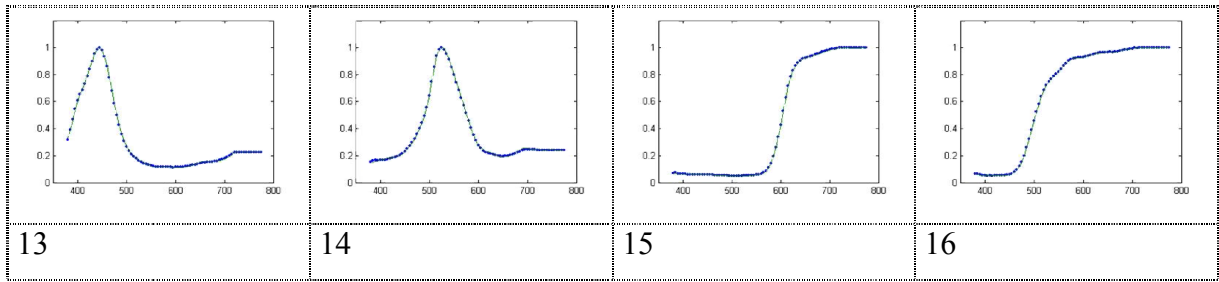


Table 5.d: Spectral reconstruction using the LM Neural Network

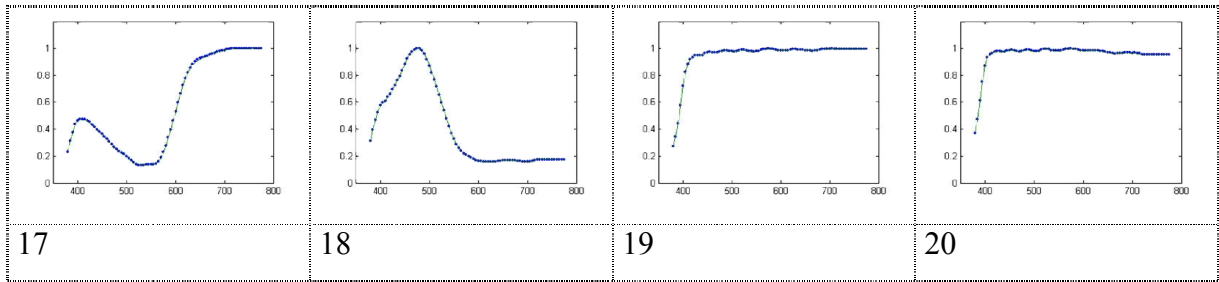


Table 5.e: Spectral reconstruction using the LM Neural Network

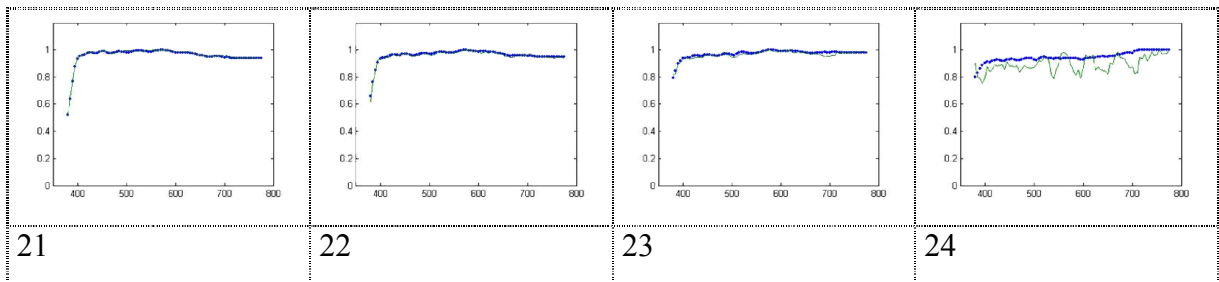


Table 5.f: Spectral reconstruction using the LM Neural Network

Number of layer neurone	Input	Layer 1	Layer 2	Output Layer	Mean error	Time (mn)	Iteration	Computer
2 layers	3	10	80	_80_	6.42	40	20	Intel, Bi-Processor , 1G Hz
3 layers	3	6	20	80	1.23	305	50	Intel, Bi-Processor, 1Go Hz
3 layers	3	6	20	80	0.55	57	70	Alfa, Quadri-Processor, 667 M Hz

Table 6: Neural implementation and computer specification

II.6. Conclusion

In the image processing chain, the acquisition of these images is a key element of the process. In this paper we have proposed a method based on the neural network so as to improve the spectral response estimation starting from a color triad (or set of filters).

This tool is precursor of experimental work allowing improving the quality of multi-component images and acquisition systems.

To the two existing models, we have added a third one:

The first model is used in the field of image synthesis. The image reconstruction method lies on a decomposition of the spectral reflectance in a space of circular functions or exponential functions. The aim of the work is to give the color image a rendering that has no connection with the physical reality of the colors. The reconstruction errors calculated from a choice of color ranges drawn from the Macbeth color chart show that the method using the circular functions is closer to reality. The approach used here is not different from the models below. Consequently, from the real spectral response of the object, we can make it undergo the required transformations.

The second model is used in the field of acquisition of multi-component images called multi-spectral image. The main concern in this field focuses on the colorimetric quality of the objects and on the reproducibility so as to avoid the effects of light and metamerism. This requires the power to model the acquisition system. Two methods were used in this field. One consisted in using the Penrose inverse (singular value method) and the other approach uses the Wiener inverse (or smooth inverse). Out of these two methods, the first one gives the best results on the rebuilt spectrum.

The third model we propose is to exploit the neural approaches that are subjacent in the second model. It is not the first time that the neural networks are used in the identification of systems. We can mention the frequent case in automatism. Considering the complexity of the system to be identified, we have opted for a multi-layer network with backpropagation error. To avoid getting trapped in local minima for the quadratic error, we use second order optimization methods. The Bayesian Regularization method was preferred since our data allowed it and furthermore it converges very quickly (43 seconds), after 243 iterations with 2 layers. The best result is obtained when we increase the learning time and it gives the lowest reconstruction error which is less than 0.09%.

In the context of this Optimization mentioned above, we have oriented our study towards an innovative field and in exploration: nanostructures, nanomaterials, and optical filters made from these nanomaterials thin films.

CHAPTER III: DESCRIPTION OF ANALYTICAL DEVICES AND THE METHODS FOR THE GROWTH AND SYNTHESIS OF NANOSTRUCTURED THIN FILMS

Beyond the presentation of nanotechnologies or nanosciences and a State of play on the situation of research and progress made in chapter one, we thought it was important for the continuation of our study, to go to the meeting of experimental methods and process of nanostructures realization in general and nanoscale thin layer filters in particular. The purpose of this chapter is to establish conditions of nanostructures samples realization, operating in transmittance under any impact. To describe development experimental devices and procedures for deposition of thin films on glass substrate. Nanostructured thin film (NSTF) is composed of thin layers of nanostructured objects such as nanoparticles, nanorods, and nanotubes, nanowires, and nanoporous networks. Fabrication and synthesis of those nanostructured thin films are essential for exploring their properties and creating advanced applications.

This chapter also points out the main problems faced by filing processes thin films, and the choice of the method of achieving desired nanostructures samples filters. How to work the material at the nanoscale? How are manufactured nano-objects? In this chapter, we will try to also provide satisfactory answers to these two fundamental questions. Subsequently we will exhibit the methods used for the characterization of thin films made.

III.1. How to work the matter on the nanometric scale?

The two current tools of nanotechnology are Scanning Tunneling Microscope (STM) and the Atomic Force Microscope (AFM). The scanning tunneling microscope is the essential tool in the history of the development of nanotechnologies because he was the first to allow the observation of objects at this scale.

The STM was invented in 1981 by researchers from IBM, Gerd Binnig and Heinrich Rohrer, who received the Nobel Prize in Physics for this invention in 1986. This microscope, uses a very thin metal tip that moves to a few nanometers to a conductor or semiconductor surface. The electric current flowing between the tip and the surface is called “tunneling current”. We can save by computer processing, depending on the position of the tip on the surface, variations in the electron current which crosses the space between the tips of the surface and infer the topology and some properties.

The AFM atomic force microscope is a derivative of the STM microscope, which can be used to visualize the topology of the surface of a sample not leading electricity, because it measures a force of contact instead of an electric current. The principle is based on interactions (ionic repulsive forces,

Van Der Waals forces, electrostatic forces, friction forces, magnetic forces...) between the atoms of the sample and a tip, Atomic ideally mounted on a cantilever. The tip scans surface to represent leading the cantilever deflection. A computer registers this movement and can reconstruct an image of the surface. To perform the manipulation on a nanometric scale, two approaches are used:

- the “top-down” approach;
- the “bottom-up approach.

III.2. Manufacturing processes of nano-objects and nanomaterials

Fabrication and synthesis of nanostructured thin films (NSTFs) are essential for exploring their properties and creating advanced applications. In general, the nanostructured thin film (NSTF) is defined as an assembly of a thin layer. It is different from individual or bundles of nanometer scale objects.

Nano-objects and nanomaterials manufactured and intended for industrial uses can be synthesized according to two different approaches. One differentiates between the "bottom-up" methods of the so-called "top-down" method.

- The "bottom-up" approach comes from research and nanoscience laboratories. It is to build nano-objects, and the nanomaterials atom by atom, molecule by molecule or aggregate by aggregate. These aggregates are then integrated into larger systems, in order to obtain the properties or the desired functions. The assembly or positioning of atoms, molecules or clusters occurs precisely, controlled and exponentially, thereby allowing the development of functional materials whose structure is completely controlled.
- The "top-down" approach comes from microelectronics. It is to reduce and more specifically to miniaturize systems by optimizing existing industrial technologies. This is the way that is followed by electronics for 30 years, causing a technological revolution which the computer is the most remarkable result. Devices or structures are thus gradually undersized or spanned up to nanoscale dimensions.

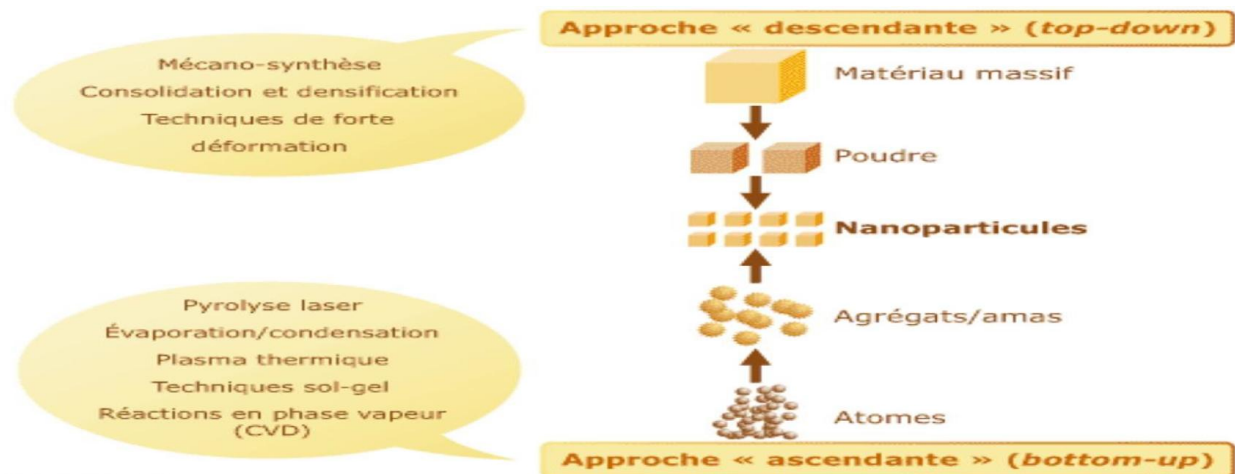


Figure 25: The two approaches of development of nano-objects and the nanostructures

Both approaches tend to converge in terms of range of size of objects. The 'Bottom-up' approach, nevertheless, seems richer in terms of type of material; diversity of architecture and nanoStatecontrolwhilethe"top-down"approachallowsobtaininglargerquantitiesofmaterial but the nano State control turns out to be trickier.

The current processes for the manufacture of nano-objects, nanostructured and nanomaterials are classified into three broad categories as shown in table 7.

Table 7: Methods of manufacturing nano-objects or nanostructured thin films

Methods of manufacturing nano-objects or nanostructured thin films		
Physical channel processes	Chemical channel processes	Mechanical channel processes
<ul style="list-style-type: none"> -the evaporation / condensation, - laser ablation - electric shock, - the flames of combustion, - laser pyrolysis, - the microwave, - ion or electron irradiation, - catalytic decomposition, - physical vapor deposition phase collectively known as PVD (Physical Vapor 	<ul style="list-style-type: none"> -The vapor phase reactions collectively known as CVD (Chemical Vapor Deposition), -The reactions in liquid medium: chemical coprecipitation, hydrolysis, etc. -The reactions in solid medium -supercritical fluids with chemical reaction, 	<ul style="list-style-type: none"> -The high energy milling or mechanosynthesis -Consolidation and densification -The strong deformation techniques: torque, friction, rolling, etc.

Deposition), etc.	-sol - gel techniques: sol - gel silica-based, metal alkoxide, etc.	
-------------------	---	--

The 'bottom-up' approach involves processes of developing chemical and physical while «top down» approach induces, mainly, the use of mechanical methods. The top-down approach refers to machine or carved macroscopic structures down to nanometer scales, whereas the bottom-up approach refers to controlled or directed self-assembly of atoms and molecules into nanostructures. The top-down approach usually consists of at least one lithography step or another size definition step and one etching step. Because there is a host of nanofabrication techniques and a variety of NSTF morphologies for each individual fabrication technique, we need to pay attention to a number of parameters listed in table 3 in order to further integrate the process with other nano or microfabrication processes for device fabrication.

Table 8: Process conditions and NSTF structures for NSTF fabrication or synthesis

Fabrication or Synthesis conditions	NSTF Structures
Approaches: bottom-up or top-down	Morphology: nanoparticles, nanorods, nanotubes, nanowires, nanoporous network, or mixture
Mechanism: physical or chemical process	Orientation: aligned or misaligned
Environment: gas or liquid phase	Regularity: ordered or disordered
Temperature: high or low	Layered structure: single layer or multilayer, single material or different materials
Other factors, such as pressure, carrier gas, plasma, substrate, etc.	

According to the general synthesis conditions, we discuss five major synthesis methods: the thermal vapor transport method, the catalyst-assisted fabrication method, the physical vapor deposition method and the chemical vapor deposition method

III.2.1. Physical channel processes

Physical Vapor Deposition Methods: PVD (Physical Vapor Deposition)

The physical Vapor Deposition method (PVD) usually represents a clean environment fabrication or synthesis because most NSTF fabrications are under vacuum. It is a conventional process for thin-film deposition. As shown in figure 26, the PVD process involves at least the following step:

- The material to be deposited is converted from condensed phase into vapor phase by physical means,
- The vapor transports from its source to the substrate, and
- The vapor condenses on the substrate to form the thin film.

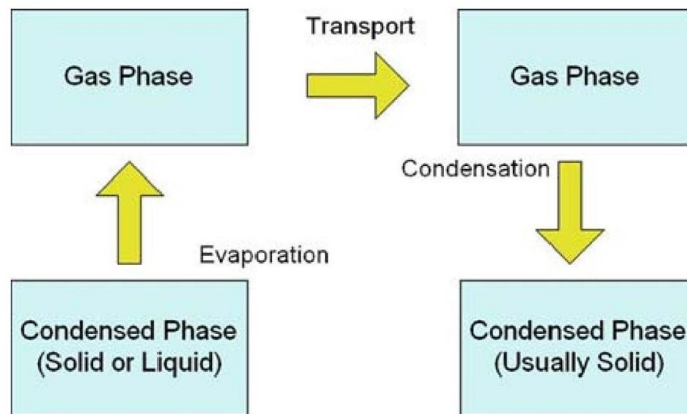


Figure 26: schematics illustrating the general steps and physical mechanism for a PVD process

There are several ways to resolve the key step for the PVD process, that is, to convert the solid phase into the gas phase. In general, we extract from a source material by a vapor phase heating ((a): thermal evaporation) or using a beam of electrons ((b): sputtering growth) or laser pyrolysis ((c): pulsed laser deposition). The steam is cooled by a neutral gas collisions and the material is collected as soon as possible on a cold wall. Another way of obtaining nano-powder is to use the action of microwave on the millimeter size powders. Finally, thin films with nanometer thickness can be achieved through PVD (Physical Vapor Deposition) or by epitaxial growth. The basic experimental setups for these three fabrication techniques are illustrated in figure 27.

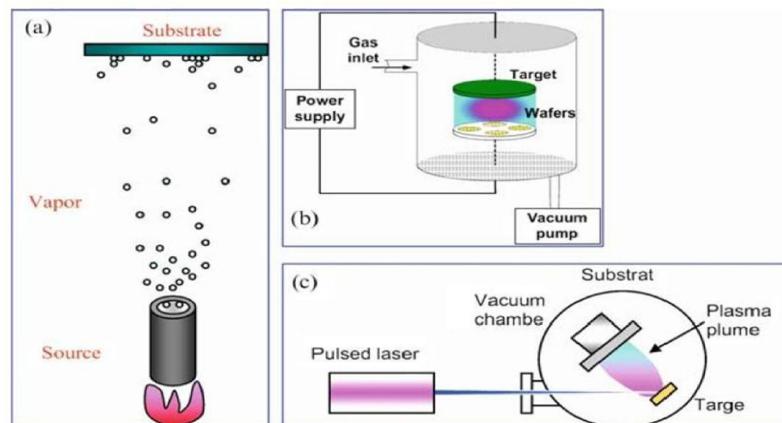


Figure 15: Three major processes for PVD: (a) thermal evaporation, (b) sputtering growth, and (c) pulsed laser deposition

In most cases, the PVD methods are used to produce island like ultrathin films especially with films of Au, Pt, or Ag for plasmonic applications [46], or to produce nanocluster films by co-deposition of metal and dielectrics [47]. Recently, a so-called glancing angle deposition (GLAD)

technique has been developed to fabricate aligned nanorods array structures, and the details of GLAD are discussed in the section, “Glancing Angle Deposition”.

III.2.2. Chemical channel processes

- **Chemical Vapor Deposition methods: CVD (Chemical Vapor Deposition)**

The chemical vapour deposition (CVD) technique is a widely used method for depositing thin film and nanostructures for a large variety of materials. In a typical CVD process, as shown in figure 16, reactant gases or precursors diluted in a carrier gas at room temperature enter the reaction chamber. The gas mixture is heated as it approaches the deposition surface. Depending on the process and operating conditions, the reactant gases may undergo homogeneous chemical reaction in the vapour phase before striking the surface, and the reactions result in a condensed phase thin film forming onto the substrates with the corresponding volatile reactants being pumped from the chamber. This technique is used for the development of certain nanomaterials such as semiconductor quantum, ceramic nanostructured materials, carbon nanotubes or diamond.

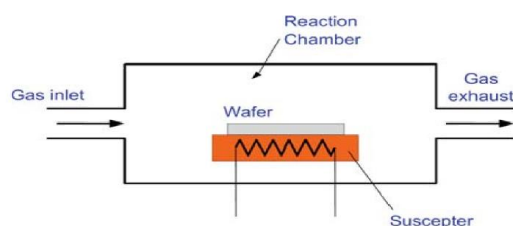


Figure 16: schematic of a conventional CVD reactor

CVD primarily is a thin film deposition technique. With the help of different catalysts, the CVD has become a major technique to make NSTFs over the past 20 years.

In chemical channel processes, there are other methods of synthesis of thin layers such as, "Liquid Phase Fabrication Techniques". In Liquid Phase Fabrication Techniques: precipitation of nanoparticles is obtained by a change in the conditions of the physico-chemical equilibrium. Liquid phase fabrication techniques refer to the synthesized NSTFs under a wet environment. These processes usually occur at relatively low temperatures but involve chemical reactions. This process consists of several other methods, such as:

- Sol-Gel Methods; the sol-gel process is a versatile solution process for making ceramic and glass NSTFs [48]. The sol - gel techniques are based on inorganic polymerization reactions from solutions of alkoxides or colloidal solutions. The sol-gel process involves the transition of a system from a liquid “sol” into a solid “gel” phase. The “sol” is made of solid particles with a diameter of few hundred nanometers that are suspended in the liquid phase. The particles condense into a new phase (gel) in which a solid macromolecule is immersed in a liquid phase (solvent) [49]. The main benefits of sol-gel processing are the high purity and uniform nanostructure achievable at low temperatures.

- Spin coating Methods; which is a simple but well-known technique to prepare thin films from liquid. One of the most important applications of spin coating is to cast photoresistant films for the lithography processes during microfabrication.

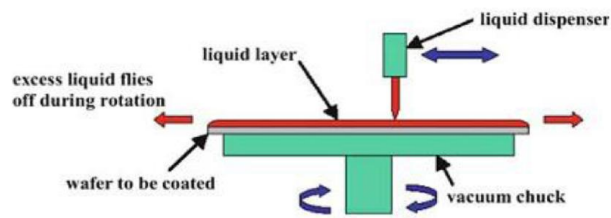


Figure 17: A schematic of spin coating process

III.2.3. Mechanical channel processes

The mechanosynthesis generally consists of grinding micrometric powders from several alloys to incorporate. This technique is suitable for the production of amount of materials which are expressed in kilograms, or tones, unlike other techniques. It has several other methods such as:

- The method of Consolidation and densification: the process involves two steps: a mechanical compaction operation and an operation of sintering, free or under load.
- The method of high deformation of crystalline material (metal, ceramic) causes a refinement of its structure until to obtain a grain size of several tens of nm. Different techniques can be used (by twisting, extrusion...). In particular, High Pressure Torsion (HPT) (figure 18 (a)), which has been recently established as the SPD (Severe Plastic Deformation) (figure 18 (b)) technique for the synthesis of nanostructured metals and alloys possessing sub-micron or even nanometer-sized grains. For many alloys HPT offers a powerful tool for microstructure design, texture formation, mechanically driven phase transformation, and the formation of metastable phases [50].

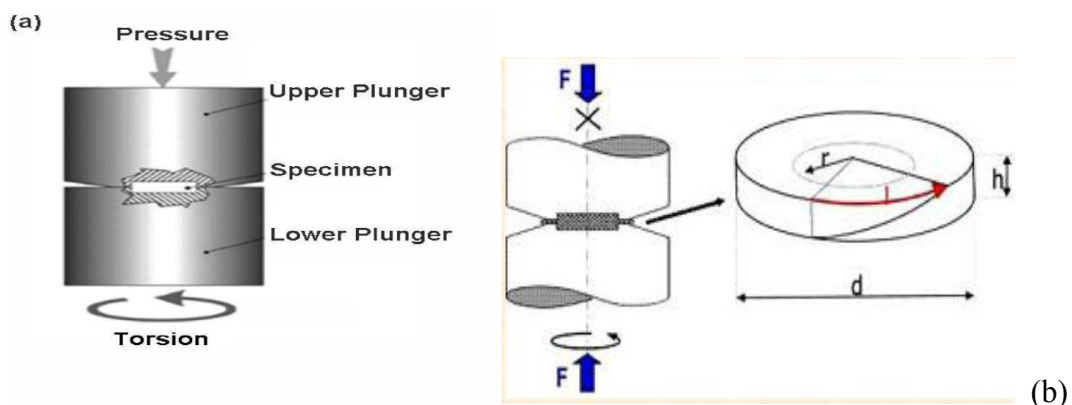


Figure 18: (a) Schematic diagram explaining the principle of high pressure torsion. (b) Schematic diagram explaining the principle of SPD.

III.2.4. Glancing Angle Deposition methods (GLAD)

The glancing angle deposition technique is the result of Template-based synthesis techniques. The GLAD is based on a simple modification of the deposition configuration of a physical vapour deposition system [51]. Any thin film physical vapour deposition system such as thermal evaporation, sputtering growth, or pulsed laser deposition, and the like, can be readily converted into a GLAD system. In fact, the Glad technique is the extension of the commonly used oblique angle deposition (OAD) which has been practiced for many years by the thin-film deposition community. Most of its fundamental growth mechanisms are similar to the oblique angle deposition although deviation may be expected. The GLAD principles are shown in figure 19.

A technique capable of fabricating ordered arrays of nanostructures is Glancing angle deposition, Glad. It was first reported in 1959 by Smith [51], and Knorr and Hoffman [52]. The technique utilizes a flow of atoms or molecules from gas phase impinging on a substrate from an oblique angle in a vacuum which results in a deposited film showing a columnar morphology. The angle of incidence controls the tilt of the columns and affects the degree of shadowing and thus the porosity of the film. If the substrate is rotated around the substrate normal, the morphology of the film is dramatically changed. A porous film consisting of isolated evenly spaced columns is demonstrated by [53] using this technique. The morphology of the columns can be controlled by changing the substrate angular frequency and substrate position relative to the evaporation source. Thin films containing complex structures can be grown by rotating the substrate in predefined cycles with a number of different frequencies. By utilizing GLAD it is furthermore possible to grow multi-component nanostructures by changing the source material during deposition. These structures are expected to enhance the complex functionality achieved by conventional single-component layers. Structures with accurate predetermined properties can thus be designed and grown utilizing GLAD. Finally the Glad technique has the following advantages in terms of fabricating NSTFs. First it can form vertical aligned nanorods arrays. Second, the size and density of the nanorods can be controlled by the vapour incident angle. Third, there is virtually no materials limit. As long as the material can be evaporated, it can form vertical aligned nanorods structures. Four, the shape, alignment, and orientation of the nanorods can be easily changed by programming the rotation procedures. Five, three-dimensional-shaped nanorods structures, multilayered nanostructures can be sculptured.

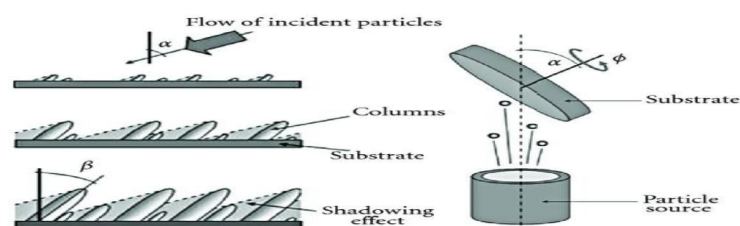


Figure 19: Schematic diagram explaining the principles of glancing angle deposition.

III.2.5. Lithography methods

Lithography is a technique to transfer patterns from either a master hard mask or a master soft mask (computer layout) to a photon or charged-particle sensitive polymer film (known as resist) coated on the substrate to which the pattern ought to be transferred. It is concerned with the study and application of fabricating nanometer-scale structures, meaning patterns with at least one lateral dimension between the size of an individual atom and approximately 100nm. This method is included in three large areas or approaches summarized in table 9.

Table 9: Capabilities and summary of various lithography methods

Approach	technique	Minimum feature	resolution	pattern
Optical approaches	photolithography	37 nm	90 nm	Parallel generation of arbitrary patterns
	Molding, embossing and printing	≈ 5 nm	30 nm	Parallel formation of arbitrary patterns
Charged-particle beam approaches	Scanning Beam lithography	5 nm	20 nm	Serial writing of arbitrary patterns
	Electron beam lithography	3 to 5 nm	Below 10 nm it is generally accepted to have the highest practical resolution capability	Periodic structures can be fabricated, 3D structures too
Other lithographic approaches	Scanning probe lithography	< 1 nm	1 nm	Serial positioning of atoms in arbitrary patterns

	Edge lithography	8 nm	16 nm	Parallel generation of noncrossing features
	Self-assembly	>1 nm	>1 nm	Parallel assembly or regular, repeating structures

Table 9 compares the current capabilities of lithography methods for patterning nanostructures. This table summarizes the current minimum feature size (minimum lateral dimension), the highest resolution (pitch), and the types of patterns that can be generated reproducibly by each technique.

III.2.5.1. Optical Approaches:

- **Photolithography**

Photolithography is the method of choice for manufacturing in the microelectronics industry, is the most commonly used technique/method for pattern transfer. The most advanced photolithographic systems project collimated light through a quartz plate that supports a patterned chromium coating. Typically, this quartz plate with chromium pattern is used as the master mask. The master mask has openings with linear dimensions approximately four times larger than the final image projected onto a photoresist located at the focal plane. A photosensitive resist is spun onto the substrate, to which the pattern needs to be transferred, depending on the optics used for light exposure; three types of optical lithography methods can be distinguished. These methods are contact printing, proximity printing, and projection printing. The light exposure dosage, including light intensity and exposure time, and the development conditions, including the purity of developer and development time, are key parameters that affect the photoresist vertical wall profile and hence the quality of pattern transfer. Thus, photolithography has a number of advantages over scanning beam lithography in nanofabrication, but the time and cost required to fabricate the photo-mask; typically patterned by scanning beam lithography can be a significant drawback. There is, however, one photolithographic method that can produce simple patterns (e.g., diffraction gratings) without using a photomask. This process is interferometric lithography, which involves the constructive and destructive interference of multiple laser beams at the surface of a photoresist. Immersion lithography is used to extend the resolution of optical lithography below 100 nm by replacing and is thermally

baked at elevated temperature before exposure to light at the appropriate wavelength. This projection lithography can expose an $\sim 8 \text{ cm}^2$ area of photoresist coated on a planar substrate; typically a semiconductor wafer in a few seconds. The quartz mask and the photoresist coated substrate are then loaded into the aligner to perform alignment and ultraviolet (UV) exposure. The exposed photoresist is immersed in solvents that dissolve the exposed (positive photoresist) or unexposed (negative photoresist) regions and provide patterned access to the surface of the substrate.

Depending on the optics used for light exposure, three types of optical lithography methods can be distinguished. These methods are contact printing, proximity printing, and projection printing. The light exposure dosage, including light intensity and exposure time, and the development conditions, including the purity of developer and development time, are key parameters that affect the photoresist vertical wall profile and hence the quality of pattern transfer. Thus, photolithography has a number of advantages over scanning beam lithography in nanofabrication, but the time and cost required to fabricate the photo-mask; typically patterned by scanning beam lithography can be a significant drawback. There is, however, one photolithographic method that can produce simple patterns (e.g., diffraction gratings) without using a photomask. This process is interferometric lithography, which involves the constructive and destructive interference of multiple laser beams at the surface of a photoresist. Immersion lithography is used to extend the resolution of optical lithography below 100 nm by replacing an air gap between the optics and the wafer with a liquid [54]. This results in dividing the diffraction limited feature size by the refractive index of the liquid which is chosen to be greater than one. The shorter the wavelength of the light used in immersion lithography the smaller is the minimum achievable feature size.

- **Molding, Embossing and printing**

A number of different procedures molding, embossing, and printing have been developed for patterning nanoscale structures. We divide molding and embossing techniques into two categories:

- moulding and embossing of nanostructures with a hard mould and;
- molding and embossing of nanostructures with a soft (elastomeric) mold. Molding involves curing a precursor (usually a monomer or a prepolymer) against a topographically patterned substrate. This method of pattern transfer is used by techniques such as step-and-flash imprint lithography (SFIL), replica molding (RM) with a soft mask, microtransfer molding (μTM), and micromolding in capillaries (MIMIC). Embossing (or imprinting) techniques transfer a mold with a structured topography into an initially flat polymer film. These techniques include nanoimprint lithography (NIL) and solvent-assisted micromolding (SAMIM).

The resolution of nanofabrication by molding and embossing is primarily limited by five factors:

- the practicality of fabricating masters with small features;
- the ability of a material to mold, with high fidelity, the features of the master;
- the distortion of features in the transferred pattern;
- the swelling of the master by the monomers used or the solvent used to dissolve polymers; and;
- the ability of the molded material to fill the mold completely, the tendency of the system to trap bubbles of gas, the kinetics of filling of the mold, the thickness of the residue or “scum” layer (if any) between isolated features, and related issues concerning the mold, substrate, and polymer as a system.

Molding and embossing are the most widely pursued and successful techniques for unconventional nanofabrication. There are a number of molding and embossing techniques that can pattern, in parallel, nanometer-scale features over large areas (i.e., entire silicon wafers). These techniques have been used to pattern functional structures for inorganic- and organic-based microelectronics and optics.

III.2.5.2. Charged-Particle-Beam Approaches:

Conventional charged-particle-beam lithographic techniques include electron-beam lithography (EBL) [55] and ion-beam lithography (IBL) [56].

- **Scanning Beam Lithography**

Scanning beam lithography is a slow process relative to photolithography. This serial technique can, however, generate high resolution features with arbitrary patterns. There are three main classes of scanning beam lithography:

- scanned laser beams with ~250-nm resolution are the least expensive;
- focused electron beams with sub-50-nm resolution (depending on tool settings and the choice of photoresist) are expensive to purchase and maintain; and;
- focused ion beam (FIB) systems with sub-50-nm resolution are primarily (and extensively) used in research. Typically, high-resolution photomasks are patterned using laser writers and electron-beam tools.

These techniques are capable of producing high-resolution micro and nano features.

- **Electronic Beam Lithography (EBL)**

EBL and IBL offer the advantages of maskless exposure, submicrometer resolution, and precise dimensional control. The overall processing steps of charged-particle-beam lithography are very similar to steps followed in photolithography. In order to overcome the diffraction limitation of light in photolithography, electron-beam lithography provides a high-resolution pattern transfer technique using high-energy electron beams (100 eV to 30 KeV) to expose electron-sensitive resist,

such as polymethyl methacrylate (PMMA). There are tradeoffs for high-resolution patterning with an electron or ion beam. Increasing the resolution requires decreasing the diameter of the particle beam, which decreases the beam current (charge-charge repulsion makes small, high-current beams unstable). These changes increase the time necessary to achieve the same imaging dose. The EBL resolution is not only affected by the focused beam spot size but also highly influenced by the scattering inside the resist and backscattering from the substrate. To compensate for the scattering and backscattering problems, proximity correction algorithms provided with EBL systems are typically utilized. One disadvantage EBL suffers is the low throughput. The direct writing time for large-area patterning is long and is not acceptable for some applications. Electron-beam projection lithography (EBPL) has been developing to overcome this limitation [57], [58], [59], [60]. In contrast to EBL, IBL uses a high-energy ion beam instead of an electron beam to expose the resist. Compared to any other lithographic approaches, IBL provides the smallest beam spot size, down to 8 nm, and the generated ion energy is lower with negligible scattering in resist and backscattering from the substrate. These features enable the best resolution among all lithographic techniques [56]. However, as with EBL, the long direct writing time and high vacuum exposure requirement became the major limitation for this charged-particle-beam technique.

III.2.5.3. Other Lithographic Approaches

- **Scanning Probe Lithography (SPL)**

Scanning probe lithography uses scanning tunnelling microscopes or atomic force microscopes to pattern nanometer scale features [61]. SPL provides a versatile set of tools for both manipulating and imaging the topography of a surface with atomic-scale resolution [62], [63]. When a voltage bias is applied between a sharp probe tip and the substrate, an electric field is generated around the tip and can be used to locally oxidize Si or to expose resist [34]. This local oxidation process is powerful because of its fine resolution (sub-50 nm) and the robust oxide etch mask that is created. In addition, the electrons generated around the tips have lower energy (<50 eV) compared to EBL (100 eV to 30 KeV). This lower energy prevents the scattering in the resist and backscattering from the substrate and thus enhances the resolution. At present, these tools seem well suited for applications in research but will require substantial development before they can be used for patterning large areas in manufacturing. The most important SPL techniques include scanning tunnelling microscopy (STM), atomic force microscopy (AFM), and near-field scanning optical microscopy (NSOM). This atomic scale manipulation is interesting scientifically but is not yet a practical technology. Scanning probe lithography is a versatile method for depositing clusters of atoms or molecules onto a surface in a well-defined pattern. One approach to deposit nanoparticles or molecules selectively onto a surface is dip-pen nanolithography (DPN) [63], [64], [65].

Scanning probe lithography can precisely position atoms on a surface and selectively deposit or remove regions of etch resist to pattern surfaces. These techniques may find applications in mask or device repair and information storage. Parallel approaches in SPL are being developed to overcome the serial limitations of standard SPL technologies. Surface diffusion of molecular inks and colloidal suspensions broadens the features patterned by SPL. It is also challenging to generate reproducible structures between scans because of variations in the surface topography of the substrate and differences in the shape of the tip (and variations in this shape with time and use).

- **Edge lithography**

We define edge lithography as either pattern transfer directed by the edge of a feature [66], [68], [69], [70] or the process of transforming a feature that is thin in the vertical direction into a feature that is thin in the lateral direction, [67], [72], [66], [71] General interest, as measured by volume of publications, in these two areas has increased markedly in the past few years. These methods are, currently, limited in the types of patterns they can form but can be used to pattern arrays of <100-nm structures in parallel for a range of materials.

Edge lithographic techniques are, currently, restricted to generating certain, limited types of line structures (e.g., noncrossing lines) in one step of fabrication. Crossed lines can sometimes be generated by stacking features. These techniques are still being developed as tools for research. Recent developments include “wiring-up” nanostructures to external magnetic or electric fields and directing the formation of parallel nanowires with applications in nanoelectronics and tuneable optical polarisers. We believe the formation of more complex nanostructures will result from a combination of edge lithography with other conventional and unconventional nanofabrication techniques.

- **Self-Assembly**

Self-assembly is defined as the spontaneous organization of two (or more) components into larger aggregates using covalent and/or noncovalent bonds [73]. We described a number of techniques for nanofabrication that use top-down approaches to patterning nanostructures. Self-assembly, a bottom-up approach to nanostructures or nanostructured materials is a second strategy for nanofabrication. This approach relies on cooperative interactions of small components that assemble spontaneously in a predefined way to produce a larger structure in two or three dimensions.

Self-assembly as a stand-alone method for nanofabrication is presently unable to produce structures with precise spatial positioning and arbitrary shapes with a low concentration of defects and functionality that can be achieved using conventional nanofabrication. It is also unable to generate the range of patterns required for even simple electronic functionality. Nontemplated self-assembly may represent a useful method of generating materials for information technology. For example, crystalline arrays of magnetic nanocrystals can store large amounts of information [74].

Neither nontemplated nor templated self-assembly strategies have yet demonstrated a route to the level of functionality necessary to contribute to microelectronics other than by generating materials or positioning objects with large ($\sim 100 \mu\text{m}$) dimensions [75], [76-77]. We are, however, optimistic that self-assembly will play a significant role in nanofabrication in the future, particularly when we consider the potential for fabrication in three dimensions, the opportunity for reversible [78] and reconfigurable self-assembly, [79] and the implication that self-assembled structures can undergo self-repair or self-replication [60]. The cell is the ultimate demonstration and inspiration for continuing work in nanometer-scale self-assembly and it is much more sophisticated than current microelectronic systems. A demonstration of the principle for *very* complex and functional forms of self-assembly thus already exists.

After this comparative study of different nanostructure realization, we chose to use EBL. Choice based on high resolution and availability of equipment in laboratory.

III.3. Equipment and devices used for characterization

The laboratory ImVla of the University of Burgundy account breast two experimental classrooms: the black room and the white room with many appliances and devices dedicated to image processing, and Optronics experiments. Among these measuring apparatus we used OL series 750 and Konica Minolta CS-2000 for the characterization of our samples nanostructures filters.

III.3.1. OL Series 750

The OL Series 750 is an extremely versatile spectroradiometer measurement system capable of performing a variety of highly accurate optical radiation measurements under computer control in the ultraviolet, visible and infrared. The modular approach of the OL Series 750 coupled with an extensive selection of accessories and powerful application software packages enables the user to tailor a turn-key system to their exact requirements as well as insure expandability in the future. Both single (OL 750S) and double (OL 750D) grating monochromator versions are available in the laboratory.

The basic system, along with an extensive selection of optional items and accessories, enables the OL Series 750 to measure over all or part of the entire 200 nm to 2000 nm wavelength range. An automated system can be configured for: Source Spectral Analysis, Detector Spectral Response, Diffuse Spectral Reflectance, Specular Spectral Reflectance, and Spectral Transmittance.



Figure 20: Overview of the characterization bench with OL Series 750 in white room

The basic OL Series 750 consists of: OL 750-M-S Single or 750-M-D Double Grating Monochromator, OL 750-C Controller, OL 750 General Operating Software. Optional Items consist of: Signal Detection Systems, Detectors, Windows Application Software, Calibration Standards, Exit Optics, Blocking Filters & Gratings, Precision Power Supplies, and Input Optics.

There are two type of monochromator: a single monochromator (OL 750-S) and a double monochromator (OL750-D). OL series 750 uses the latest technologies to report a spectroradiometric sharp and accurate measurement system. OL series 750 is one of the systems of the most versatile light of products in the industry. A modular approach coupled with a wide selection of accessories allows with proper configuration to access almost all the desired experimental requirements.

With its configurable gratings, blocking filters, and slits, the OL 750 can be set up across the full solar spectral output range. It also has a wide variety of accessories for measuring reflectance (diffuse and specular components) and therefore computing both internal and external quantum efficiencies (IQE, EQE). There is even a white bias accessory, a while light source that allows the cell's active area to be brought up to a typical operating energy level while measuring the spectral response simultaneously.

III.3.2. CS-2000 spectroradiometer

This polychromator type spectroradiometer has the ability to measure 100,000:1 contrasts. Featuring premiere top level capacity, the CS-2000 spectroradiometer is designed to pick-up incredibly low luminance ranges that reach 0.003 cd / m².

The CS-2000 records highly accurate measurements. This spectroradiometers signal processing technologies and optical design give you accurate measurements of luminance and chromaticity levels, including extremely low levels. The instrument calculates measurements in only 5 seconds. The spectroradiometer measurement calculation abilities free you of the need to work with electrical and mechanical noise elements.



Figure 21: illustration of CS-2000

CS-2000 is Instruments that push the extreme boundaries of practical application and cost performance to support design and development work. Designed to thoroughly eliminate mechanical and electrical noise factors, the CS-2000 makes quick measurements with good repeatability possible even at low luminance levels. The polarization error generated when using a reflection-type

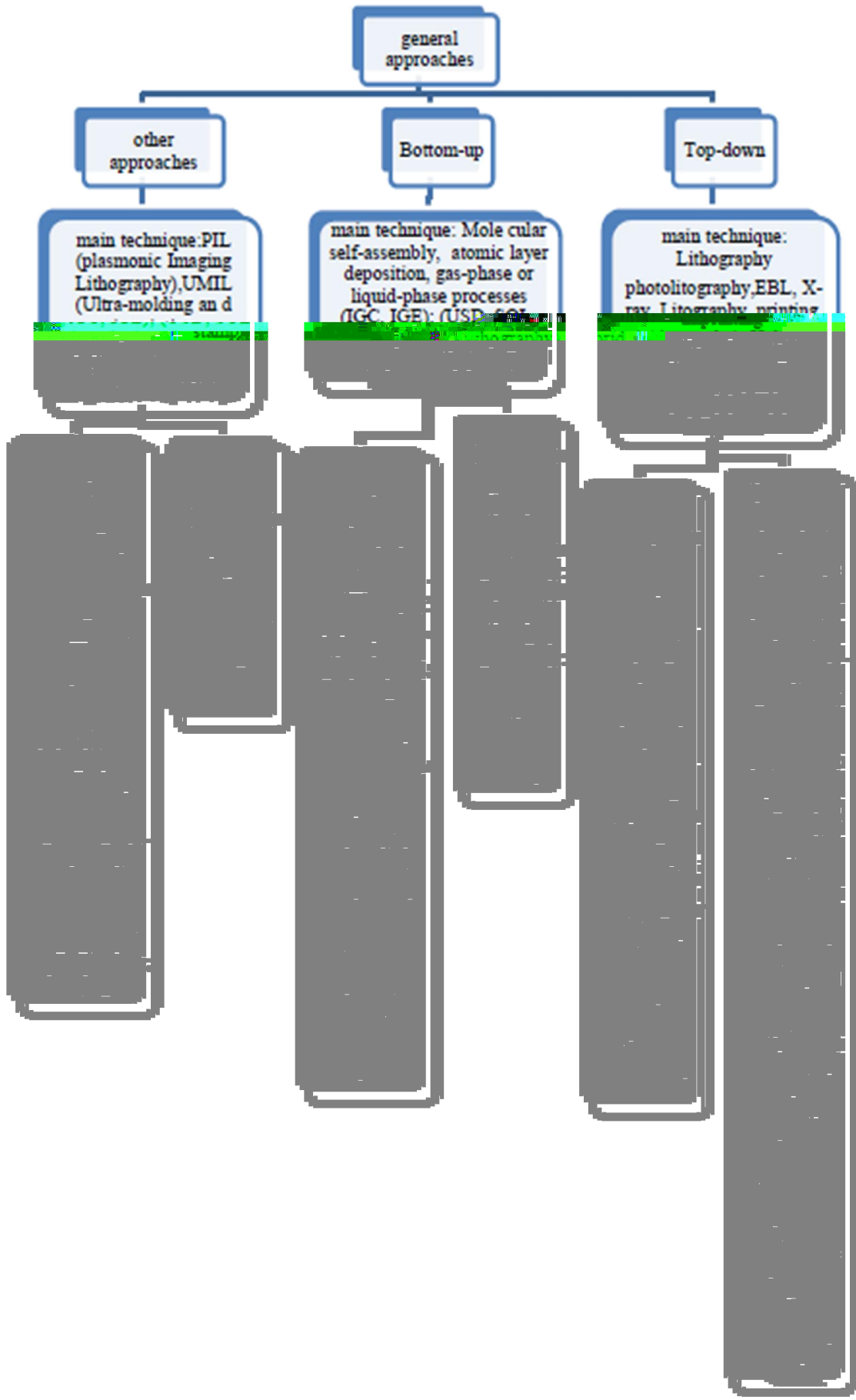
diffraction grating has been minimized to 2% (measuring angle: 1°). This ensures more stable measurements of display devices that use polarization, such as LCDs. It use in the spectral band of measurement ranging from 380 to 780 nm.

III.4. Choice of nanostructures manufacturing technique

In general it is very difficult to assemble devices on the atomic scale, as one as to position atoms on other atoms of comparable size and stickiness. Another view, put forth by Carlo Montemagno, [61] is that future nanosystems will be hybrids of silicon technology and biological molecular machines. Richard Smalley argued that mechanosynthesis are impossible due to the difficulties in mechanically manipulating individual molecules. Such bottom-up approaches should be capable of producing devices in parallel and be much cheaper than top-down methods, but could potentially be overwhelmed as the size and complexity of the desired assembly increases. Most useful structures require complex and thermodynamically unlikely arrangements of atoms. Nevertheless, there are many examples of self-assembly based on molecular recognition in biology, most notably Watson–Crick base pairing and enzyme-substrate interactions. The challenge for nanotechnology is whether these principles can be used to engineer new constructs in addition to natural ones.

Following the paragraphs 2 above the various manufacturing techniques of nanostructured filters, their advantages and disadvantages; we choose in this paragraph the proper method for the realization of our samples. In this context, a non-exhaustive of the preceding summary table methods is highlighted to allow us to make this choice for table 10. Considering the table, the choice of the method of manufacture of our samples is on lithography. This choice is justified by two main reasons: the availability at the ICB laboratory devices and equipment needed for achieving this goal, and the advantages inherent in the method. As we have pointed out in paragraph III.2 above, there are three general approaches to the synthesis of nanomaterials and the fabrication of nanostructures as shown in table 10. The current nanotechnology revolution is facing several major challengers: to manufacture nanodevices below 20nm, to fabricate complex nanostructures and to heterogeneously integrate multiple functionalities.

Table 10: general approaches of nanomaterials and nanostructures fabrication



III.5. Conclusion

In this chapter we presented several methods, manufactured techniques of nanostructured devices and analytical instruments that we used to characterize our samples.

A variety of methods of making one-dimensional structures for use in small scale devices and device elements and methods of making multilayered thin films or multifunction devices have been described. While a variety of ways of making nanostructures are available current technologies are largely insufficient to form high yield of nanostructures, particularly nanostructures having pre-selected properties (e.g. uniformity). In addition existing methods of assembling nanostructures in to create have been stated up, arrays (filter arrays) and functional devices are fairly cumbersome.

There are several important modern developments. Various techniques of nanolithography such as optical lithography that we chose to realize our filter sample, X-ray lithography, dip pen nanolithography, electron beam lithography or nanoimprint lithography were also presented as illustrated in table 5. Lithography is a top-down fabrication technique where a bulk material is reduced in size to nanoscale pattern. The top-down approach anticipates nanodevices that must be built piece by piece in stages, much as manufactured items are made. In contrast, bottom-up techniques build or grow larger structures atom by atom or molecule by molecule.

A motivation in nanoscience is to understand how materials behave when sample sizes are close to atomic dimensions. This leads to unique properties and the opportunity to use such nanostructured materials in novel applications and devices. Phenomena occurring on this length scale are of interest to physicists, chemists, biologists, electrical and mechanical engineers, and computer scientists, making research in nanotechnology a frontier activity in materials science. There are hopes for applying nanorobots in medicine, [62] [63] [64] but it may not be easy to do such a thing because of several drawbacks of such devices [65]. Nevertheless, progress on innovative materials and methodologies has been demonstrated with some patents granted about new nanomanufacturing devices for future commercial applications, which also progressively helps in the development towards nanorobots with the use of embedded nanobioelectronics concepts [66] [67].

Ultimately, by considering this contention, it appears at the outset necessary to present the instruments of experimental analyses of samples as shown in figures 20, 21 and tools for theoretical simulation, the adaptability and the implementation of experimental bench illustrated in figure 20. Some essential tools for the creation and implementation of certain devices or accessories necessary for the characterization of our samples were directed from a 3-d printer. These are devices bearing the samples to characterize on the experimental bench.

CHAPTER IV: THEORY, DESIGN AND SYNTHESIS OF THE NANOFILMS FILTER: METHODOLOGIES

When we reduce the size of an object; its surface decreases less rapidly in proportion than its volume. At the nanoscale, this means that the proportion of atoms at the surface increased compared to those in interior. The atoms on the surface then behave differently and are generally more reactive because they are not completely surrounded by atoms or molecules. This explains why nanometric objects often have chemical, electrical, magnetic properties, different from objects, of the same composition, but of macro size or microscopic (such as flexibility, resistance, adhesion or repulsion). The ability to understand, predict, and control the light interaction phenomena is essential for many industrial applications, such as aerodynamic shape design, oil recovery from an underground reservoir, or multiphase/multicomponent flows in furnaces, heat exchangers, and chemical reactors. This ability offers substantial economic benefits and contributes to human well-being. We take such things for granted and hardly ever think about the physics and mathematics behind them. The traditional approach to investigation of a physical process is based on observations, experiments, and measurements. The amount of information that can be obtained in this way is usually very limited and subject to measurement errors. Moreover, experiments are only possible when a small-scale model or the actual equipment has already been built. An experimental investigation may be very time-consuming, dangerous, prohibitively expensive, or impossible for another reason. Getting Started Alternatively, an analytical or computational study can be performed on the basis of a suitable mathematical model. As a rule, such a model consists of several differential and/or algebraic equations which make it possible to predict how the quantities of interest evolve and interact with one another. A drawback to this approach is the fact that complex physical phenomena give rise to complex mathematical equations that cannot be solved analytically, i.e., using paper and pencil.

The specific properties of nanomaterials are multiple: physical, magnetic, mechanical, optical, electrical, chemical, where still thermal. These specific properties result in particular from two characteristics of the nano-objects, consequences of their very small size: the virtual absence of defects and the strong relationship between surface and volume dimensions. Moreover, because of their very small size, nano-objects also have properties very different from solid materials in the domains of optical, electrical, magnetic, etc. The laws of classical physics do not explain their behaviour and we must then use the laws of quantum physics to understand and identify these new properties. Artificially engineered nanomaterials warrant innovative research to develop novel design methodologies by exploiting exotic electromagnetic (EM) physical behaviours that are not normally found to occur in nature [68], [69]. For instance, specific resonant elements can be used to generate extraordinary EM behaviours, thereby enabling the design of novel devices for enhancing resonant

behaviours. Most nanomaterials are based on split-ring resonators (SRRs) or similar geometries in order to achieve extraordinary physical behaviours for promising applications such as the fabrication of negative refractive materials [70], superlenses [71], smart power management applications [72], acoustic devices [73], and cloaking devices [74], [75]. More recently, increasing interest has been evinced in developing sensing platforms based on SRR arrays [76], [77]. For example, Hu Tao et al. have successfully developed label-free sensing platforms with SRR elements patterned on paper [78]. The EM resonant behaviours produced from SRR elements provide unique EM signatures in sensor applications. Because the resonant frequency ω_0 can be easily modulated by the device structure rather than composition, sensing parameters such as the resonant frequency ω_0 and bandwidth B can be easily controlled and achieved by properly designed subwavelength elements. Nonetheless, when compared with the performance of conventional plasmonics devices, SPR nanomaterial biosensors require further improvements in their sensing capability particularly in the light of their current low EM localization and low selectivity generated from the basic physics of nanomaterials.

In this chapter, because of all these properties and the reasons mentioned above, we use for two approaches for analyses, design and synthesis our device. The analytical approach which use RCW model and the experimental approach using the equipment available in the multispectral, ICB and IMVIA laboratories. The content of this chapter and the following was the subject of an article which was published in the journal of Electronic Image SPIE [96].

IV.1. analytical and computational method: Basic theory

In this part of the chapter, we developed as much as possible reported less cumbersome of the theoretical basis necessary for understanding and, to the characterization of properties coatings thin layers where multilayer.

IV.1.1. Maxwell's Equations and Plane Electromagnetic Waves

We begin our attack on thin-film problems by solving Maxwell's equations together with the appropriate material equations. In isotropic media, these are:

$$\text{curl}\vec{H}=\vec{\nabla}\wedge\vec{H}=\vec{j}+\partial\vec{D}/\partial t \quad (36)$$

$$\text{curl}\vec{E}=\vec{\nabla}\wedge\vec{E}=-\partial\vec{B}/\partial t \quad (37)$$

$$\text{div}\vec{D}=\vec{\nabla}\cdot\vec{D}=\rho \quad (38)$$

$$\text{div}\vec{B}=\vec{\nabla}\cdot\vec{B}=0 \quad (39)$$

$$\vec{j}=\sigma\vec{E} \quad (40)$$

$$\vec{D}=\epsilon\vec{E} \quad (41)$$

$$\vec{B}=\mu\vec{H} \quad (42)$$

where the symbols in bold are vector quantities. In anisotropic media, Equations 36 through 42

become much more complicated with σ , ϵ , and μ being tensor rather than scalar quantities. Anisotropic media are covered by Yeh [79] and Hodgkinson and Wu [80]. To the equations, we can add:

$$\epsilon = \epsilon_r \epsilon_0 \quad (43)$$

$$\mu = \mu_r \mu_0 \quad (44)$$

$$\epsilon_0 = 1/\mu_0 c^2 \quad (45)$$

where ϵ_0 and μ_0 are the permittivity and permeability of free space, respectively; ϵ_r and μ_r are the relative permittivity and permeability, respectively; and c is a constant that can be identified as the velocity of light in free space. ϵ_0 , μ_0 , and c are important constants, the values of which are given and known.

In the normal way, the parameters in Equations (43) through (45) do not depend on either \vec{E} or \vec{H} and so the phenomena are linear.

The following analysis is brief and incomplete. For a full, rigorous treatment of the electromagnetic field equations, the reader is referred to Born and Wolf [81].

First we assume an absence of space charge so that ρ is zero. This implies

$$\text{div} \vec{D} = \epsilon (\vec{\nabla} \cdot \vec{E}) = 0 \quad (46)$$

and solving for \vec{E}

$$\vec{\nabla} \wedge (\vec{\nabla} \wedge \vec{E}) = \vec{\nabla} (\vec{\nabla} \cdot \vec{E}) - \nabla^2 \vec{E} = -\mu \frac{\partial}{\partial t} (\vec{\nabla} \wedge \vec{H}) = -\mu \sigma \frac{\partial \vec{E}}{\partial t} - \mu \epsilon \frac{\partial^2 \vec{E}}{\partial t^2}$$

Equation (46) gives after reduction:

$$\nabla^2 \vec{E} = \epsilon \mu \frac{\partial^2 \vec{E}}{\partial t^2} + \mu \sigma \frac{\partial \vec{E}}{\partial t} \quad (47)$$

A similar expression holds for \vec{H}

First, we look for a solution of Equation (47) in the form of a linearly polarized plane harmonic wave (or plane polarized, a term meaning the same as linearly polarized), and we choose the complex form of this wave, the physical meaning being associated with either the real or the imaginary part of the expression.

$$\mathbf{E} = \mathbf{E} \exp[i\omega(t - z/v)] \quad (48)$$

represents such a wave propagating along the z -axis with velocity v . \mathbf{E} is the vector amplitude and ω is the angular frequency of this wave. Note that because we are dealing with linear phenomena, ω is invariant as the wave propagates through media with differing properties. The advantage of the complex form of the wave is that phase changes can be dealt with very readily by including them in complex amplitude. If we include a relative phase, φ , in Equation (48), then it becomes:

$$\mathbf{E} = \mathbf{E} \exp[i\omega(t - z/v + \varphi)] = \mathbf{E} \exp(i\varphi) \exp[i\omega(t - z/v)] \quad (49)$$

where $\mathbf{E} \exp(i\varphi)$ is the complex vector amplitude. The complex scalar amplitude is given by

$\mathcal{E}\exp(i\varphi)$ where $\mathcal{E} = |\mathcal{E}|$. Equation 2.15, which has phase φ relative to Equation (48), is simply Equation (48) with the amplitude replaced by the complex amplitude.

In Equation (48), we chose to place the time variable first and the spatial variable second in the argument of the exponential. This is a convention, because we could have chosen the alternative of the spatial variable first. However, to reverse the direction of the wave in this convention, we simply change the minus sign to a plus sign, reversing the spatial direction. In the alternative convention, it is tempting to reverse the wave again by changing the sign from minus to plus, but that would reverse the time axis, not the spatial direction. We shall stick to the convention in Equation (48) throughout this work. For Equation (48) to be a solution of Equation (47), it is necessary that:

$$\omega^2/v^2 = \omega^2\varepsilon\mu - i\omega\mu\sigma \quad (50)$$

In a vacuum we have $\sigma=0$ and $v=c$, so that from Equation (50) we have:

$$c^2 = 1/\varepsilon_0\mu_0 \quad (51)$$

which is identical to Equation (45). Multiplying Equation (50) by Equation (51) and dividing through by ω^2 , we obtain:

$$\frac{c^2}{v^2} = \frac{\varepsilon\mu}{\varepsilon_0\mu_0} - i \frac{\mu\sigma}{\omega\varepsilon_0\mu_0}$$

where c/v is clearly a dimensionless parameter of the medium, which we denote by N :

$$N^2 = \varepsilon_r\mu_r - i\mu_r\sigma/\omega\varepsilon_0 \quad (52)$$

This implies that N is of the form

$$N = c/v = n - ik \quad (53)$$

There are two possible values of N from Equation (52), but for physical reasons we choose that which gives a positive value of n . N is known as the complex refractive index, n is known as the real part of the refractive index (or often simply as the refractive index, because N is real in an ideal dielectric material), and k is known as the extinction coefficient.

If the various parameters are real (which is not always the case), then from Equation (52) we have:

$$n^2 - k^2 = \varepsilon_r\mu_r \quad (54)$$

$$2nk = \frac{\mu_r\sigma}{\omega\varepsilon_r} \quad (55)$$

Then Equation (48) can now be written

$$\mathbf{E} = \mathcal{E}\exp[i\omega t - (2\pi N/\lambda)z] \quad (56)$$

where we have introduced the wavelength in free space, $\lambda = (2\pi c/\omega)$.

Substituting $n - ik$ for N in Equation (56) gives

$$\mathbf{E} = \mathcal{E}\exp[-(2\pi k/\lambda)z]\exp[i\omega t - (2\pi n/\lambda)z] \quad (57)$$

and the significance of k emerges as being a measure of absorption in the medium. The distance

$\lambda/(2\pi k)$ is that in which the amplitude of the wave falls to $1/e$ of its original value. The way in which the power carried by the wave falls off will be considered shortly.

The change in phase produced by a traversal of distance z in the medium is the same as that produced by a distance nz in a vacuum. Because of this, nz is known as the optical distance, as distinct from the physical or geometrical distance. Generally, in thin-film optics, one is more interested in optical distances and optical thicknesses than in geometrical ones.

Since E is constant, Equation 2.18 represents a linearly polarized plane wave propagating along the z -axis. For a similar wave propagating in a direction given by direction coefficient (α, β, γ) , the expression becomes

$$E = \mathcal{E} \exp[i\omega t - (2\pi N/\lambda)(\alpha x + \beta y + \gamma z)] \quad (58)$$

This is the simplest type of wave in an absorbing medium. In an assembly of absorbing thin films, we shall see that we are occasionally forced to adopt a slightly more complicated expression for the wave.

There are some important relationships for this type of wave which can be derived from Maxwell's equations.

IV.1.2. Background

Developed in 1980's, by Dr. M. G. "Jim" Moharam, and Dr. Thomas K. Gaylord; Rigorous coupled Wave Analysis Method (RCWA) which Alternate Names for the Method is:

– Rigorous Coupled-Wave analysis – Fourier Modal Method – Transfer Matrix Method with a plane wave basis.

A commonly-employed modelling approach for grating diffraction is known as the rigorous coupled wave analysis (RCWA). The RCWA is based on retaining a finite number of diffraction orders in the calculation, thereby allowing Maxwell's equations for the grating diffraction problem to be expressed as a system of matrix equations. The RCWA is well known and is described in many references, including Moharam et al [82], [83]. Since it is usually necessary to run a large number of cases to fit a modelled grating response to a measured grating response, methods of reducing RCWA calculation time are of special interest, and many approaches for reducing RCWA calculation time have been described. For example, in the second Moharam paper cited above, a layer by layer solution approach is described, where the system of matrix equations is basically solved one interface at a time, as opposed to solving for all interfaces simultaneously. This layer by layer approach can dramatically reduce the computation time compared to the simultaneous approach.

In this Moharam paper, it is also noted that in cases where it is not necessary to calculate both reflectance (R) and transmittance (T), the calculations can be modified to provide only the desired quantity and to significantly reduce computation time. This is in contrast to the more familiar case of

R and T calculations relating to planar multi-layer stacks, where calculating only R or only T is not significantly faster than calculating both **R** and **T**.

Other approaches have also been considered for reducing RCWA calculation time. In some cases see figure (22), it is possible to exploit symmetry to reduce calculation time.

Although the various known approaches for reducing RCWA calculation time can be more or less effective, depending on circumstances see figure (23), there remains an ongoing need to further reduce RCWA calculation time.

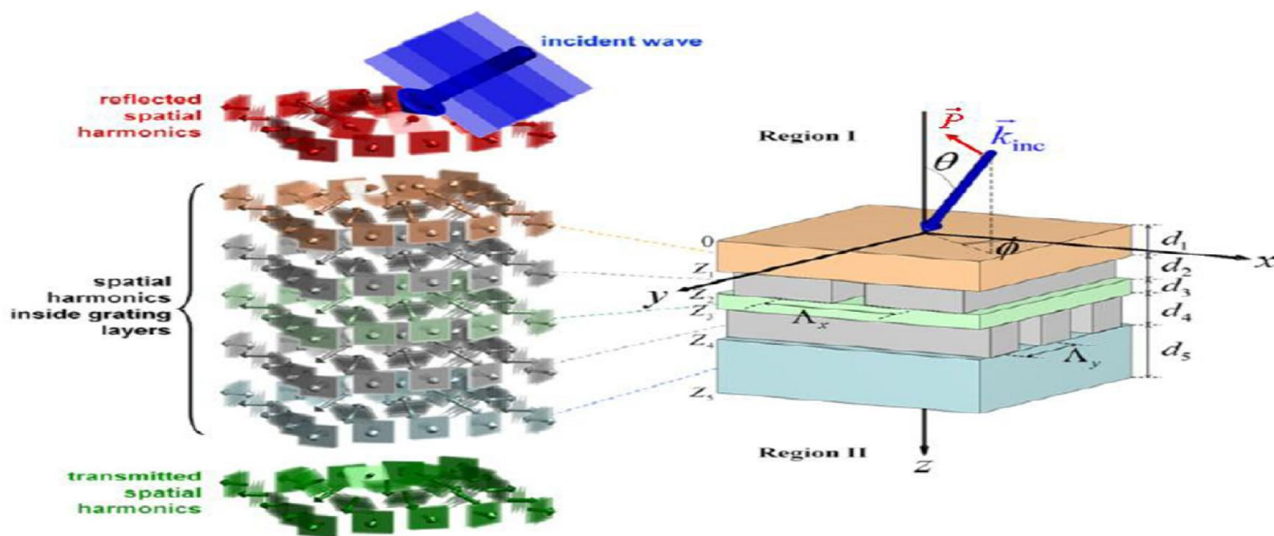


Figure 22: Geometry of RCWA

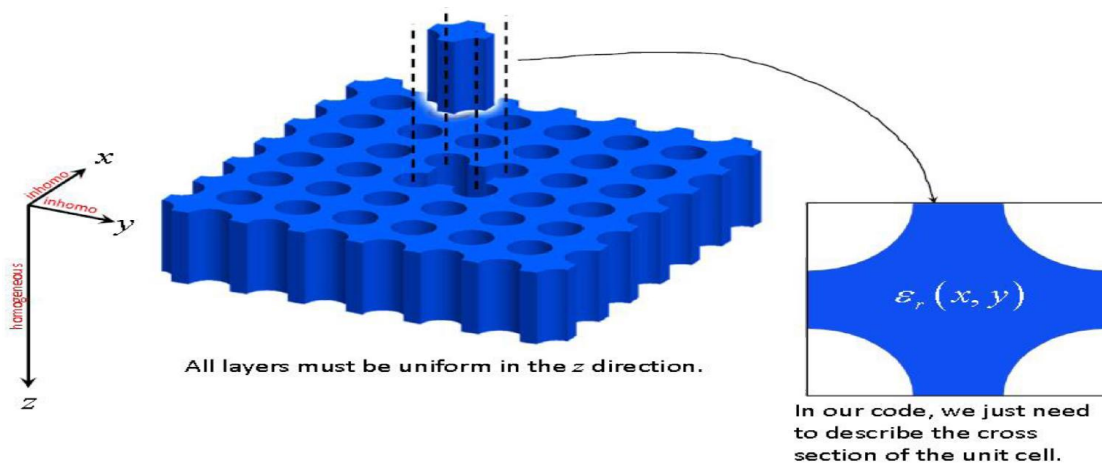


Figure 23: The 2D Unit Cell for Single Layer

For further understanding of the method development, we adopt a necessary sign convention as mentioned in the paragraph above. A wave travelling in the $+z$ direction:

$$e^{jkz} \tag{59}$$

IV.1.3. Semi-analytical form of Maxwell's

IV.1.3.1. Starting Point for RCWA

We start with Maxwell's equations in the following form

$$\frac{\partial E_z}{\partial y} - \frac{\partial E_y}{\partial z} = K_0 \mu_r \tilde{H}_x \frac{\partial \tilde{H}_z}{\partial y} - \frac{\partial \tilde{H}_y}{\partial z} = K_0 \varepsilon_r E_x \quad (60)$$

$$\frac{\partial E_x}{\partial z} - \frac{\partial E_z}{\partial x} = K_0 \mu_r \tilde{H}_y \frac{\partial \tilde{H}_x}{\partial z} - \frac{\partial \tilde{H}_z}{\partial x} = K_0 \varepsilon_r E_y \quad (61)$$

$$\frac{\partial E_y}{\partial x} - \frac{\partial E_x}{\partial y} = K_0 \mu_r \tilde{H}_z \frac{\partial \tilde{H}_y}{\partial x} - \frac{\partial \tilde{H}_x}{\partial y} = K_0 \varepsilon_r E_z \quad (62)$$

Recall that we normalized the magnetic field according

$$\vec{\tilde{H}} = -j \sqrt{\frac{\mu_0}{\varepsilon_0}} \vec{H} \quad (63)$$

IV.1.3.2.z-Uniform Media

We are going to consider Maxwell's equation inside a medium that is uniform in the z direction. The medium may still be inhomogeneous in the x - y plane, but it must be uniform in the z direction.

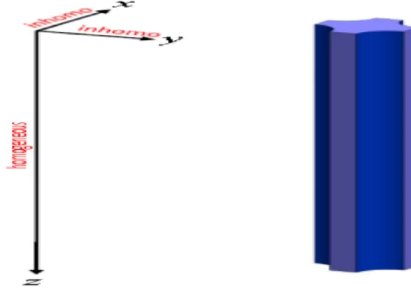


Figure 24: z- uniform media

IV.1.3.3 Fourier Transform in x and y Only

Unlike PWEM, RCWA only Fourier transforms along x and y . The z parameter remains analytical and unchanged. The Fourier expansion of the materials in the x - y plane is:

$$\varepsilon_r(x, y) = \sum_{m=-\infty}^{+\infty} \sum_{n=-\infty}^{+\infty} a_{m,n} e^{j\left(\frac{2\pi m x}{\Lambda_x} + \frac{2\pi n y}{\Lambda_y}\right)} \quad (64)$$

$$\mu_r(x, y) = \sum_{m=-\infty}^{+\infty} \sum_{n=-\infty}^{+\infty} b_{m,n} e^{j\left(\frac{2\pi m x}{\Lambda_x} + \frac{2\pi n y}{\Lambda_y}\right)} \quad (65)$$

Where $a_{m,n}$ and $b_{m,n}$ are Fourier coefficient given by:

$$a_{m,n} = \frac{1}{\Lambda_x \Lambda_y} \int_{-\Lambda_x/2}^{+\Lambda_x/2} \int_{-\Lambda_y/2}^{+\Lambda_y/2} \varepsilon_r(x, y) e^{-j\left(\frac{2\pi m x}{\Lambda_x} + \frac{2\pi n y}{\Lambda_y}\right)} dx dy \quad (66)$$

$$b_{m,n} = \frac{1}{\Lambda_x \Lambda_y} \int_{-\Lambda_x/2}^{+\Lambda_x/2} \int_{-\Lambda_y/2}^{+\Lambda_y/2} \mu_r(x, y) e^{-j\left(\frac{2\pi m x}{\Lambda_x} + \frac{2\pi n y}{\Lambda_y}\right)} dx dy \quad (67)$$

It follows that the Fourier expansion of the field are:

$$E_x(x, y, z) = \sum_{m=-\infty}^{+\infty} \sum_{n=-\infty}^{+\infty} S_x(m, n, z) e^{-j[K_x(m)x + K_y(n)y]} \quad (68.a)$$

$$E_y(x, y, z) = \sum_{m=-\infty}^{+\infty} \sum_{n=-\infty}^{+\infty} S_y(m, n, z) e^{-j[K_x(m)x + K_y(n)y]} \quad (68.b)$$

$$E_z(x, y, z) = \sum_{m=-\infty}^{+\infty} \sum_{n=-\infty}^{+\infty} S_z(m, n, z) e^{-j[K_x(m)x + K_y(n)y]} \quad (68.c)$$

And for magnetic field

$$\tilde{H}_x(x, y, z) = \sum_{m=-\infty}^{+\infty} \sum_{n=-\infty}^{+\infty} U_x(m, n, z) e^{-j[K_x(m)x + K_y(n)y]} \quad (69.a)$$

$$\tilde{H}_y(x, y, z) = \sum_{m=-\infty}^{+\infty} \sum_{n=-\infty}^{+\infty} U_y(m, n, z) e^{-j[K_x(m)x + K_y(n)y]} \quad (69.b)$$

$$\tilde{H}_z(x, y, z) = \sum_{m=-\infty}^{+\infty} \sum_{n=-\infty}^{+\infty} U_z(m, n, z) e^{-j[K_x(m)x + K_y(n)y]} \quad (69.c)$$

IV.1.3.4. Wave Vector Components

The transverse components of the wave vectors are equal throughout all layers of the device.

$$\begin{cases} K_x(m) = K_{x,inc} - \frac{2\pi m}{\Lambda_x} m = -\infty, \dots, -2, -1, 0, 1, 2, \dots, +\infty \\ K_y(n) = K_{y,inc} - \frac{2\pi n}{\Lambda_y} n = -\infty, \dots, -2, -1, 0, 1, 2, \dots, +\infty \end{cases} \quad (70)$$

For generalized symmetry, the transverse components are expanded along the reciprocal lattice vectors \vec{T}_1 and \vec{T}_2 so that we have

$$\vec{K}_T(m, n) = \vec{K}_{T,inc} - m\vec{T}_1 - n\vec{T}_2 \quad (71)$$

We need the longitudinal components of the wave vectors for:

Calculating diffraction efficiencies,

- Calculating the Eigen-modes of a homogeneous layer analytically.

These are calculated from the dispersion relation in the medium of interest.

$$K_z(m, n) = \left\{ \sqrt{K_0^2 \mu_r^* \epsilon_r^* - K_x^2 - K_y^2(n)} \right\}^* \quad (72)$$

Note that the conjugate operations enforce our negative sign convention.

By substitute Expansions Equations (68-b), (68-c), (68-a) and (65) into Maxwell's Equations (60) we then obtained semi-Analytical Form of Maxwell's Equations in Fourier Space.

If we do this for all of Maxwell's equations, we get...

- **Real-Space**

given by Equations (60), (61), and (62).

- **Semi-Analytical Fourier-Space**

Given by equations below:

$$-jK_y(n)U_z(m, n, z) - \frac{dU_y(m, n, z)}{dz} = K_0 \sum_{q=-\infty}^{+\infty} \sum_{r=-\infty}^{+\infty} a_{m-q, n-r} S_x(q, r, z)$$

$$\frac{dU_x(m, n, z)}{dz} + jK_x(m)U_z(m, n, z) = K_0 \sum_{q=-\infty}^{+\infty} \sum_{r=-\infty}^{+\infty} a_{m-q, n-r} S_y(q, r, z)$$

$$-jK_x(m)U_y(m, n, z) + jK_y(n)U_x(m, n, z) = K_0 \sum_{q=-\infty}^{+\infty} \sum_{r=-\infty}^{+\infty} a_{m-q, n-r} S_z(q, r, z)$$

We finally get with the magnetic field vector replacing U with S and a by b

$$-jK_y(n)S_z(m, n, z) - \frac{dS_y(m, n, z)}{dz} = K_0 \sum_{q=-\infty}^{+\infty} \sum_{r=-\infty}^{+\infty} b_{m-q, n-r} U_x(q, r, z)$$

$$\frac{dS_x(m, n, z)}{dz} + jK_x(m)S_z(m, n, z) = K_0 \sum_{q=-\infty}^{+\infty} \sum_{r=-\infty}^{+\infty} b_{m-q, n-r} U_y(q, r, z)$$

$$-jK_x(m)S_y(m, n, z) + jK_y(n)S_x(m, n, z) = K_0 \sum_{q=-\infty}^{+\infty} \sum_{r=-\infty}^{+\infty} b_{m-q, n-r} U_z(q, r, z)$$

Note that U (m, n, z) and S (m, n, z) are function of z. μ_z , a and b are not.

IV.1.4. Matrix form of Maxwell's equations

Taking into account the Equations in the Fourier space, and normalizing them by definition of the wave vectors, we obtain standardized coordinates that allow us to define the matrix form of Maxwell's Equations.

Define normalized wave vectors. We ask:

$$\tilde{K}_x = \frac{K_x}{K_0} \tilde{K}_y = \frac{K_y}{K_0} \tilde{K}_z = \frac{K_z}{K_0}$$

Normalize z coordinate

$$\tilde{z} = K_0 z$$

$$-j\tilde{K}_y(n)U_z(m, n, \tilde{z}) - \frac{dU_y(m, n, \tilde{z})}{d\tilde{z}} = \sum_{q=-\infty}^{+\infty} \sum_{r=-\infty}^{+\infty} a_{m-q, n-r} S_x(q, r, \tilde{z})$$

$$\frac{dU_x(m, n, \tilde{z})}{d\tilde{z}} + j\tilde{K}_x(m)U_z(m, n, \tilde{z}) = \sum_{q=-\infty}^{+\infty} \sum_{r=-\infty}^{+\infty} a_{m-q, n-r} S_y(q, r, \tilde{z})$$

$$-j\tilde{K}_x(m)S_y(m, n, \tilde{z}) + j\tilde{K}_y(n)S_x(m, n, \tilde{z}) = \sum_{q=-\infty}^{+\infty} \sum_{r=-\infty}^{+\infty} a_{m-q, n-r} U_z(q, r, \tilde{z})$$

and

$$-j\tilde{K}_y(n)S_z(m, n, \tilde{z}) - \frac{dS_y(m, n, \tilde{z})}{d\tilde{z}} = \sum_{q=-\infty}^{+\infty} \sum_{r=-\infty}^{+\infty} b_{m-q, n-r} U_x(q, r, \tilde{z})$$

$$\frac{dS_x(m, n, \tilde{z})}{d\tilde{z}} + j\tilde{K}_x(m)S_z(m, n, \tilde{z}) = \sum_{q=-\infty}^{+\infty} \sum_{r=-\infty}^{+\infty} b_{m-q, n-r} U_y(q, r, \tilde{z})$$

$$-j\tilde{K}_x(m)S_y(m,n,\tilde{z}) + j\tilde{K}_y(n)S_x(m,n,\tilde{z}) = \sum_{q=-\infty}^{+\infty} \sum_{r=-\infty}^{+\infty} b_{m-q,n-r} U_z(q,r,\tilde{z})$$

Start with the first equation.

$$-j\tilde{K}_y(n)U_z(m,n,\tilde{z}) - \frac{dU_y(m,n,\tilde{z})}{d\tilde{z}} = \sum_{q=-\infty}^{+\infty} \sum_{r=-\infty}^{+\infty} a_{m-q,n-r} S_x(q,r,\tilde{z})$$

This equation is written once for every combination of m and n . This large set of equations can be written in matrix form as

$$-j\tilde{K}_y \mathbf{U}_z - \frac{d\mathbf{U}_y}{d\tilde{z}} = \llbracket \varepsilon_r \rrbracket \mathbf{S}_x \quad (73)$$

Where

$$\tilde{K}_y = \begin{bmatrix} \tilde{K}_y(1,1) & \dots & 0 \\ \vdots & \ddots & \vdots \\ 0 & \dots & \tilde{K}_y(m,n) \end{bmatrix} \quad (74)$$

$$\mathbf{u}_z = \begin{bmatrix} U_z(1,1) \\ U_z(1,2) \\ \vdots \\ U_z(M,N) \end{bmatrix} \quad \mathbf{u}_y = \begin{bmatrix} U_y(1,1) \\ U_y(1,2) \\ \vdots \\ U_y(M,N) \end{bmatrix} \quad \mathbf{s}_x = \begin{bmatrix} S_x(1,1) \\ S_x(1,2) \\ \vdots \\ S_x(M,N) \end{bmatrix}$$

$$\llbracket \varepsilon_r \rrbracket = \begin{bmatrix} \text{Toeplitz} \\ \text{convolution} \\ \text{matrix} \end{bmatrix}$$

Note that only truly Toeplitz symmetry for 1D gratings.

Applying this development to the other Equations, we arrive at the following other matrix forms which are written below (75a, 75b).

$$\begin{aligned} -j\tilde{k}_y(n)U_z(m,n;\tilde{z}) - \frac{dU_y(m,n;\tilde{z})}{d\tilde{z}} &= \sum_{q=-M/2}^{M/2} \sum_{r=-N/2}^{N/2} a_{m-q,n-r} S_x(q,r;\tilde{z}) \\ \frac{dU_x(m,n;\tilde{z})}{d\tilde{z}} + j\tilde{k}_x(m)U_z(m,n;\tilde{z}) &= \sum_{q=-M/2}^{M/2} \sum_{r=-N/2}^{N/2} a_{m-q,n-r} S_y(q,r;\tilde{z}) \\ -j\tilde{k}_x(m)U_y(m,n;\tilde{z}) + j\tilde{k}_y(n)U_x(m,n;\tilde{z}) &= \sum_{q=-M/2}^{M/2} \sum_{r=-N/2}^{N/2} a_{m-q,n-r} S_z(q,r;\tilde{z}) \end{aligned} \quad \Rightarrow \quad \begin{aligned} -j\tilde{K}_y \mathbf{u}_z - \frac{d}{d\tilde{z}} \mathbf{u}_y &= \llbracket \varepsilon_r \rrbracket \mathbf{s}_x \\ \frac{d}{d\tilde{z}} \mathbf{u}_x + j\tilde{K}_x \mathbf{u}_z &= \llbracket \varepsilon_r \rrbracket \mathbf{s}_y \\ \tilde{K}_x \mathbf{u}_y - \tilde{K}_y \mathbf{u}_x &= j \llbracket \varepsilon_r \rrbracket \mathbf{s}_z \end{aligned} \quad (75a)$$

$$\begin{aligned}
-jk_y(n)S_z(m,n;z) - \frac{dS_y(m,n;z)}{dz} &= k_0 \sum_{q=-M/2}^{M/2} \sum_{r=-N/2}^{N/2} b_{m-q,n-r} U_x(q,r;z) \\
\frac{dS_x(m,n;z)}{dz} + jk_x(m)S_z(m,n;z) &= k_0 \sum_{q=-M/2}^{M/2} \sum_{r=-N/2}^{N/2} b_{m-q,n-r} U_y(q,r;z) \\
-jk_x(m)S_y(m,n;z) + jk_y(n)S_x(m,n;z) &= k_0 \sum_{q=-M/2}^{M/2} \sum_{r=-N/2}^{N/2} b_{m-q,n-r} U_z(q,r;z)
\end{aligned}
\Rightarrow
\boxed{
\begin{aligned}
-j\tilde{\mathbf{K}}_y \mathbf{s}_z - \frac{d}{d\tilde{z}} \mathbf{s}_y &= \llbracket \mu_r \rrbracket \mathbf{u}_x \\
\frac{d}{d\tilde{z}} \mathbf{s}_x + j\tilde{\mathbf{K}}_x \mathbf{s}_z &= \llbracket \mu_r \rrbracket \mathbf{u}_y \\
\tilde{\mathbf{K}}_x \mathbf{s}_y - \tilde{\mathbf{K}}_y \mathbf{s}_x &= j \llbracket \mu_r \rrbracket \mathbf{u}_z
\end{aligned}
} \quad (75b)$$

IV.1.5. Matrix wave equation

The search for solutions of these Equations (73), (75-a), et (75-b) gives for the longitudinal components of field leads to matrix wave Equation. To do this, we wish to eliminate the longitudinal field components S_z and U_z .

We start by solving the third and sixth equation for these terms.

$$\begin{aligned}
-j\tilde{\mathbf{K}}_y \mathbf{u}_z - \frac{d}{d\tilde{z}} \mathbf{u}_y &= \llbracket \varepsilon_r \rrbracket \mathbf{s}_x \\
\frac{d}{d\tilde{z}} \mathbf{u}_x + j\tilde{\mathbf{K}}_x \mathbf{u}_z &= \llbracket \varepsilon_r \rrbracket \mathbf{s}_y \\
\tilde{\mathbf{K}}_x \mathbf{u}_y - \tilde{\mathbf{K}}_y \mathbf{u}_x &= j \llbracket \varepsilon_r \rrbracket \mathbf{s}_z \longrightarrow \mathbf{s}_z = -j \llbracket \varepsilon_r \rrbracket^{-1} (\tilde{\mathbf{K}}_x \mathbf{u}_y - \tilde{\mathbf{K}}_y \mathbf{u}_x) \\
-j\tilde{\mathbf{K}}_y \mathbf{s}_z - \frac{d}{d\tilde{z}} \mathbf{s}_y &= \llbracket \mu_r \rrbracket \mathbf{u}_x \\
\frac{d}{d\tilde{z}} \mathbf{s}_x + j\tilde{\mathbf{K}}_x \mathbf{s}_z &= \llbracket \mu_r \rrbracket \mathbf{u}_y \\
\tilde{\mathbf{K}}_x \mathbf{s}_y - \tilde{\mathbf{K}}_y \mathbf{s}_x &= j \llbracket \mu_r \rrbracket \mathbf{u}_z \longrightarrow \mathbf{u}_z = -j \llbracket \mu_r \rrbracket^{-1} (\tilde{\mathbf{K}}_x \mathbf{s}_y - \tilde{\mathbf{K}}_y \mathbf{s}_x)
\end{aligned}$$

Eliminate Longitudinal Field components; we substitute S_z and U_z back into the remaining four equations. So that we get

$$\begin{aligned}
\left. \begin{aligned}
-j\tilde{\mathbf{K}}_y \mathbf{u}_z - \frac{d}{d\tilde{z}} \mathbf{u}_y &= \llbracket \varepsilon_r \rrbracket \mathbf{s}_x \\
\frac{d}{d\tilde{z}} \mathbf{u}_x + j\tilde{\mathbf{K}}_x \mathbf{u}_z &= \llbracket \varepsilon_r \rrbracket \mathbf{s}_y \\
\mathbf{s}_z &= -j \llbracket \varepsilon_r \rrbracket^{-1} (\tilde{\mathbf{K}}_x \mathbf{u}_y - \tilde{\mathbf{K}}_y \mathbf{u}_x)
\end{aligned} \right\} \begin{aligned}
-\tilde{\mathbf{K}}_y \llbracket \mu_r \rrbracket^{-1} (\tilde{\mathbf{K}}_x \mathbf{s}_y - \tilde{\mathbf{K}}_y \mathbf{s}_x) - \frac{d}{d\tilde{z}} \mathbf{u}_y &= \llbracket \varepsilon_r \rrbracket \mathbf{s}_x \\
\frac{d}{d\tilde{z}} \mathbf{u}_x + \tilde{\mathbf{K}}_x \llbracket \mu_r \rrbracket^{-1} (\tilde{\mathbf{K}}_x \mathbf{s}_y - \tilde{\mathbf{K}}_y \mathbf{s}_x) &= \llbracket \varepsilon_r \rrbracket \mathbf{s}_y
\end{aligned} \\
\left. \begin{aligned}
-j\tilde{\mathbf{K}}_y \mathbf{s}_z - \frac{d}{d\tilde{z}} \mathbf{s}_y &= \llbracket \mu_r \rrbracket \mathbf{u}_x \\
\frac{d}{d\tilde{z}} \mathbf{s}_x + j\tilde{\mathbf{K}}_x \mathbf{s}_z &= \llbracket \mu_r \rrbracket \mathbf{u}_y \\
\mathbf{u}_z &= -j \llbracket \mu_r \rrbracket^{-1} (\tilde{\mathbf{K}}_x \mathbf{s}_y - \tilde{\mathbf{K}}_y \mathbf{s}_x)
\end{aligned} \right\} \begin{aligned}
-\tilde{\mathbf{K}}_y \llbracket \varepsilon_r \rrbracket^{-1} (\tilde{\mathbf{K}}_x \mathbf{u}_y - \tilde{\mathbf{K}}_y \mathbf{u}_x) - \frac{d}{d\tilde{z}} \mathbf{s}_y &= \llbracket \mu_r \rrbracket \mathbf{u}_x \\
\frac{d}{d\tilde{z}} \mathbf{s}_x + \tilde{\mathbf{K}}_x \llbracket \varepsilon_r \rrbracket^{-1} (\tilde{\mathbf{K}}_x \mathbf{u}_y - \tilde{\mathbf{K}}_y \mathbf{u}_x) &= \llbracket \mu_r \rrbracket \mathbf{u}_y
\end{aligned}
\end{aligned}$$

Next, we expand the equations and rearrange the terms. We get from then

$$\begin{aligned}
-\tilde{\mathbf{K}}_y \llbracket \mu_r \rrbracket^{-1} (\tilde{\mathbf{K}}_x \mathbf{s}_y - \tilde{\mathbf{K}}_y \mathbf{s}_x) - \frac{d}{d\tilde{z}} \mathbf{u}_y &= \llbracket \varepsilon_r \rrbracket \mathbf{s}_x \\
\frac{d}{d\tilde{z}} \mathbf{u}_x + \tilde{\mathbf{K}}_x \llbracket \mu_r \rrbracket^{-1} (\tilde{\mathbf{K}}_x \mathbf{s}_y - \tilde{\mathbf{K}}_y \mathbf{s}_x) &= \llbracket \varepsilon_r \rrbracket \mathbf{s}_y
\end{aligned}
\begin{aligned}
\frac{d}{d\tilde{z}} \mathbf{u}_x &= \tilde{\mathbf{K}}_x \llbracket \mu_r \rrbracket^{-1} \tilde{\mathbf{K}}_y \mathbf{s}_x + \left(\llbracket \varepsilon_r \rrbracket - \tilde{\mathbf{K}}_x \llbracket \mu_r \rrbracket^{-1} \tilde{\mathbf{K}}_x \right) \mathbf{s}_y \\
\frac{d}{d\tilde{z}} \mathbf{u}_y &= \left(\tilde{\mathbf{K}}_y \llbracket \mu_r \rrbracket^{-1} \tilde{\mathbf{K}}_y - \llbracket \varepsilon_r \rrbracket \right) \mathbf{s}_x - \tilde{\mathbf{K}}_y \llbracket \mu_r \rrbracket^{-1} \tilde{\mathbf{K}}_x \mathbf{s}_y
\end{aligned}$$

$$\begin{aligned}
-\tilde{\mathbf{K}}_y \llbracket \varepsilon_r \rrbracket^{-1} (\tilde{\mathbf{K}}_x \mathbf{u}_y - \tilde{\mathbf{K}}_y \mathbf{u}_x) - \frac{d}{dz} \mathbf{s}_y &= \llbracket \mu_r \rrbracket \mathbf{u}_x & \frac{d}{dz} \mathbf{s}_x &= \tilde{\mathbf{K}}_x \llbracket \varepsilon_r \rrbracket^{-1} \tilde{\mathbf{K}}_y \mathbf{u}_x + (\llbracket \mu_r \rrbracket - \tilde{\mathbf{K}}_x \llbracket \varepsilon_r \rrbracket^{-1} \tilde{\mathbf{K}}_x) \mathbf{u}_y \\
\frac{d}{dz} \mathbf{s}_x + \tilde{\mathbf{K}}_x \llbracket \varepsilon_r \rrbracket^{-1} (\tilde{\mathbf{K}}_x \mathbf{u}_y - \tilde{\mathbf{K}}_y \mathbf{u}_x) &= \llbracket \mu_r \rrbracket \mathbf{u}_y & \frac{d}{dz} \mathbf{s}_y &= (\tilde{\mathbf{K}}_y \llbracket \varepsilon_r \rrbracket^{-1} \tilde{\mathbf{K}}_y - \llbracket \mu_r \rrbracket) \mathbf{u}_x - \tilde{\mathbf{K}}_y \llbracket \varepsilon_r \rrbracket^{-1} \tilde{\mathbf{K}}_x \mathbf{u}_y
\end{aligned}$$

IV.1.5.1 Block Matrix Form

When a layer is homogeneous, the \mathbf{P} and \mathbf{Q} matrices reduce to

$$\begin{aligned}
\mathbf{P} &= \varepsilon_r^{-1} \begin{bmatrix} \tilde{\mathbf{K}}_x \tilde{\mathbf{K}}_y & \mu_r \varepsilon_r \mathbf{I} - \tilde{\mathbf{K}}_x^2 \\ \tilde{\mathbf{K}}_y^2 - \mu_r \varepsilon_r \mathbf{I} & -\tilde{\mathbf{K}}_y \tilde{\mathbf{K}}_x \end{bmatrix} & \mathbf{Q} &= \mu_r^{-1} \begin{bmatrix} \tilde{\mathbf{K}}_x \tilde{\mathbf{K}}_y & \mu_r \varepsilon_r \mathbf{I} - \tilde{\mathbf{K}}_x^2 \\ \tilde{\mathbf{K}}_y^2 - \mu_r \varepsilon_r \mathbf{I} & -\tilde{\mathbf{K}}_y \tilde{\mathbf{K}}_x \end{bmatrix} \\
& & & = \frac{\varepsilon_r}{\mu_r} \mathbf{P}
\end{aligned}$$

Notice that these matrices do not contain computationally intensive convolution matrices.

Therefore, they are very fast and efficient to calculate for this special case.

We can therefore give the matrix wave Equation by following these three steps mentioned below.

From here, we can derive a wave equation just as we did for TMM. Doing that with equation (76) we obtain

$$\frac{d}{dz} \begin{bmatrix} \mathbf{S}_x \\ \mathbf{S}_y \end{bmatrix} = \mathbf{P} \begin{bmatrix} U_x \\ U_y \end{bmatrix} \quad (76) \quad \frac{d}{dz} \begin{bmatrix} U_x \\ U_y \end{bmatrix} = \mathbf{Q} \begin{bmatrix} \mathbf{S}_x \\ \mathbf{S}_y \end{bmatrix} \quad (77)$$

First, differentiate Equation (76) with respect to z .

$$\frac{d^2}{dz^2} \begin{bmatrix} \mathbf{S}_x \\ \mathbf{S}_y \end{bmatrix} = \mathbf{P} \frac{d}{dz} \begin{bmatrix} U_x \\ U_y \end{bmatrix} \quad (78)$$

Second, substitute Equation (77) in to Equation (78) to eliminate the magnetic fields we obtain.

$$\frac{d^2}{dz^2} \begin{bmatrix} \mathbf{S}_x \\ \mathbf{S}_y \end{bmatrix} = \mathbf{PQ} \begin{bmatrix} \mathbf{S}_x \\ \mathbf{S}_y \end{bmatrix} \quad (79)$$

Third, the final matrix wave equation is

$$\frac{d^2}{dz^2} \begin{bmatrix} \mathbf{S}_x \\ \mathbf{S}_y \end{bmatrix} - \Omega^2 \begin{bmatrix} \mathbf{S}_x \\ \mathbf{S}_y \end{bmatrix} = 0 \quad \text{With } \Omega^2 = \mathbf{PQ} \quad (80)$$

So that, we arrived at our standard PQ “form”.

IV.1.5.3. Solution to the matrix wave equation

- **Analytical Solution in the z Direction**

The matrix wave equation is given by Equation (80).

$$\frac{d^2}{dz^2} \begin{bmatrix} \mathbf{S}_x \\ \mathbf{S}_y \end{bmatrix} - \Omega^2 \begin{bmatrix} \mathbf{S}_x \\ \mathbf{S}_y \end{bmatrix} = 0$$

This is really a large set of ordinary differential equations that can each be solved analytically.

This set of solutions is

$$\begin{bmatrix} \mathbf{S}_x(\tilde{z}) \\ \mathbf{S}_y(\tilde{z}) \end{bmatrix} = e^{-\Omega \tilde{z}} \mathbf{S}^+(0) + e^{\Omega \tilde{z}} \mathbf{S}^-(0) \quad (81)$$

The terms $\mathbf{S}^+(0)$ and $\mathbf{S}^-(0)$ are the initial values for this differential equation. The \pm superscripts indicate whether they pertain to forward propagating waves (+) or backward propagating waves (-).

- **Computation of $e^{\pm\Omega z}$**

Recall from Lecture paragraph IV.1, we can put this function in the form

$$(\mathbf{A}) = \mathbf{W} \cdot (\boldsymbol{\lambda}) \cdot \mathbf{W}^{-1} \quad (82)$$

Where:

$\mathbf{A} \equiv$ Arbitrary matrix (full rank).

$\mathbf{W} \equiv$ Eigen vector matrix calculated from \mathbf{A}

$\boldsymbol{\lambda} \equiv$ Diagonal Eigen value matrix calculated from \mathbf{A}

We can use this relation to compute the matrix exponentials.

$$e^{-\Omega z'} = \mathbf{W} e^{-\boldsymbol{\lambda} z'} \mathbf{W}^{-1} \qquad e^{\Omega z'} = \mathbf{W} e^{\boldsymbol{\lambda} z'} \mathbf{W}^{-1}$$

$$\begin{aligned} \mathbf{W} &\equiv \text{Eigen-vector matrix of } \Omega^2 \\ \boldsymbol{\lambda}^2 &\equiv \text{Eigen-value matrix of } \Omega^2 \end{aligned} \qquad e^{\boldsymbol{\lambda} z'} = \begin{bmatrix} e^{\sqrt{\lambda_1^2} z'} & & & \\ & e^{\sqrt{\lambda_2^2} z'} & & \\ & & \ddots & \\ & & & e^{\sqrt{\lambda_N^2} z'} \end{bmatrix}$$

We start with the following solution which is given by Equation (81).

$$\begin{bmatrix} \mathbf{S}_x(\tilde{z}) \\ \mathbf{S}_y(\tilde{z}) \end{bmatrix} = e^{-\Omega \tilde{z}} \mathbf{S}^+(0) + e^{\Omega \tilde{z}} \mathbf{S}^-(0) \quad (83) \quad \left. \begin{aligned} e^{-\Omega \tilde{z}} &= \mathbf{W} \exp(-\boldsymbol{\lambda} \tilde{z}) \cdot \mathbf{W}^{-1} \\ e^{\Omega \tilde{z}} &= \mathbf{W} \exp(\boldsymbol{\lambda} \tilde{z}) \mathbf{W}^{-1} \end{aligned} \right\} \quad (84)$$

Substituting Equation (81) into Equation (80) yields we get (85)

$$\begin{bmatrix} \mathbf{s}_x(\tilde{z}) \\ \mathbf{s}_y(\tilde{z}) \end{bmatrix} = \mathbf{W} e^{-\boldsymbol{\lambda} \tilde{z}} \underbrace{\mathbf{W}^{-1} \mathbf{s}^+(0)}_{\mathbf{c}^+} + \mathbf{W} e^{\boldsymbol{\lambda} \tilde{z}} \underbrace{\mathbf{W}^{-1} \mathbf{s}^-(0)}_{\mathbf{c}^-} \quad (85)$$

The terms $\mathbf{S}^+(0)$ and $\mathbf{S}^-(0)$ are the initial values that have yet to be calculated. Therefore \mathbf{W}^{-1} can be combined with these terms to produce column vectors of proportionality constants \mathbf{c}^+ and \mathbf{c}^- .

$$\begin{bmatrix} \mathbf{s}_x(\tilde{z}) \\ \mathbf{s}_y(\tilde{z}) \end{bmatrix} = \mathbf{W} e^{-\boldsymbol{\lambda} \tilde{z}} \mathbf{c}^+ + \mathbf{W} e^{\boldsymbol{\lambda} \tilde{z}} \mathbf{c}^- \qquad \begin{aligned} \mathbf{c}^+ &= \mathbf{W}^{-1} \mathbf{s}^+(0) \\ \mathbf{c}^- &= \mathbf{W}^{-1} \mathbf{s}^-(0) \end{aligned}$$

- **Solution for the Magnetic Fields**

We can similarly write a solution for the magnetic fields.

$$\begin{bmatrix} \mathbf{U}_x(\tilde{z}) \\ \mathbf{U}_y(\tilde{z}) \end{bmatrix} = -\mathbf{V} e^{-\boldsymbol{\lambda} \tilde{z}} \mathbf{c}^+ + \mathbf{V} e^{\boldsymbol{\lambda} \tilde{z}} \mathbf{c}^- \quad (86)$$

We need to calculate \mathbf{V} from the Eigen-value solution of Ω^2 . To put this equation in terms of the electric field, we differentiate with respect to z . so that we get:

$$\frac{d}{d\tilde{z}} \begin{bmatrix} \mathbf{U}_x(\tilde{z}) \\ \mathbf{U}_y(\tilde{z}) \end{bmatrix} = \boldsymbol{\lambda} \mathbf{V} e^{-\boldsymbol{\lambda} \tilde{z}} \mathbf{c}^+ + \boldsymbol{\lambda} \mathbf{V} e^{\boldsymbol{\lambda} \tilde{z}} \mathbf{c}^- \quad (87)$$

The negative sign is needed so both terms will be positive after differentiation.

- **Solution for the Magnetic Fields**

The solution for the magnetic fields is given by:

First we recall equation (77), (85) and (87)

$$\frac{d}{d\tilde{z}} \begin{bmatrix} U_x \\ U_y \end{bmatrix} = Q \begin{bmatrix} S_x \\ S_y \end{bmatrix}$$

$$\begin{bmatrix} S_x(\tilde{z}) \\ S_y(\tilde{z}) \end{bmatrix} = W e^{-\lambda\tilde{z}} c^+ + W e^{\lambda\tilde{z}} c^-$$

$$\frac{d}{d\tilde{z}} \begin{bmatrix} U_x(\tilde{z}) \\ U_y(\tilde{z}) \end{bmatrix} = \lambda V e^{-\lambda\tilde{z}} c^+ + \lambda V e^{\lambda\tilde{z}} c^-$$

Substitute Equation, (85) into Equation, (77). We obtain expression (88)

$$\frac{d}{d\tilde{z}} \begin{bmatrix} U_x(\tilde{z}) \\ U_y(\tilde{z}) \end{bmatrix} = Q W e^{-\lambda\tilde{z}} c^+ + Q W e^{\lambda\tilde{z}} c^- \quad (88)$$

When we compare this Equation (88) to Equation (86) we have

$$V\lambda = QW \Rightarrow V = QW\lambda^{-1} \quad (89)$$

- **Overall Field Solution**

The field solutions for both the electric and magnetic fields were

$$\begin{bmatrix} S_x(\tilde{z}) \\ S_y(\tilde{z}) \end{bmatrix} = W e^{-\lambda\tilde{z}} c^+ + W e^{\lambda\tilde{z}} c^-$$

$$\begin{bmatrix} U_x(\tilde{z}) \\ U_y(\tilde{z}) \end{bmatrix} = -V e^{-\lambda\tilde{z}} c^+ + V e^{\lambda\tilde{z}} c^-$$

Combining these into a single matrix equation yields,

$$\psi(\tilde{z}) = \begin{bmatrix} S_x(\tilde{z}) \\ S_y(\tilde{z}) \\ U_x(\tilde{z}) \\ U_y(\tilde{z}) \end{bmatrix} = \begin{bmatrix} W & W \\ -V & V \end{bmatrix} \begin{bmatrix} e^{-\lambda\tilde{z}} & 0 \\ 0 & e^{\lambda\tilde{z}} \end{bmatrix} \begin{bmatrix} c^+ \\ c^- \end{bmatrix} \quad (90)$$

Where $V = QW\lambda^{-1}$

- **Interpretation of the Solution**

The overall solution is can be writing by this equation.

$$\psi(\tilde{z}) = QW e^{-\lambda\tilde{z}} C \quad (91)$$

- $\psi(\tilde{z})$ represent Overall solution which is the sum of all the modes at plane z'
- W is square matrix who's column vectors describe the “modes” that can exist in the material. These are essentially pictures of the modes which quantify the relative amplitudes of E_x , E_y , H_x , and H_y .
- $e^{-\lambda\tilde{z}}$ is diagonal matrix describing how the modes propagate. This includes accumulation of

phase as well as decaying (loss) or growing (gain) amplitude.

- **C** is Column vector containing the amplitude coefficient of each of the modes. These quantities how much energy is in each mode.

• Visualization of this Solution

The visualization of this solution and different modes are given at figure 25.

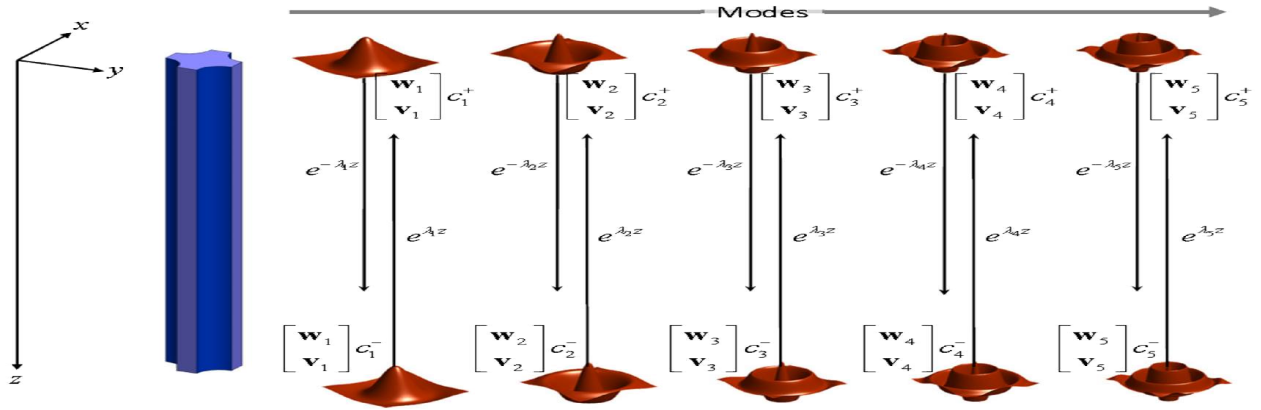


Figure 25: visualization of solution and different modes

• Solution in Homogeneous Layers

Recall that in homogeneous layers we have

$$P = \epsilon_r^{-1} \begin{bmatrix} K_x \tilde{K}_y & \mu_r \epsilon_r I - \tilde{K}_x^2 \\ \tilde{K}_y^2 - \mu_r \epsilon_r I & -\tilde{K}_y \tilde{K}_x \end{bmatrix} \quad Q = \frac{\epsilon_r}{\mu_r} P \quad (92)$$

The solution to the Eigen value problem is

$$\Omega^2 = PQ, \text{ Eigen vectors } W = \begin{bmatrix} I & 0 \\ 0 & I \end{bmatrix}, \text{ Eigen values, } \lambda^2 = \begin{bmatrix} -\tilde{K}_z^2 & 0 \\ 0 & -\tilde{K}_z^2 \end{bmatrix}, \lambda = \begin{bmatrix} j\tilde{K}_z & 0 \\ 0 & j\tilde{K}_z \end{bmatrix}, \text{ and}$$

$$\tilde{K}_z = \left(\sqrt{\mu_r^* \epsilon_r^* I - \tilde{K}_x^2 - \tilde{K}_y^2} \right)^* . \text{ The Eigen-modes for the magnetic fields are simply } V = Q\lambda^{-1}, \text{ thus}$$

no need to actually solve the Eigen value problem in homogeneous layers.

IV.1.6 Multilayer framework: scattering matrices

• Geometry of a Multilayer Device

So far, we have treated substrates as being one-sided slabs of material of infinite depth. In almost all practical cases, the substrate will have finite depth with rear surfaces that reflect some of the energy and affect the performance of the assembly.

The depth of the substrate will usually be much greater than the wavelength of the light, and variations in the flatness and parallelism of the two surfaces will be appreciable fractions of a wavelength. In case, the description of the multilayer nanofilms is necessary, taking into account certain assumptions or conditions as shown in the figure 26 below

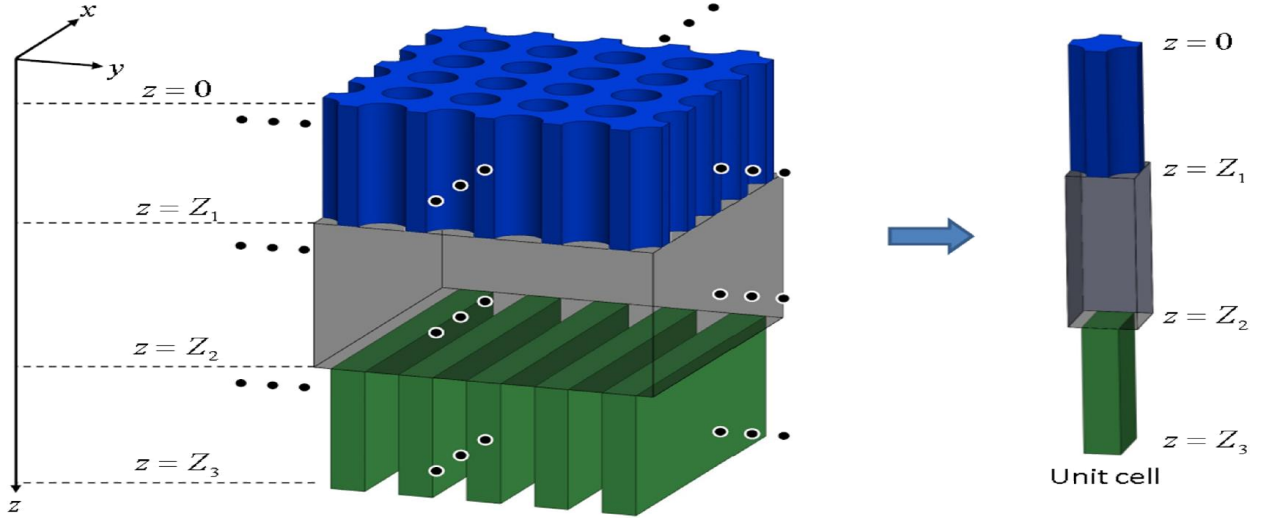


Figure 26: Sample of an infinitely periodic lattice

- **Eigen System in Each Layer**

We can then, taking into account the different solutions obtained in the above paragraphs write the equations giving the Eigen system of each layer.

Boundary conditions require that all layers have the same \mathbf{K}_x and \mathbf{K}_y matrices.

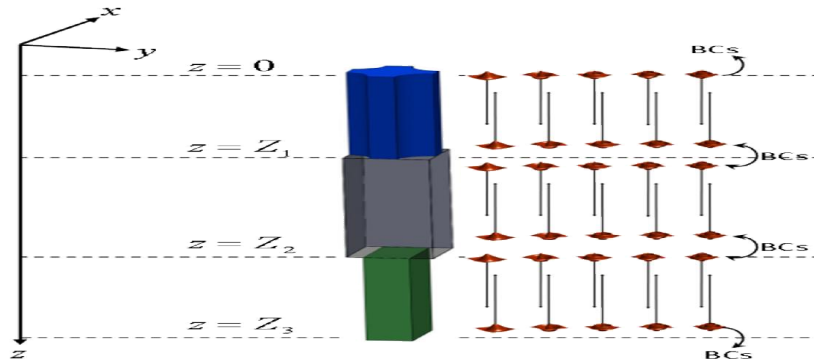


Figure 27: sample of multilayer's with finite thickness, and different modes

Figure 26 above shows a multilayer structure (3 layers) with different and finite thicknesses, each layer defines a zone that is 1, 2, 3, delimited the layers. For the three layers we have:

Layer 1: Equation (93)

$$P_1 = \begin{bmatrix} \tilde{K}_x[\epsilon_{r,1}]^{-1}\tilde{K}_y & \mu_{r,1} - \tilde{K}_x[\epsilon_{r,1}]^{-1}\tilde{K}_x \\ \tilde{K}_y[\epsilon_{r,1}]^{-1}\tilde{K}_y - \mu_{r,1} & -\tilde{K}_y[\epsilon_{r,1}]^{-1}\tilde{K}_x \end{bmatrix}$$

$$Q_1 = \begin{bmatrix} \tilde{K}_x[\mu_{r,1}]^{-1}\tilde{K}_y & [\varepsilon_{r,1}] - \tilde{K}_x[\mu_{r,1}]^{-1}\tilde{K}_x \\ \tilde{K}_y[\mu_{r,1}]^{-1}\tilde{K}_y - [\varepsilon_{r,1}] & -\tilde{K}_y[\mu_{r,1}]^{-1}\tilde{K}_x \end{bmatrix}$$

$$\Omega_1^2 = P_1 Q_1 \rightarrow W_1, \lambda_1 \rightarrow V_1, c_1^+, c_1^-$$

Layer 2: Equations(94)

$$P_2 = \begin{bmatrix} \tilde{K}_x[\varepsilon_{r,2}]^{-1}\tilde{K}_y & \mu_{r,2} - \tilde{K}_x[\varepsilon_{r,2}]^{-1}\tilde{K}_x \\ \tilde{K}_y[\varepsilon_{r,2}]^{-1}\tilde{K}_y - \mu_{r,2} & -\tilde{K}_y[\varepsilon_{r,2}]^{-1}\tilde{K}_x \end{bmatrix}$$

$$Q_2 = \begin{bmatrix} \tilde{K}_x[\mu_{r,2}]^{-1}\tilde{K}_y & [\varepsilon_{r,2}] - \tilde{K}_x[\mu_{r,2}]^{-1}\tilde{K}_x \\ \tilde{K}_y[\mu_{r,2}]^{-1}\tilde{K}_y - [\varepsilon_{r,2}] & -\tilde{K}_y[\mu_{r,2}]^{-1}\tilde{K}_x \end{bmatrix}$$

$$\Omega_2^2 = P_2 Q_2 \rightarrow W_2, \lambda_2 \rightarrow V_2, c_2^+, c_2^-$$

Layer 3: Equations (95)

$$P_3 = \begin{bmatrix} \tilde{K}_x[\varepsilon_{r,3}]^{-1}\tilde{K}_y & \mu_{r,3} - \tilde{K}_x[\varepsilon_{r,3}]^{-1}\tilde{K}_x \\ \tilde{K}_y[\varepsilon_{r,3}]^{-1}\tilde{K}_y - \mu_{r,3} & -\tilde{K}_y[\varepsilon_{r,3}]^{-1}\tilde{K}_x \end{bmatrix}$$

$$Q_3 = \begin{bmatrix} \tilde{K}_x[\mu_{r,3}]^{-1}\tilde{K}_y & [\varepsilon_{r,3}] - \tilde{K}_x[\mu_{r,3}]^{-1}\tilde{K}_x \\ \tilde{K}_y[\mu_{r,3}]^{-1}\tilde{K}_y - [\varepsilon_{r,3}] & -\tilde{K}_y[\mu_{r,3}]^{-1}\tilde{K}_x \end{bmatrix}$$

$$\Omega_3^2 = P_3 Q_3 \rightarrow W_3, \lambda_3 \rightarrow V_3, c_3^+, c_3^-$$

• Field Relations & Boundary Conditions

Taking into account the boundary conditions the values of the field inside the i th layer are given by the following relations.

Recall Equation (90) we have considering the figure (27) below:

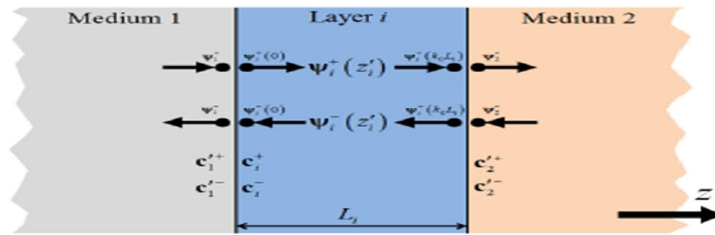


Figure 28: multilayer structure showing optical phenomena

$$\psi(\tilde{z}) = \begin{bmatrix} S_x(\tilde{z}) \\ S_y(\tilde{z}) \\ U_x(\tilde{z}) \\ U_y(\tilde{z}) \end{bmatrix} = \begin{bmatrix} W & W \\ -V & V \end{bmatrix} \begin{bmatrix} e^{-\lambda\tilde{z}} & 0 \\ 0 & e^{\lambda\tilde{z}} \end{bmatrix} \begin{bmatrix} c^+ \\ c^- \end{bmatrix} \quad (93)$$

Boundary conditions at the first interface:

$$\Psi_1 = \Psi_i(0)$$

$$\begin{bmatrix} W_1 & W_1 \\ -V_1 & V_1 \end{bmatrix} \begin{bmatrix} c_1'^+ \\ c_1'^- \end{bmatrix} = \begin{bmatrix} W_i & W_i \\ -V_i & V_i \end{bmatrix} \begin{bmatrix} c_1^+ \\ c_1^- \end{bmatrix} \quad (94)$$

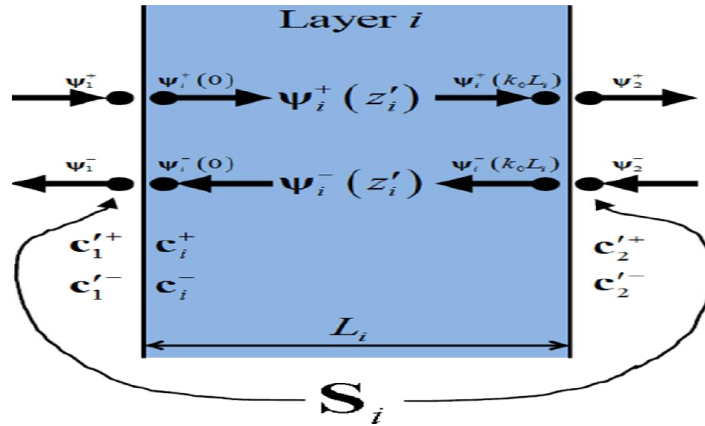
Boundary conditions at the second interface:

$$\Psi_1(K_0 L_i) = \Psi_2$$

$$\begin{bmatrix} W_i & W_i \\ -V_i & V_i \end{bmatrix} \begin{bmatrix} e^{-\lambda_i K_0 L_i} & 0 \\ 0 & e^{\lambda_i K_0 L_i} \end{bmatrix} \begin{bmatrix} c_1^+ \\ c_1^- \end{bmatrix} = \begin{bmatrix} W_2 & W_2 \\ -V_2 & V_2 \end{bmatrix} \begin{bmatrix} c_2'^+ \\ c_2'^- \end{bmatrix} \quad (95)$$

- **Adopt the Symmetric S-Matrix Approach**

The scattering matrix S_i of the i^{th} layer is still defined, considering from the figure (29) below as



:Figure 29: multilayer structure highlighting scattering phenomena free between two free space separated by a material medium (layer 1).

$$\begin{bmatrix} C_1'^- \\ C_2'^+ \end{bmatrix} = S^{(i)} \begin{bmatrix} C_1'^+ \\ C_2'^- \end{bmatrix} S^{(i)} = \begin{bmatrix} S_{11}^{(i)} & S_{12}^{(i)} \\ S_{21}^{(i)} & S_{22}^{(i)} \end{bmatrix} \quad (96)$$

But the elements are calculated as

$$s_{11}^{(i)} = (A_i - X_i B_i A_i^{-1} X_i B_i)^{-1} (X_i B_i A_i^{-1} X_i A_i - B_i) \quad (97.a)$$

$$s_{12}^{(i)} = A_i - (X_i B_i A_i^{-1} X_i B_i^{-1} X_i) A_i - (B_i A_i^{-1} B_i) \quad (97.b)$$

$$s_{21}^{(i)} = s_{12}^{(i)} \quad (97.c)$$

$$s_{22}^{(i)} = s_{11}^{(i)} \quad (97.d)$$

Note that Layers are symmetric so the scattering matrix elements have redundancy. Scattering matrix equations are simplified. Fewer calculations. Less memory storage.

- **Global Scattering Matrix**

By generalizing all the considerations made above on the other layers, we obtain globally a matrix equation of the scattering phenomena for all the layers.

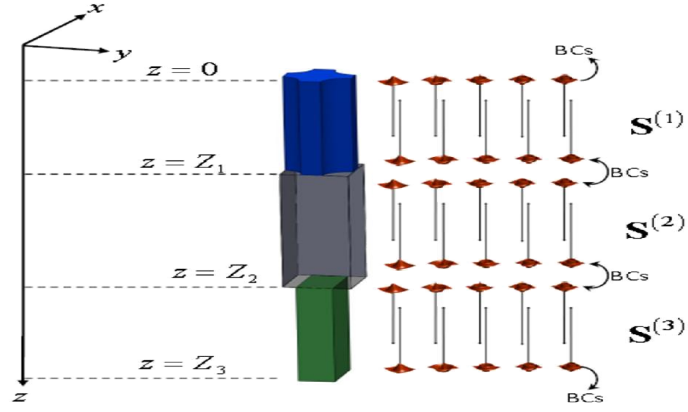


Figure 30: modes and scattering phenomena in all layers

First we write scattering matrix for all layers. By looking device, Equation (98).

$$\mathcal{S}^{(device)} = \mathcal{S}^{(1)} \mathcal{S}^{(2)} \mathcal{S}^{(3)} \quad (98)$$

Second according to figure 28, we write scattering matrix connection to outside regions and we get Equation (99).

$$\mathcal{S}^{(global)} = \mathcal{S}^{(ref)} \mathcal{S}^{(device)} \mathcal{S}^{(tm)} \quad (99)$$

Now we can address some essential properties for the optical color filters that are the reflection and the transmission.

- **Reflection/Transmission Side Scattering Matrices**

The reflection-side scattering matrix is given by relations (69) and (70) the scattering phenomena is explained by figure (31)

$$s_{11}^{(ref)} = -A_{ref}^{-1} B_{ref} \quad (100.a)$$

$$s_{12}^{(ref)} = 2 A_{ref}^{-1} \quad (100.b)$$

$$s_{21}^{(i)} = 0,5 (A_{ref} - B_{ref} A_{ref}^{-1} B_{ref}) \quad (100.c)$$

$$s_{22}^{(i)} = B_{ref} A_{ref}^{-1} \quad (100.d)$$

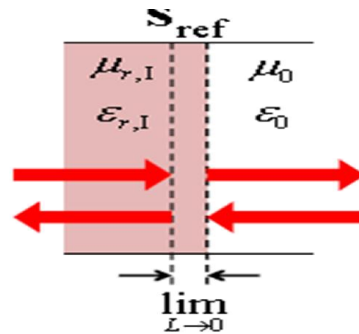


Figure 31: scattering phenomena when $\lim L=0$.

$$A_{ref} = W_0^{-1} W_{ref} + V_0^{-1} V_{ref} \quad (101.a)$$

$$B_{ref} = W_0^{-1} W_{ref} - V_0^{-1} V_{ref} \quad (101.b)$$

The transmission-side scattering matrix is according to figure (32)

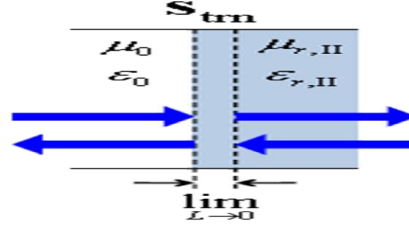


Figure 32: scattering phenomena explained transmission. When $L=0$.

$$A_{tm} = W_0^{-1}W_{tm} + V_0^{-1}V_{tm} \quad (102.a)$$

$$B_{tm} = W_0^{-1}W_{tm} - V_0^{-1}V_{tm} \quad (102.b)$$

$$s_{11}^{(tm)} = B_{tm}A_{tm}^{-1} \quad (103.a)$$

$$s_{12}^{(tm)} = 0, 5 (A_{tm} - B_{tm}A_{tm}^{-1}B_{tm}) \quad (103.b)$$

$$s_{21}^{(tm)} = 2 A_{tm}^{-1} \quad (103.c)$$

$$s_{22}^{(tm)} = -A_{tm}^{-1}B_{tm} \quad (103.d)$$

IV.1.7. Calculating transmission and reflection

The transmittance of a thin-film assembly is independent of the direction of propagation of the light. This applies regardless of whether the layers are absorbing.

A proof of this result, from Abelès [85], [86], who was responsible for the development of the matrix approach to the analysis of thin films, follows quickly from the properties of the matrices of thin film assembly.

The electric field source is calculated assuming unit amplitude polarization vector \vec{P} .

$$S_T^{(inc)} = \begin{bmatrix} p_x \delta_{0,pq} \\ p_y \delta_{0,pq} \end{bmatrix} C_{inc} = W_{ref}^{-1} S_T^{(inc)} \vec{p} = \begin{bmatrix} p_x \\ p_y \\ p_z \end{bmatrix} |\vec{p}| = 1 \quad (104)$$

Given the global scattering matrix, the coefficients for the reflected and transmitted fields are

$$C_{ref} = S_{11} C_{inc} C_{tm} = S_{21} C_{inc} \quad (105)$$

The transverse components of the reflected and transmitted fields are then

$$r_T = S_T^{(ref)} = W_{ref} C_{ref} = W_{ref} S_{11} C_{inc} r_T = \begin{bmatrix} r_x \\ r_y \end{bmatrix} \quad (106.a)$$

$$t_T = S_T^{(tm)} = W_{tm} C_{tm} = W_{tm} S_{21} C_{inc} t_T = \begin{bmatrix} t_x \\ t_y \end{bmatrix} \quad (106.b)$$

This is amplitude coefficients of the transverse components of the spatial harmonics, not reflectance or transmittance.

- **Calculating the Longitudinal Components**

The longitudinal fields components are calculated from the transverse components using the

divergence equation see Equation (60), (61), (62), (63) so we obtain these two relations (107), and (108).

$$r_z = -\tilde{K}_{z,ref}^{-1}(\tilde{K}_x r_x + \tilde{K}_y r_y)\tilde{K}_{z,ref} = -\left(\sqrt{\mu_{r,ref}^* \varepsilon_{r,ref}^* I - \tilde{K}_x^2 - \tilde{K}_y^2}\right) \quad (107)$$

$$t_z = -\tilde{K}_{z,ref}^{-1}(\tilde{K}_x t_x + \tilde{K}_y t_y)\tilde{K}_{z,tm} = \left(\sqrt{\mu_{r,tm}^* \varepsilon_{r,tm}^* I - \tilde{K}_x^2 - \tilde{K}_y^2}\right)^* \quad (108)$$

- **Calculating the Diffraction Efficiencies**

After having made and obtained these two Equations, we can then calculate the transmission and the efficiencies reflection, still called transmittance (**T**), and reflectance (**R**).

The diffraction efficiencies **R** and **T** are calculated as according to figure (33).

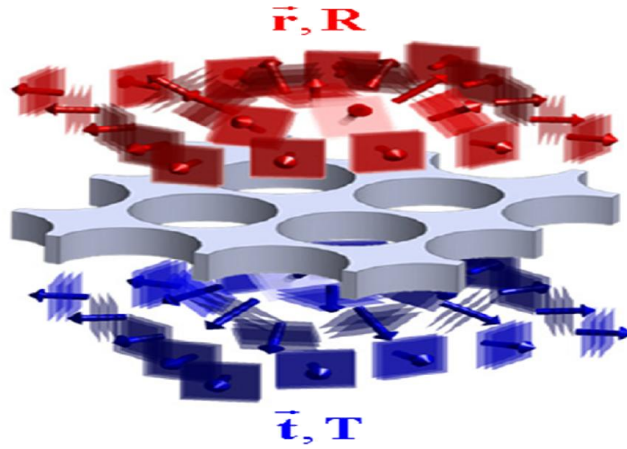


Figure 33: structure emphasizing reflection and transmission each in their plane.

$$|\vec{r}|^2 = |r_x|^2 + |r_y|^2 + |r_z|^2$$

$$|\vec{t}|^2 = |t_x|^2 + |t_y|^2 + |t_z|^2$$

$$\mathbf{R} = \frac{Re[-\tilde{K}_{z,tm}/\mu_{r,inc}]}{Re[k_z^{inc}/\mu_{r,inc}]} |\vec{r}|^2 \quad (109)$$

$$\mathbf{T} = \frac{Re[\tilde{K}_{z,tm}/\mu_{r,tm}]}{Re[k_z^{inc}/\mu_{r,inc}]} |\vec{t}|^2 \quad (110)$$

Note that these equations assume a unit amplitude source, and don't forget to reshape **R** and **T** back to 2D arrays.

- **Calculating Overall Reflectance and Transmittance**

The overall reflectance **R** and transmittance **T** are calculated by summing all of the diffraction efficiencies.

$$\mathbf{R} = \sum \mathbf{R} \quad (111)$$

$$\mathbf{T} = \sum \mathbf{T} \quad (112)$$

These two quantities can be represented in a logarithmic scale, by calculating the gain in

$$\text{decibels. } \mathbf{R}_{dB} = 10 \log_{10} \mathbf{R} \quad \mathbf{T}_{dB} = 10 \log_{10} \mathbf{T}.$$

- **Power Conservation**

It is always good practice to check for conservation of power.

$$A+R+T=1(113)$$

When no loss or gain (in a medium without absorption) is incorporated into the simulation(i.e.

$A = 0$), conservation reduces to

$$A+T=1(114)$$

We have now covered all the basic theory necessary for the understanding of the remainder of this work. It has been a somewhat long and involved discussion, so we summarize the principal results of the theory (34). We can finally successfully implement the concept of multispectral filter array-based nanofilms. There are fundamental difficulties associated with the definitions of reflectance and transmittance unless the incident medium is absorption-free.

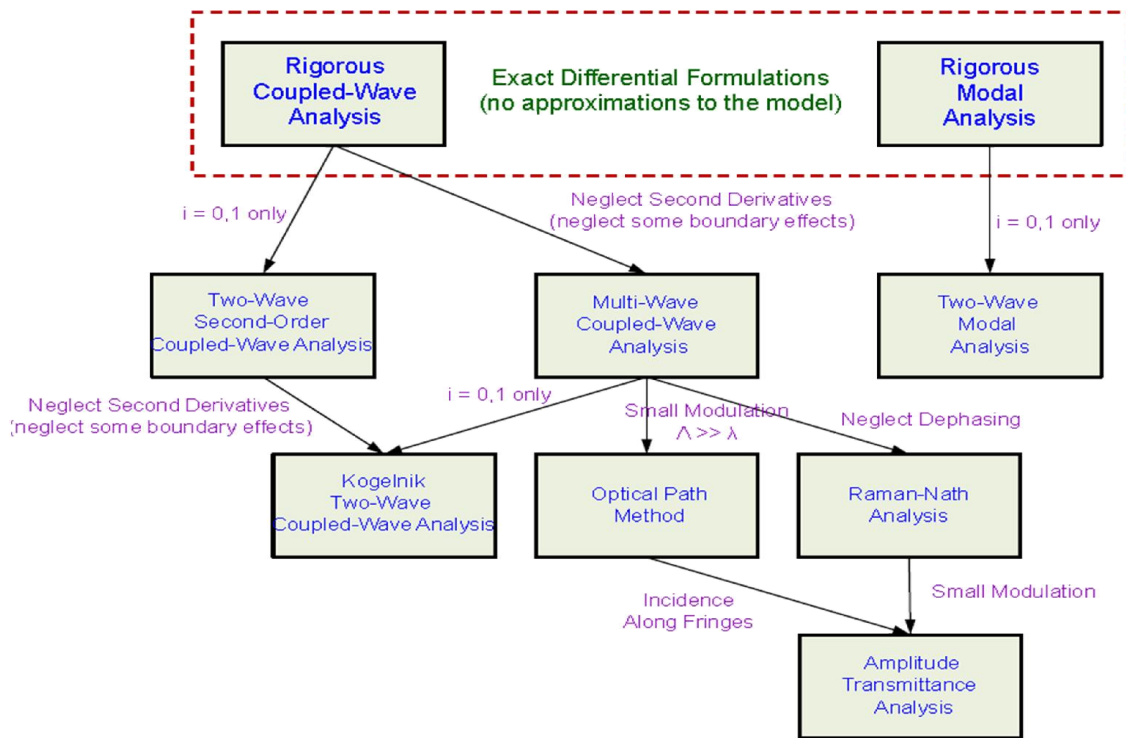


Figure 34: Differential Grating Diffraction Analysis Hierarchy

However, insight into the properties of thin-film assemblies cannot easily be gained simply by feeding the calculations into a computer, and insight is necessary if filters are to be designed and if their limitations in use are to be fully understood. Studies have been made of the properties of the characteristic matrices and some results that are particularly helpful in this context have been obtained. Approximate methods, especially graphical ones, have also been found useful. We find transmittance a rather less accessible parameter from the point of view of the theory than reflectance. Reflectance is immediately a function of the admittance of the front surface of the multilayer.

In the following section we present the second investigation approach adopted for our study.

This approach is experimental and focuses on the synthesis, the realization of nanofilms samples taking into account calculations, properties and technical considerations.

IV.2. experimental methods

In this section, we shall deal briefly with the fundamental process, the machines that are used for the thin-film deposition, and we shall discuss some aspects of the properties of thin-film materials. Subsequent sub section will include a more examination of some of the problems met in production.

Much of this paragraph is concerned with the properties of materials, ways of measuring them, and some examples of the results of the measurements of the important parameters. Probably the most important properties from the thin-film point of view are given in the following list, although the orders not that of relative importance, which will vary from one application to another.

1. Optical properties such as refractive index and region of transparency
2. The method that must be used for the production of the material in thin-film form
3. Mechanical properties of thin films such as hardness or resistance to abrasion, and the magnitude of any built-in stresses
4. Chemical properties such as solubility and resistance to attack by the atmosphere, and compatibility with other materials
5. Toxicity
6. Price and availability
7. Other properties that may be important in particular applications, for example, electrical conductivity or dielectric constant.

Item 5, 6, 7 are not ones on which we comment further here in this work. On the question of price and availability, item 6, also little can be said (chapter 1). The situation is changing all the time. Note, however, that price is of secondary importance to suitability. The cost of a failed batch of coatings is very great compared with the price of the source materials

There is a considerable number of processes that can be and are used for the deposition of optical coatings. A variety of thin films have to be deposited during the fabrication of electronic devices. The two most common deposition methods are physical vapor deposition (**PVD**) and chemical vapor deposition (**CVD**) due to their abilities to produce high quality, technologically advanced thin films in mass production. However, understanding, measuring, and controlling the properties of the resultant films is a complex process. Films can range from amorphous to single crystal, a single atomic layer to multilayer coatings, dense to porous, and have structural and chemical gradients, depending on the deposition conditions. Additionally, the materials being deposited along with their resulting structure and composition can lead to large changes in interfacial adhesion properties.

There is no handbook of mechanical and interfacial properties of deposited films, given the diversity of input parameters that dictate these quantities. These properties strongly depend on the details of the deposition process, details of film growth kinetics and mechanisms on the substrate, intermediate processes, and post-deposition processes. The ability to quantitatively measure mechanical and interfacial adhesion properties of ultra-thin films is of paramount importance to controlling thin film behavior and establishing process parameter limits.

The commonest take place under vacuum and can be classified as physical vapor deposition (PVD). In these processes, the thin film condenses directly in the solid phase from the vapor. The word “physical” as distinct from “chemical” does not imply the complete absence of chemical parameters in the formation of the film.

Chemical reactions are, in fact, involved, but the term chemical vapor deposition (CVD) is reserved for a family of technique where the growing film is formed by a chemical reaction between precursors so that the growing film differs substantially in composition and properties from the starting materials.

But at the laboratory of the ICB of the University of Burgundy, we have at our disposal machines capable of doing lithography. This is the technique we adopted for our experiments.

IV.2.1. Thin film deposition methods

- **Thin film? How thick is it?**

There are many methods to make things thin, some examples are shown here. The manufactures from optical thin film using deposition technologies as we said above that make film thickness $1\mu\text{m}$ and down to a few Å , as shown in figure 33 below.

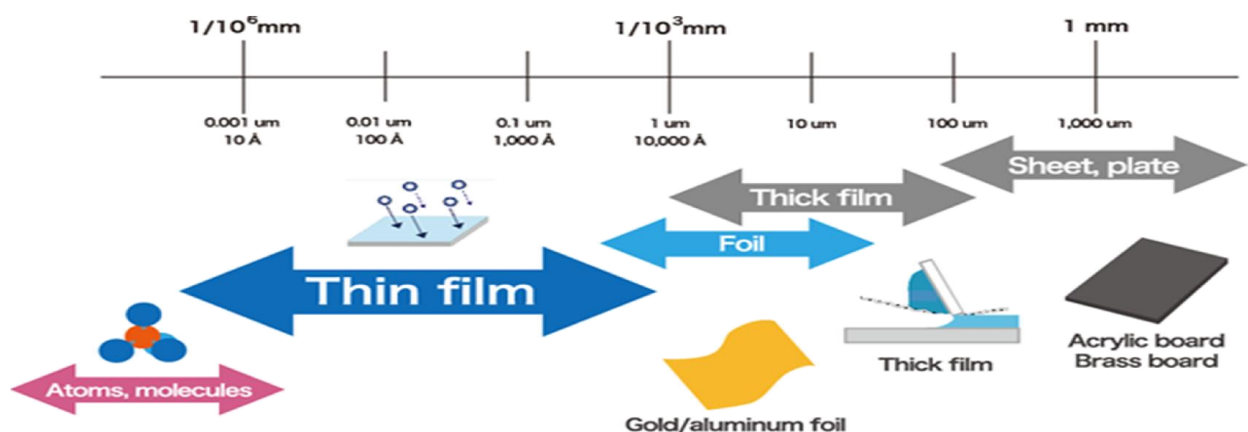


Figure 35: Highlighting the evolution of the thicknesses of thin film

- **Deposition methods**

In electronics, there are many thin film deposition methods. The manufacturers of nanofilms use several methods depending on the products and materials. Three main methods, sputtering,

plasma assisted chemical vapor deposition, and lithography are explained here as shown in figure 36.

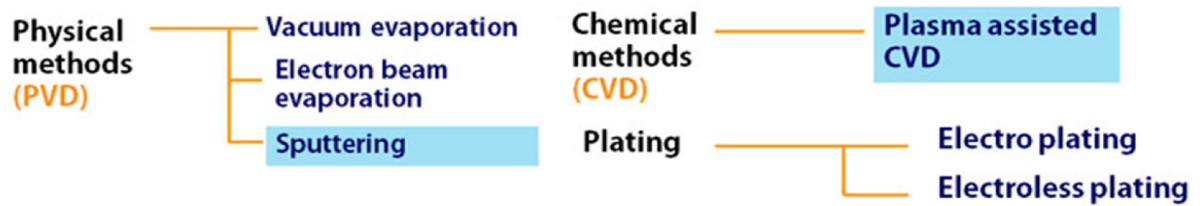


Figure 36: Principle of (PVD) and (CVD)

➤ **PVD method**

Argon ions, created by glow discharge under vacuum, sputter out target (materials for the thin film) atoms/molecules. These target atoms/molecules adhere to the substrates and form thin film. This method is ideal for depositing metal alloy thin films and high melting point materials.

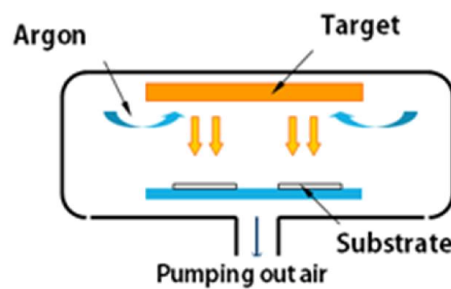


Figure 37: simplified mechanism of The PVD method

➤ **Plasma assisted Chemical Vapor Deposition (PCVD)**

In plasma (glow discharge), thin film precipitate after a series of chemical reaction. Thin film is formed under relatively low temperature. Any materials, organic or inorganic, that can be made into gas compounds can be deposited.

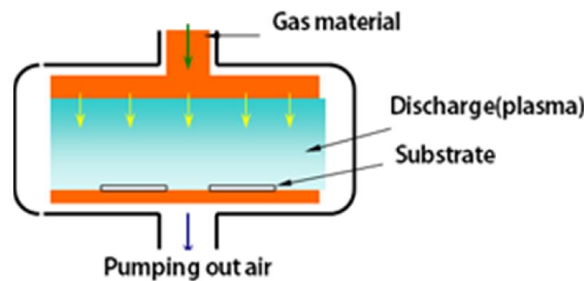


Figure 38: simplified mechanism of the PCVD method

➤ **Lithography**

Lithography is an intermediate process in electronic device fabrication. The mechanical and interfacial properties of the photoresist, as well as the potential effects of the photolithography process

on the underlying deposited film structure, need to be thoroughly characterized. Understanding the mechanical properties of the resist, such as the modulus of elasticity and glass transition temperature, are needed to assure the resist structures will withstand the various forces and environmental conditions encountered during processing.

Bruker has pioneered a comprehensive suite of test equipment and characterization techniques to enable quantitative nanoscale mechanical and interfacial adhesion measurements of thin films. Nanoindentation measurements are valuable in determining the elastic-plastic properties of thin films, and can be enhanced with dynamic measurement capabilities for viscoelastic property determination. Additional Bruker nanomechanical testing techniques provide the ability to quantify thin film interfacial adhesion properties. The ability to rapidly measure and control these properties on the nanoscale enables the material and process technologies required for next-generation electronic devices.

Lithography is one of the 4 major processes in the top-down model Lithography Etching Deposition Doping. In order to perform the other 3 processes, we must precisely define where to do them Lithography does This! In the top-down model, we use these 4 processes to create features in certain areas of the substrate. The thin film patterns created in lithography can mask the substrate from being etched by strong chemicals or define areas where metal layers can be added for wiring. With doping, we change the physical properties of certain areas of the substrate. Lithography also masks off areas for this process.

IV.2.2. Experimental process: Lithography's Key Role in the Process

With multiple etch, deposition, and doping processes taking place in the fabrication of a device, the lithography process is repeated many times. The precision and accuracy of lithography in the manufacturing process controls, to a first degree, the success in building a device. The lithography process is repeated many times during fabrication of a device, since there are often several "layers" of materials added to a substrate. With this multilayer manufacturing method, if one layer doesn't line up with the one below it or if the areas overlap each other, the final device will not work.

IV.2.2.1. Principles and methods

The lithography module, typically lithography is performed as part of a well-characterized module which includes the wafer surface preparation; photoresist deposition alignment of the mask and wafer, exposure, develop and appropriate resist conditioning.

Silicon wafers are commonly used substrates in the top-down process. The first step is to coat the clean surface of the wafer with a light sensitive chemical emulsion known as photoresist by exposure to radiant energy. Typically, the photoresist chemicals are in a liquid solution that is applied to a silicon wafer in a device called a spinner. The silicon wafer must be clean, flat, and dry in order for

the spin process to create a flat, uniform coating of the resist. If the coating is not uniform, the pattern created will not be even (planar). Gaps or holes in the coating may allow chemicals and other physical processes to “seep through” areas where they should not be occurring and cause the device to be rejected. The “recipe” that defines the speed, temperature of the wafer and timing for each part of the spinning process is unique to the photoresist being applied. This is schematically illustrated in Figure 39 is the key technology for microstructure scaffold fabrication.

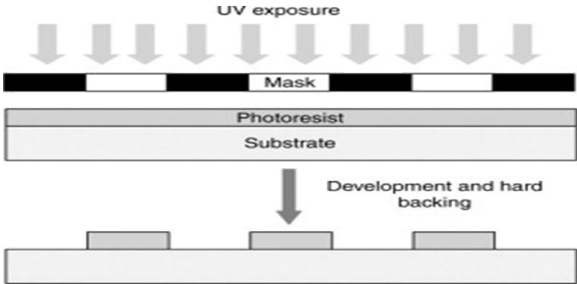


Figure 39: Schematic illustration of Lithography

These techniques can produce micro features as small as possible. Recent advances in X-ray, electron- and ion-beam lithography, nanoparticles lithography, soft lithography, colloidal lithography, and microcontact printing (μ CP) and nanocontact printing have broken the wavelength barrier to prepare patterns as small as 300 nm. To distinguish between micro and nanolithography, techniques capable of producing feature sizes of 100 nm or smaller are defined as nanolithography.

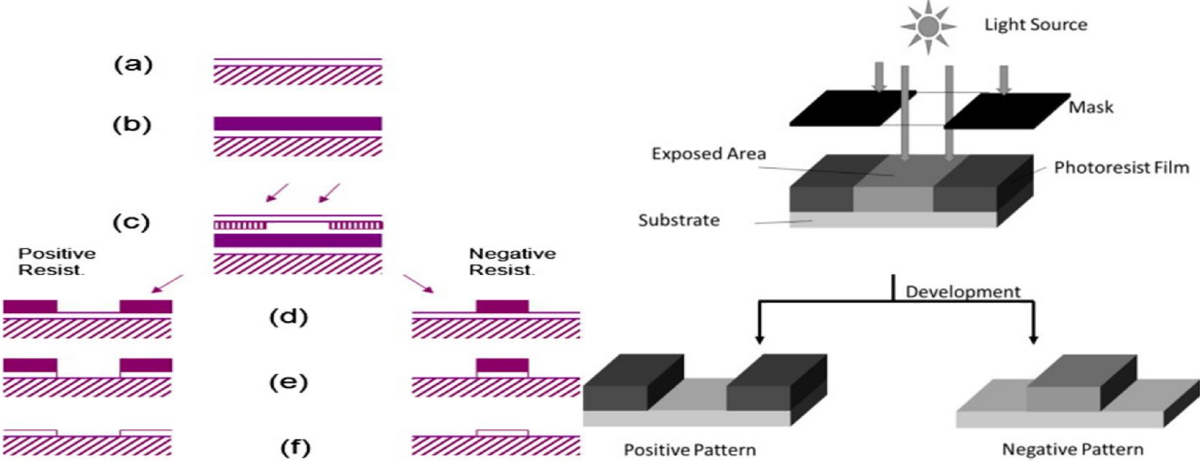


Figure 40: Schematic diagram of a Lithographic, process to transfer a positive or negative image onto a substrate.

IV.2.2.2. The general sequence of processing steps

The general sequence of processing steps for a typical photolithography process is as follows: substrate preparation, photoresist spin coat, prebake, exposure, post-exposure bake, development, and post bake. A resist strip is the final operation in the lithographic process, after the resist pattern has been transferred into the underlying layer. This sequence is shown diagrammatically in Figure 43, and

is generally performed on several tools linked together into a contiguous unit called a lithographic cluster. A brief discussion of each step is given below, pointing out some of the practical issues involved in photoresist processing.

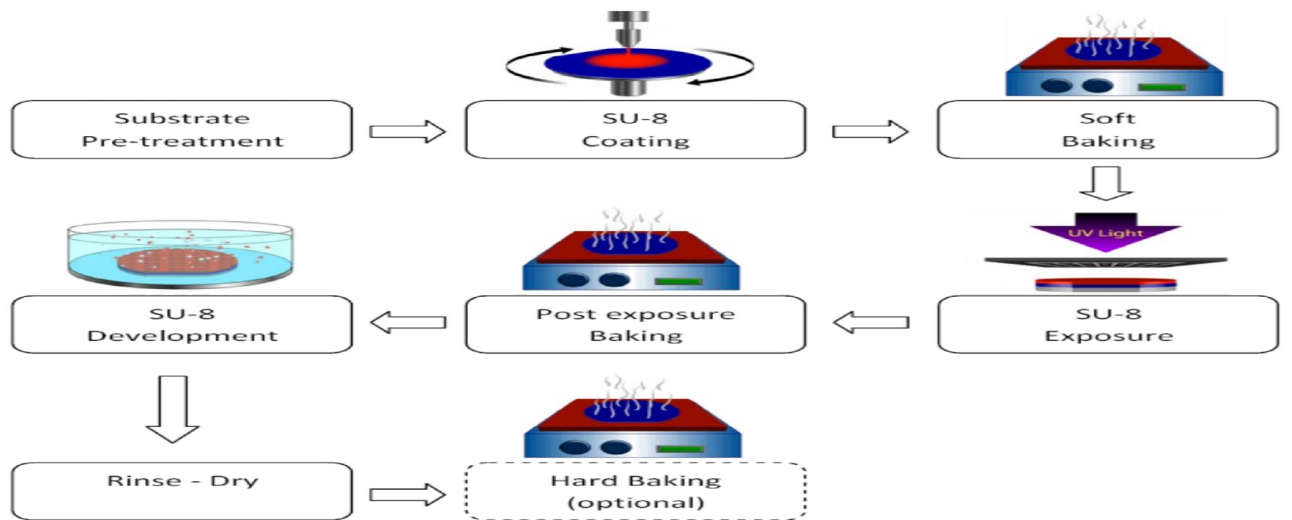


Figure 41: General sequence of processing steps for a typical photolithography process

IV.3. Application of RCWA, and experimental study of silver, gold, germanium nanofilms filters.

In order to optimize the optical quality of the materials used in the production of color filter, we started the study and characterization of the optical properties of thin film materials of Germanium (Ge), Silver (Ag), and Gold (Au).

In this work, the method of determine optical characteristics that we have developed for multilayer thin transparent Ge, Ag, Au is based on the expressions of the reflectance R and optical transmittance T established by Abeles [85] and RCWA. Which are applicable to homogeneous layers with parallel faces and deposited on non-absorbent substrates. The thin film filters usually consist of a number of boundaries between various homogeneous media, and it is the effect of these boundaries on an incident wave that we will calculate. A single boundary is the simplest case.

First we consider absorption free media, i.e., $k = 0$.

The arrangement is sketched in figure 40. A plane harmonic wave is incident on a plane surface separating the incident medium from a second, or emergent, medium. The plane containing the normal to the surface and the direction of propagation of the incident wave is known as the plane of incident and the sketch corresponds to this plane. We take the z -axis as the normal into the surface in the sense of the incident wave and the x -axis as normal to it and also in the plane of incidence.

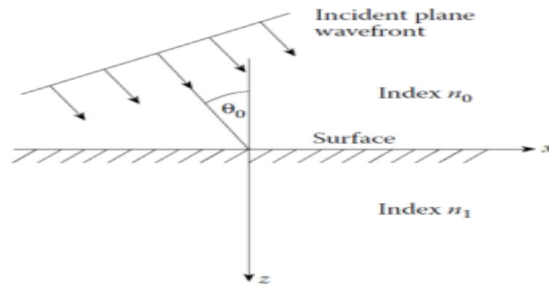


Figure 42: Plane wave front incident on a single surface.

At a boundary, the tangential components of E and H along the boundary are continuous across it because there are no mechanisms that will change them [84] figure 43.

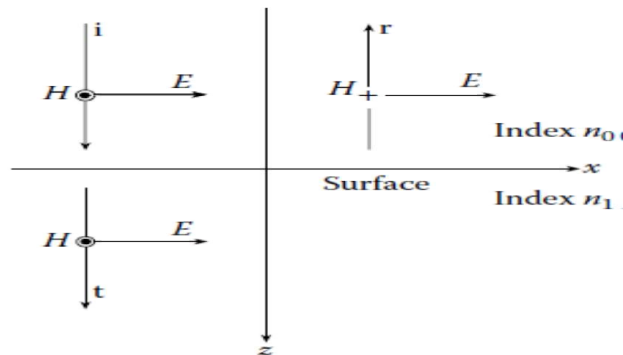


Figure 43: orientation of the components of the electromagnetic fields of the incident wave: case of normal incidents.

For the case of oblique incidents Figure 44, the application of the boundary conditions leads us into complicated and difficult expressions for the vector amplitudes of the reflected and transmitted waves. Fortunately, there are two orientations of the incident wave that lead to reasonably straightforward calculations; by using Mie or RCWA theory we fine up the solution.

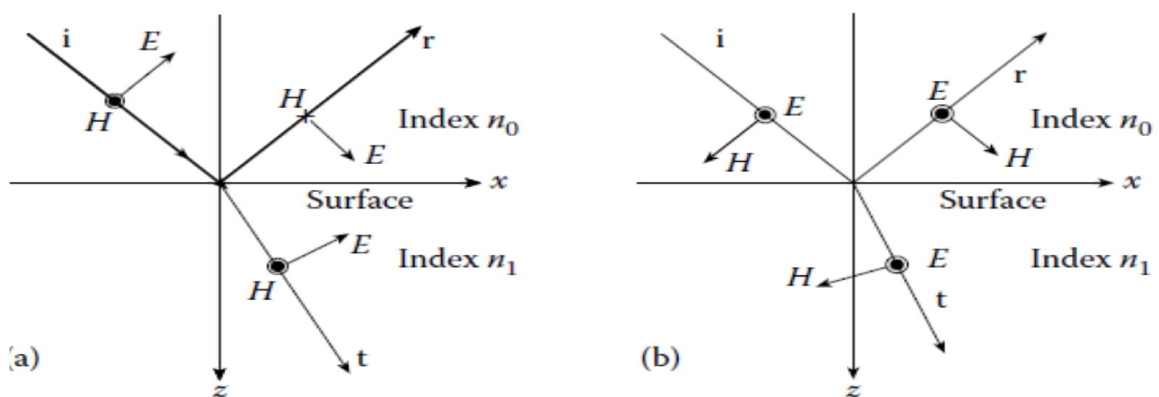


Figure 44: (a) Convention defining the positive directions of the electric and magnetic vectors for p-polarized light (TM waves); (b) Convention defining the positive directions of the electric and magnetic vectors for s-polarized light (TE waves).

Our objective is to obtain the calculation of the relative parameters of the three waves: incident, reflected, and transmitted. However, this introduces a further complication. We will use the

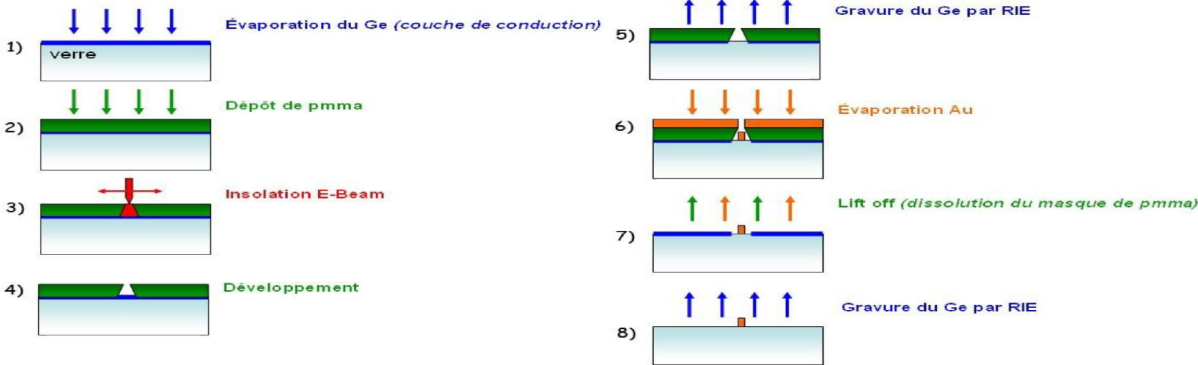
boundary conditions to set up a set of equations from which we will extract the required relations and the algorithm of calculation by using RCWA theory to define electromagnetic field. The optical properties of metal layers are influenced by their thickness and topography. This occurs especially when the layers reach nanometric dimensions and when inserted in resonant systems [85].

Our study focuses on layers of silver, germanium and gold. It has been shown that thin metal nanoscale behaves in reflection and transmission completely different from that of the bulk material. In particular, the real part as the imaginary part of the refractive index is changed [86]. The experimental analysis of the samples of thin layers of gold, silver and germanium in order to obtain the optical properties is performed by a monochromatic, and Mie spectroscopy.

To calculate and compute the optical response of a stack of thin layers, we use the matrix representation of Abeles and that derived from the RCWA model RCWA described in the paragraph above. That models each thin layer of a matrix used to express the transformation of electric and magnetic fields in the portion of the thin layer equations ((93), (94), (95), (96), (90), (109) (110)).

The thickness of each layer is a crucial parameter of the equations. There is no question of reversing the steps to go back to the index and layer thickness. It is therefore necessary to solve the system: $R = f(n_i, k_i, d_i)$ and $T = g(n_i, k_i, d_i)$ for each wavelength. You must know this fact all the unknowns except 2! The continuity equations of electromagnetic fields at the interfaces of the system as possible to establish an expression for the amplitudes of the reflection and transmittance, with n_0 , n_s , respectively indices output settings (substrate) and input (air) see equations (109), (110).

We investigate theoretically (computational methods simulation) and experimentally transmission color filters using nanostructured thin film (NSTF) of Germanium (Ge), silver (Ag) and Gold (Au) gratings on glass substrates. Each grating area is $100\mu\text{m}$ -square, which is a suitable pixel size for display and multichannel detectors. In the fabrication, electron beam lithography is used. Lithography is a technique to transfer patterns from either a master hard mask or a master soft mask (computer layout) to a photon or charged-particle sensitive polymer film (known as resist) coated on the substrate to which the pattern ought to be transferred [86] figure 45.



CHAPTER V: THEORETICAL SIMULATION, EXPERIMENTAL SETUP: RESULTS AND DISCUSSION

The British research company Edmund Optics Ltd [87] recalls that although filters share many specifications with other optical components, there are a number of unique specifications specific to optical filters that must be known and understood in order to determine the best filter, suitable for an application. In this article, he describes a Terminology concerning filters. These specifications are: Central Wavelength (CWL); Bandwidth; Full Width-Half Maximum (FWHM); Slope; Cut-On Cutting Wavelength; Cut-Off Cutting Wavelength and Reflectivity.

- **Central Wavelength (CWL)**

The central wavelength, used in the qualification of band-pass filters, corresponds to the wavelength having the maximum transmittance over the whole spectrum chosen.

- **Bandwidth**

Bandwidth is a range of wavelengths used to designate a specific part of the spectrum in which 50% of the energy is transmitted. Bandwidth is also called FWHM

- **Full Width-Half Maximum (FWHM)**

The width at half height designates the spectral band over which a notch filter transmits. The upper and lower limits of this band are defined at the wavelength level where the filter reaches 50% of the maximum transmission.

- **Slope**

Slope is a specification often defined on cutoff filters, such as low pass and high pass filters, to describe the bandwidth over which the filter goes from high blocking to high transmission (and vice versa). Indicated as a percentage of blocking wavelength, the slope can be specified from a multitude of start and end points.

- **Cut-On Cutting Wavelength**

Cut-On Wavelength is a term used to refer to the wavelength from which the transmission will be greater than 50% in a high-pass filter.

- **Cut-Off Cutting Wavelength**

Cut-Off Cutting Wavelength is a term used to refer to the wavelength from which the transmission will be less than 50% in a low-pass filter.

- **Reflectivity**

In the case of interference filters, light travels through a lower index material and is reflected on a higher index material. Only light from a certain angle and wavelength will constructively

interfere with the incoming beam and pass through the material, while any other light will destructively interfere with and reflect on the material. The following figure illustrates this phenomenon.

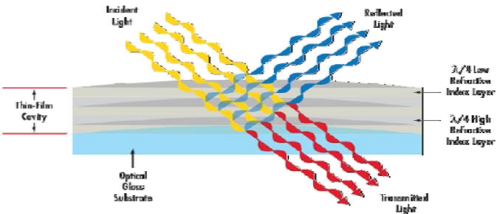
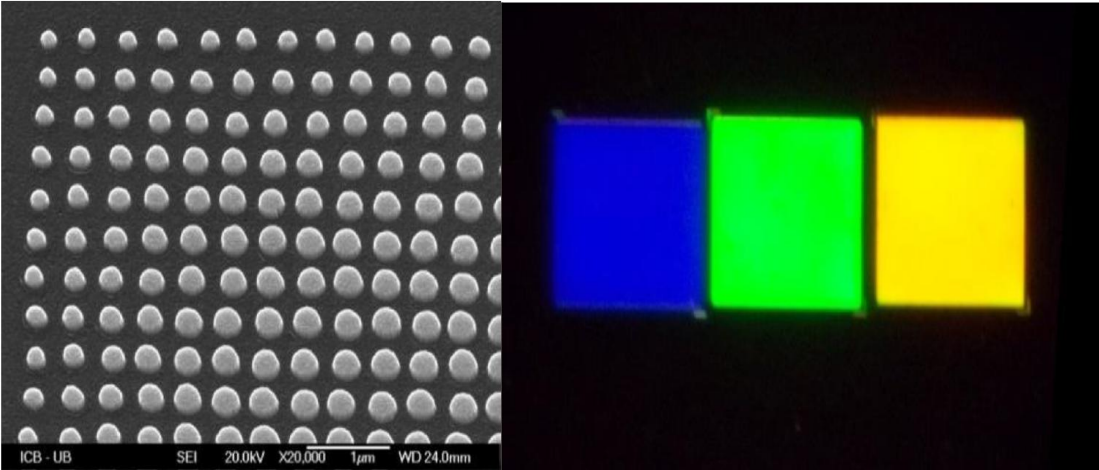


Figure 46: Light path in a laminate material

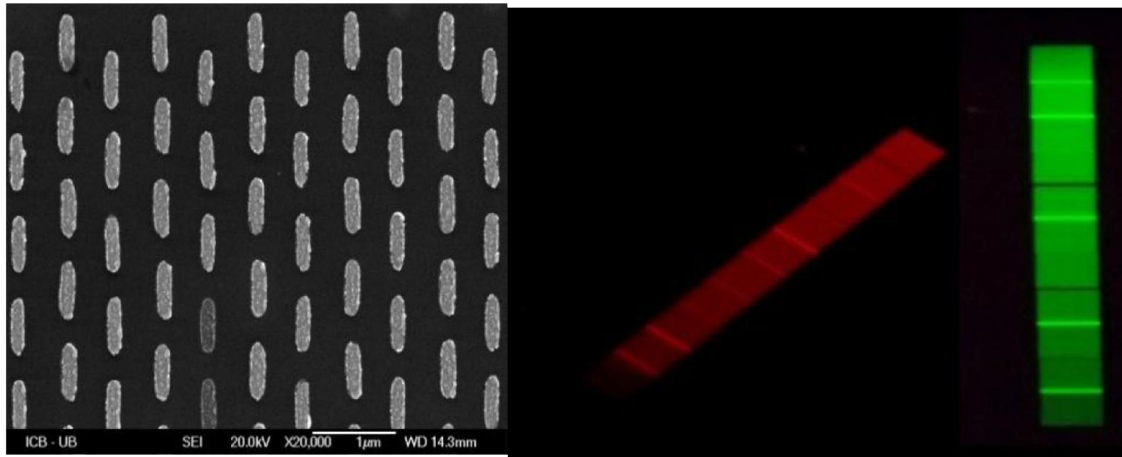
V.1 global results

The RCWA method an algorithm optimization described in the previous section was implemented in MATLAB. For each of the three materials structures in figure 48, the algorithm was used to optimize values of the grating period, filing factor and grating thickness as the angle of incident light θ was increased from 0° to 45° over the wavelength range of 380nm to 1100nm. Having obtained the optimal design parameters for each of the three materials (reflectance, transmittance, absorbency) we have evaluated and compared the properties of each devices in terms of their reflectance and transmission efficiencies and extinction ratios. The simulation parameters for the reflectance the transmittance and of the absorbency of the three materials are: The indices of refraction for different metals Ge=4 Au=1.74 Ag=0.1. Numbers of undercoat =2. The refractive indices of the layers in layer 1=1.5, layer 2= 1.52, the thickness of the under layer. Thickness of layer 1=350nm. Thickness of layer 2=175nm.



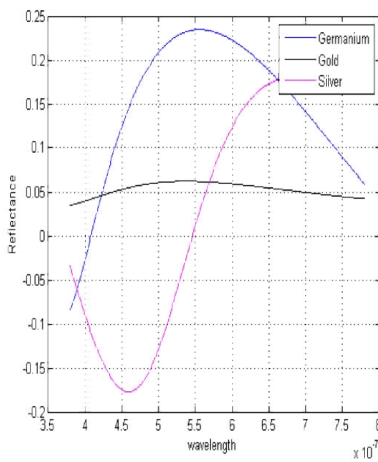
(a)

(b)

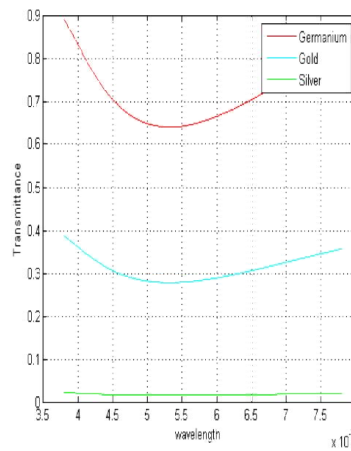


(c)

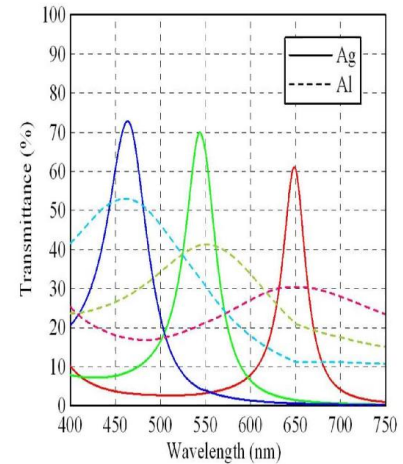
(d)



(e)



(f)



(g)

Figure 47: (a) Cartoon illustration of nanoshell fabrication; (b) Electron microscope observation noted intensities vivid colors; (C) SEM image of nanoshell arrays; (d) Electron microscope observation; (e) Reflectance of the thin layers of Ag, Au, and Ge; (f) Transmittance of the thin layers of Ag, Au, and Ge, (g) transmittance of Ag, and Al with R, G, B

The theoretical and experimental researches on multilayer are many [85]. Theoretical models for the calculation of reflection, transmittance, and a multilayer absorbency have been developed and adjusted based on experimental results. To search for peak reflection at large angles of incidence, these models use the structure factor of the material which appears in the elements of the characteristic matrix connecting the electromagnetic fields at the entrance and exit of the material. The matrix is obtained from the equations of continuity of the electromagnetic field, written at the interfaces of the multilayer. In our case, figures 47 (e), (f) and (g) shows the simulation results of the three materials studied. It appears that in Figure 47 (e), for wavelengths between 350 nm and 750 nm, the reflectance which varies a little (constant) compared to the other two materials. Ag has a low reflectance for wavelengths between 380 nm and 500 nm, which believes in following the higher wavelengths. Ge has a reflectance which is believed to 380 nm to 550 nm which is a maximum and

then decreases to high wavelengths.

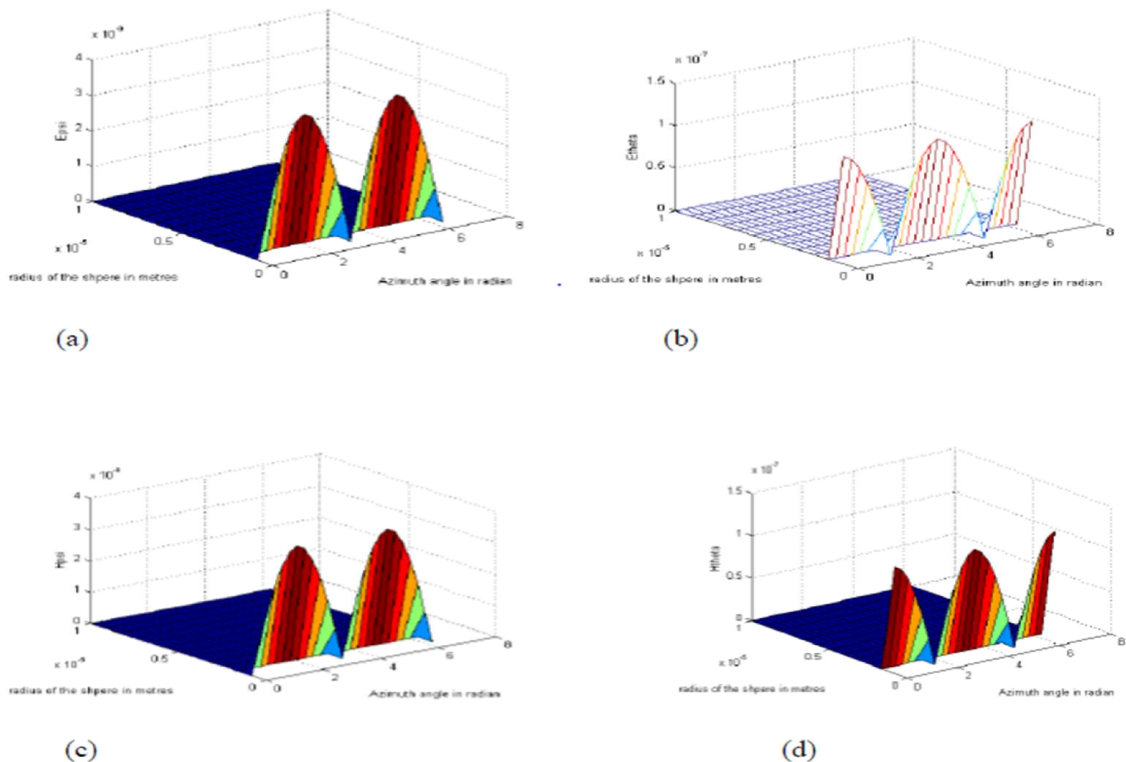
Figure 47 (f), shows a transmittance close to zero for Ag, Au medium, and high for Ge in the visible spectrum. Figure 47 (g) has a zero absorbency for germanium, average for gold and high to silver. Optical properties depend on the ratio $n_i d_i / \lambda$. Changes in optical properties are increasingly steep toward shorter wavelengths.

V.2. 3D Electromagnetic wave simulation using RCWA

The indices of refraction for different materials Ge=4, Au=1.74, Ag=0.1. Size parameter 0.2. Initial sequence of Legendre polynomials =1. Amplitude max of electric field $E_0 = 1V/m$. Amplitude max of magnetic field $H_0 = 1H/m$. The azimuth angle in radians = $\pi/4$. Radius of the sphere = 10. Wavelength of incidence = 700nm. The simulation results are shown in figure 48.

• 3D simulation for germanium material

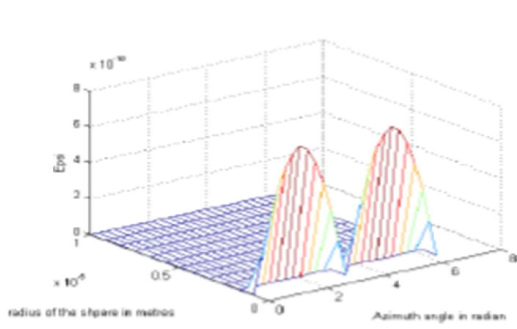
We present the evolution of the electric and magnetic fields in the figures 48 ((a), (b), (c), (d)) below obtained by 3-D simulation taking into account the amplitude, the radius of spheres of the Germanium layers and the angle of incidence of the light beam.



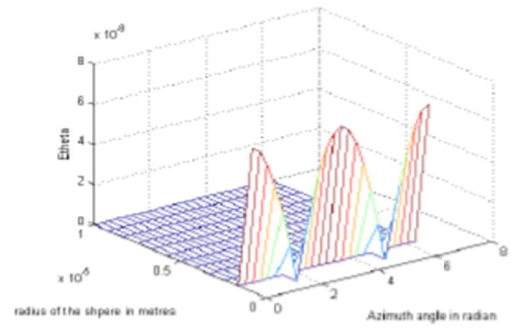
• 3D simulation for silver material

The evolution of the electric and magnetic fields is shown in the figures 48 ((e), (f), (g), (h)) below obtained by 3-D simulation taking into account the amplitude, the radius of spheres of the silver layers and the

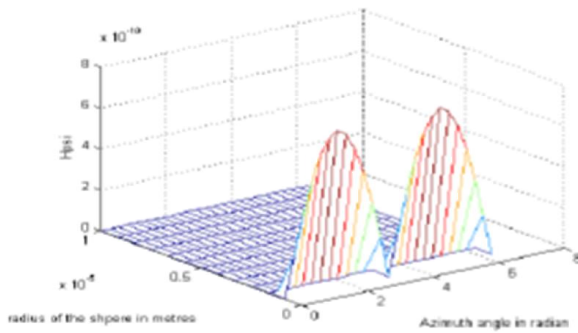
angle of incidence of the light beam.



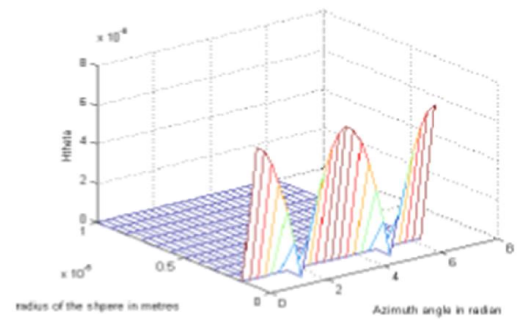
(e)



(f)



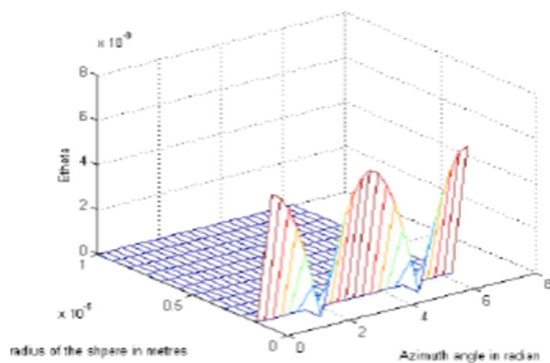
(g)



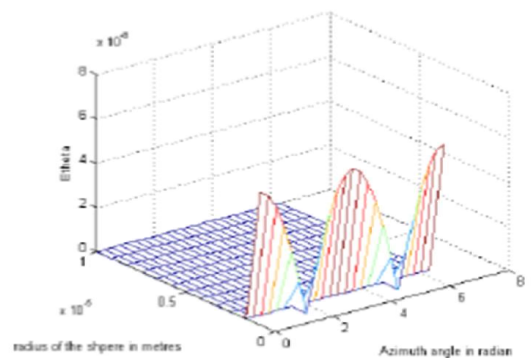
(h)

- **3D simulation for gold material**

The figures 48 ((i), (j), (k), (l)) below obtained by 3-D simulation taking into account the amplitude, the radius of spheres of the gold layers and the angle of incidence of the light beam highlight the evolution of the electric and magnetic fields.



i)



(j)

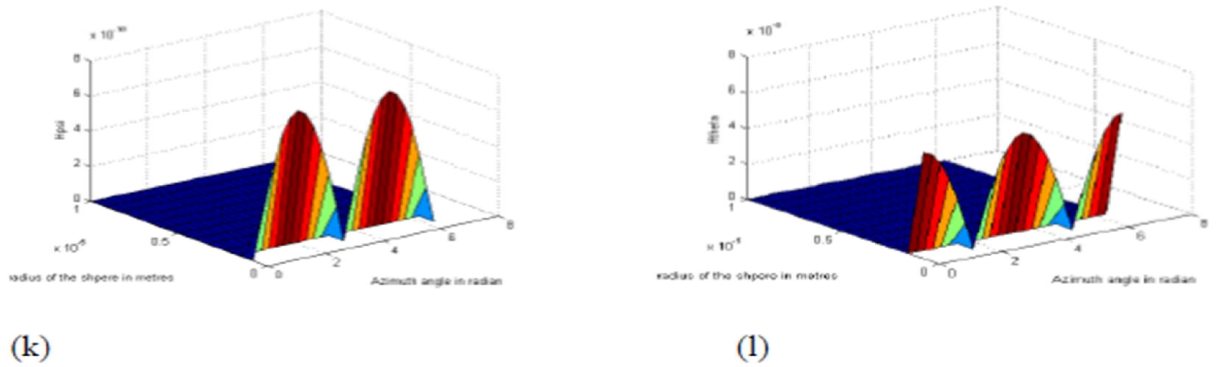


Figure 48: 3D simulation of electric and magnetic field for the three materials; (a) E_{psi} field intensity of Ge; (b) E_{theta} : field intensity of Ge; (c) H_{psi} field intensity of Ge; (d) H_{theta} field intensity of Ge; (e) E_{psi} field intensity of Ag; (f) E_{theta} field intensity of Ag; (g) H_{psi} field intensity of Ag; (h) H_{theta} field intensity of Ag; (i) E_{psi} field intensity of Au; (j) E_{theta} field intensity of Au; (k) H_{psi} field intensity of Au; (l) H_{theta} field intensity of Au.

Figure 49 highlights the 3D simulation of the distribution of electromagnetic energy on a thin film structure made up of the metamaterials used.

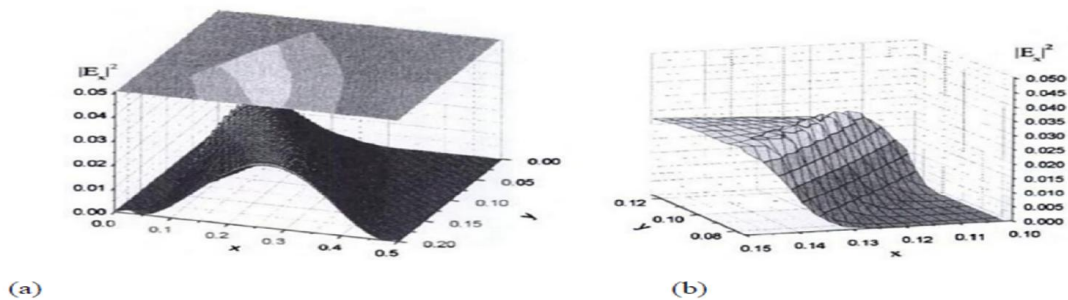


Figure 49: spatial distribution of $|E_x|^2$ calculated for non-discretized sinusoidal profile in TM polarization (a) the entire groove, and (b) the same region as multilayer.

V.3. Transmittance, Reflectance and Absorbance of each material

We present in this part the results obtained by simulations according to parameters defined for experimentation. These parameters are as follows:

- In oblique illumination $\theta = 10^\circ, \theta = 15^\circ, \theta = 25^\circ$,
- The thicknesses of each layer are Ge = 350 nm, Au = 175 nm, AG = 190 nm.

The different results are highlighted in the diagram below

V.3.1 case of germanium thickness 350 nm

Oblique illumination: $\theta = 10^\circ, \theta = 15^\circ, \theta = 25^\circ$.

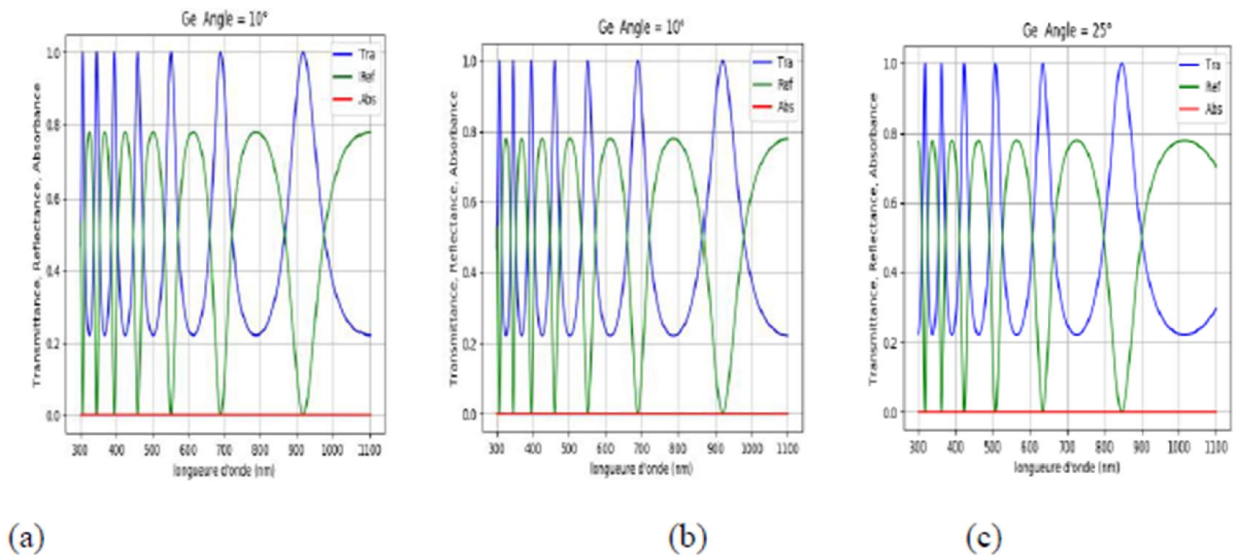


Figure 50: diagram showing variation on transmittance, reflectance and absorbance Germanium in different illumination angle (a) 10° (b) 15° (c) 25° .

By scanning the electromagnetic spectrum from 300 to 1100 nm, we notice that this material has a very low absorption. It varies according to the wavelength bands in the spectrum and has infinitesimals of $2 \cdot 10^{-16}$ close to zero. Which proves that all the energy received is transmitted or reflected. As a result, transmittance and reflectance are important in proportion of 1. We can therefore conclude that the material is operable for the manufacture of electronic components.

V.3.2. Case of gold

Oblique illumination: $\theta = 10^\circ, \theta = 15^\circ, \theta = 25^\circ$.

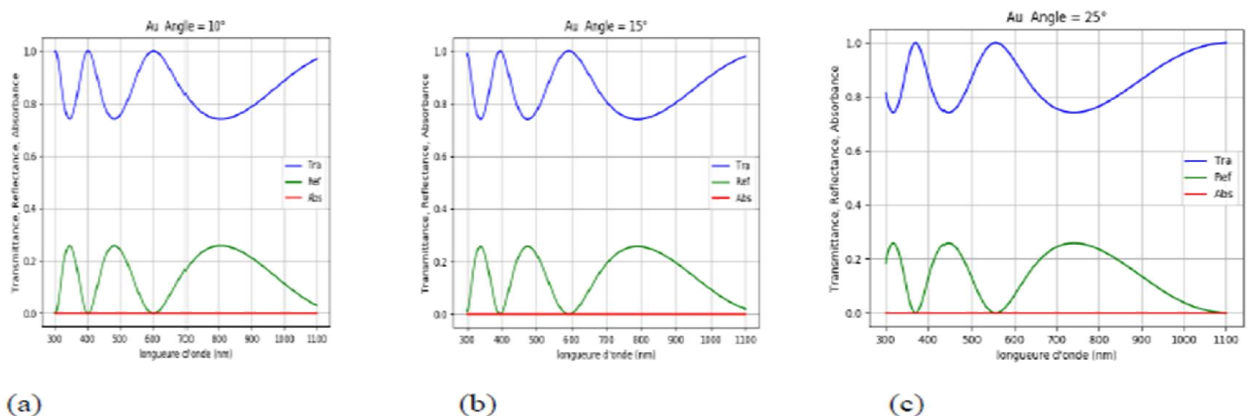


Figure 51: diagram showing variation on transmittance, reflectance and absorbance Germanium in different illumination angle (a) 10° (b) 15° (c) 25°

By scanning the electromagnetic spectrum from 300 to 1100 nm, we notice that gold has a

very low absorption. It varies according to the wavelength bands in the spectrum and has infinitesimals values of 2.10^{-16} the maximum, and $1.5.10^{-16}$ for the minimum for a reference value of 1, so very close to zero. Which proves that all the energy received is transmitted or reflected. As a result, transmittance and reflectance are important in proportion of 1. We can therefore conclude that the material is operable for the manufacture of electronic components.

V.3.3. Case of silver

Oblique illumination: $\theta = 10^\circ, \theta = 15^\circ, \theta = 25^\circ$.

In the case of the silver material, the absorption is almost a linear straight line increasing from $0.2.10^{-16}$ to the limit of the spectrum. It is always in the range of $1.2.10^{-16}$. Therefore, almost all of the radiating energy is either transmitted or reflected by this substrate.

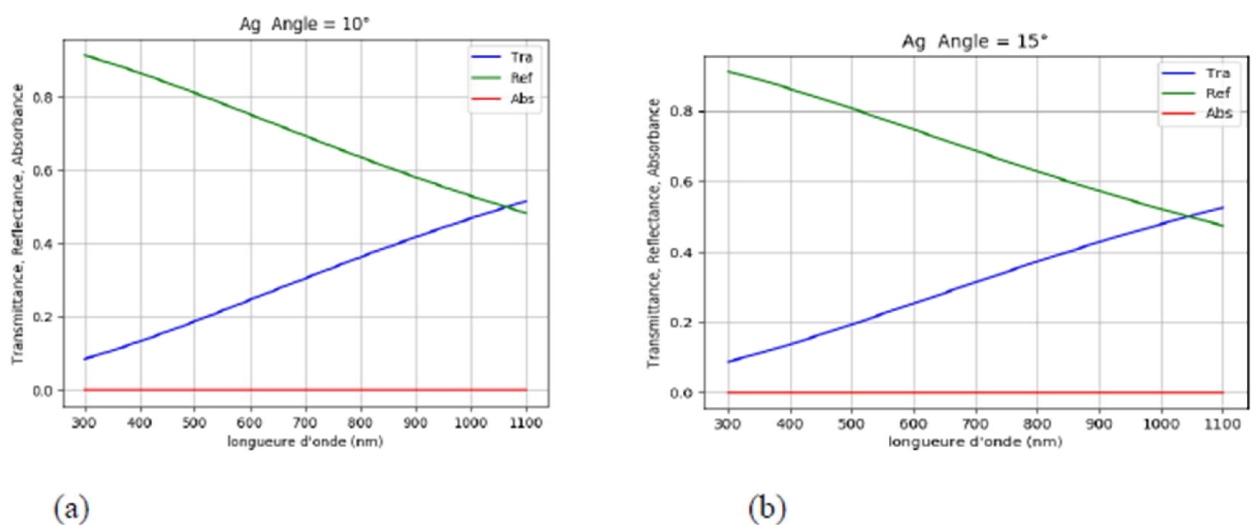


Figure 52: diagram showing variation on transmittance, reflectance and absorbance Germanium in different illumination angle (a) 10° (b) 15° .

V.4. Transmittance, Reflectance and Absorbance of multilayer system

In the following simulation cases, we consider three combinations of materials out of nine possible, to produce three multilayer samples by lithography method. The respective thicknesses are defined above; the indices of the materials as well as the angle of incidence of the illumination beam $\theta = 35^\circ$.

V.4.1. Case of multilayer combination of material: Ge-Au-Ag.

Oblique illumination: $\theta = 35^\circ$.

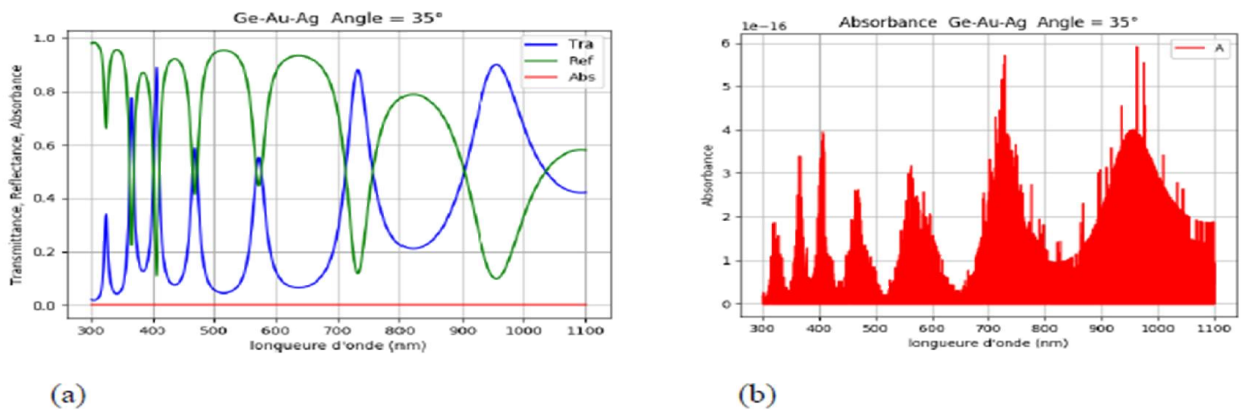


Figure 53: diagram showing variation on transmittance, reflectance and absorbance of a multilayer sample Ge-Au-Ag with different thickness (a), and absorbance of the sample (b).

V.4.2. Case of multilayer combination of material: Au-Ge-Ag.

Oblique illumination: $\theta = 35^\circ$.

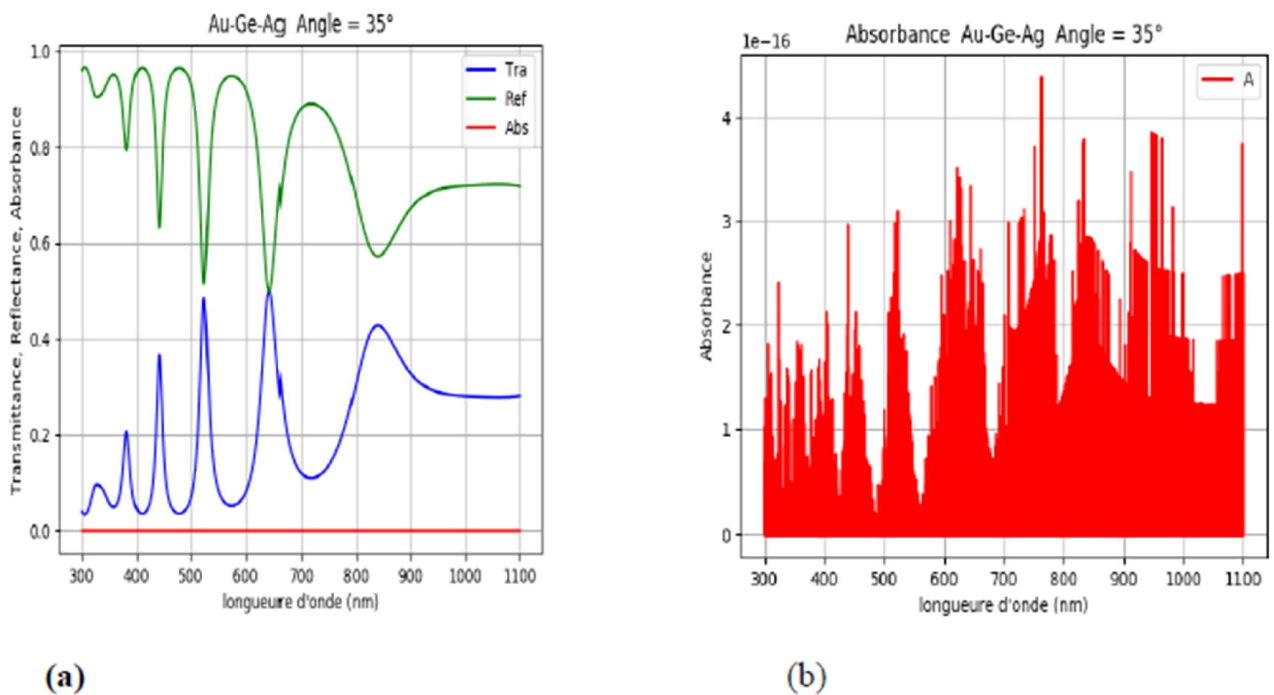


Figure 54: diagram showing variation on transmittance, reflectance and absorbance of a multilayer sample Au-Ge-Ag with different thickness (a), and absorbance of the sample (b).

V.4.3. Case of multilayer combination of material: Ag, Au, Ge.

Oblique illumination : $\theta = 35^\circ$.

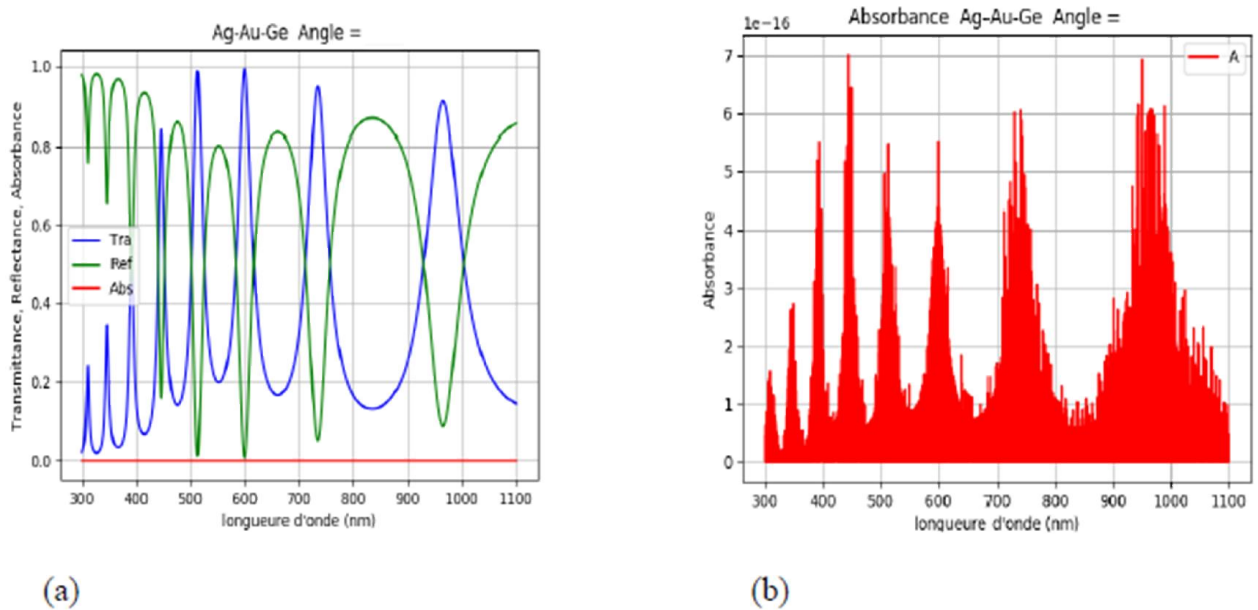


Figure 55: diagram showing variation on transmittance, reflectance and absorbance of a multilayer sample Au-Ge-Ag with different thickness (a), and absorbance of the sample (b).

V.5. Analyze and discussion

The most common metallic materials with a high reflective layer within the full-range wavelength visible light spectrum are Al and Ag. Hence, this study investigated the optical properties of combination of Au, Ge and Ag films. Figures.47, 51, 52, 53, 54, 55, shows the transmittance spectrum of R, G, and B with an (Ag, Ge, Au) film of 30 nm thickness, combine (Au, Ge, Ag) film of 15 nm, and Ag film from 100 to 170 nm. Simulation results show that the Ag film provided a better transmittance spectrum than the Al film across a range of (Ag, Au, Ge) film thicknesses. Because Ag has higher reflectivity and optical transmittance than Al [87], we selected Ag film as the reflective layer material for our three-layer sandwiched color filter. Figure47 (g), shows the effect of the Ag thickness (upper and lower layers with same thickness) on the transmittance and peak wavelength of the R, G, and B filters, using combine (Au, Ge, Ag) films of various thicknesses. The simulation results show that when the thickness of Ag reaches 25 nm, it provides higher transmittance with R,G, and B color filters.

After, the first part of the work (chapter 1,2 and3).We were able to determine geometrical parameters allowing us to realize adapted planar diffraction gratings allowing the separation of the wavelengths of the visible and the PIR.

Firstly, we made a PMMA mask (PolyMethylMethAcrylate) by electron beam Lithography.

This technique makes it possible to insulate a thin layer of photosensitive resin and then the parts insulated by the electron beam, not adherent to the substrate, are removed by rinsing with trichloroethylene. The layer of material used to carry out our network geometry by evaporation is then deposited figure 56.

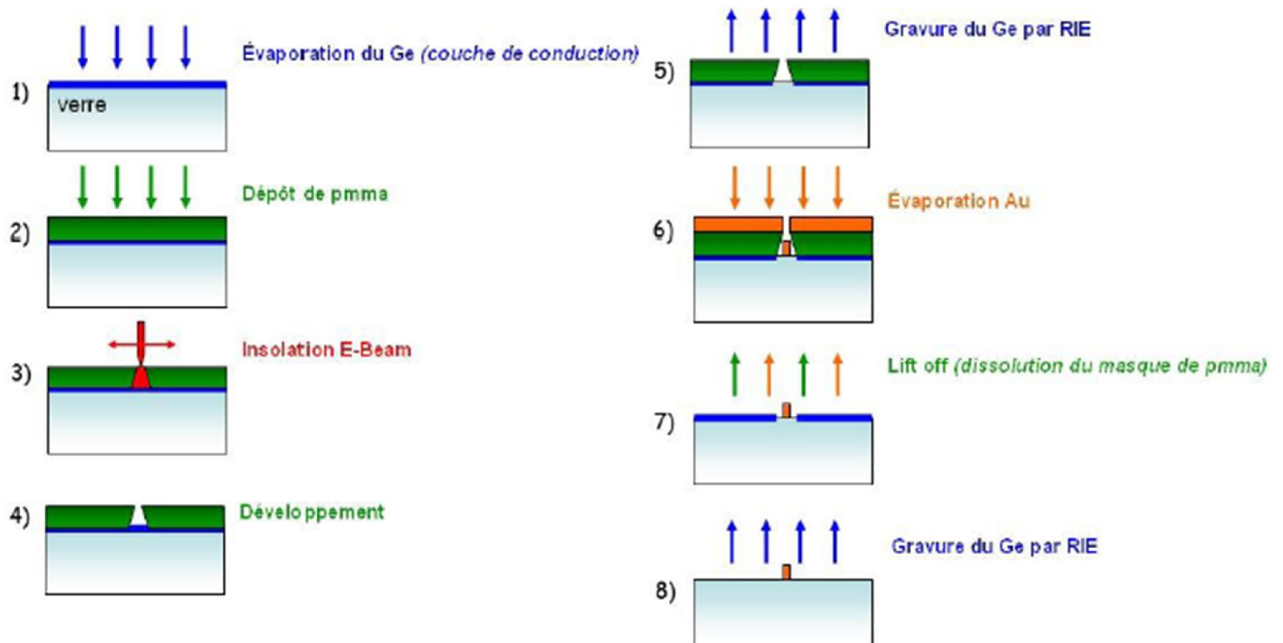


Figure 56: Diagrams showing the manufacturing mechanisms of the samples

Figures 42 to 51 show the spectral optical properties of three thin film multilayer samples between 300 nm and 1100 nm.

The diffraction gratings are a set of transmission or reflection elements separated by a distance comparable to that of the wavelengths of the light to be studied. Due to the diffraction, an electromagnetic wave incident on the electric fields, and magnetic or its phase, or both, predictably modified figure 48 ((a) to (l)). Simulation of the diffraction phenomenon through a transmission slot allowed us to design the dimensioning of the network in order to obtain the maximum yields on each of the orders. Let m be the diffraction order, which is an integer, and η , the frequency of the number of slots per mm. for a wavelength, all the values of m for which $|m\lambda/\eta| < 2$ corresponds to all the feasible diffraction orders.

We are mainly looking to use the information in order 1 which will be the most important field strength response. The interferences figures 58 (a), (b), and their theoretical energies created by the diffractions of single layer and then of a network of layers are then deduced by:

The luminous intensity on a point x of the screen,

$$\begin{bmatrix} E_a \\ H_a \end{bmatrix} = \begin{bmatrix} \cos\delta & j\frac{\sin\delta}{\eta_1} \\ j\eta_1\sin\delta & \cos\delta \end{bmatrix} \begin{bmatrix} E_b \\ H_b \end{bmatrix} \delta = \frac{2\pi\tilde{n}_1 d \cos\tilde{\theta}_1}{\lambda} \quad (115)$$

With d the network-screen distances.

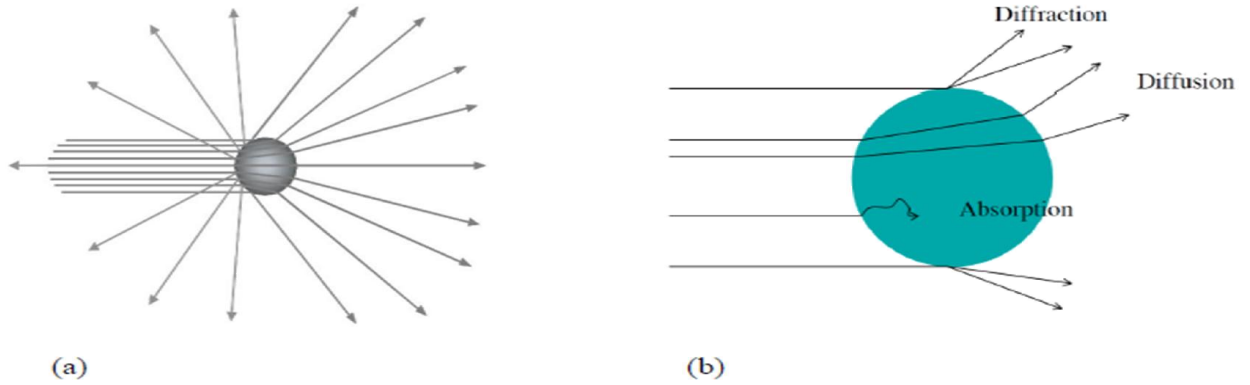


Figure 57: (a) Diffusion of a light beam by spherical particle.(b) Optical phenomena of diffusion.

A simulation tool allows us to observe the shapes of the diffraction patterns as their position on the screen. Depending on the thickness of the subwavelength layers, its width, and its height, the intensity transmitted on the screen as well as the angular dispersion of the order 1 are calculated. Following this study, the first diffraction gratings in transmission and reflection were designed figure 57 (a), (b), and 54 (a), (b).

Example of network realized: $a = 150 \text{ nm}$, $L=650 \text{ nm}$

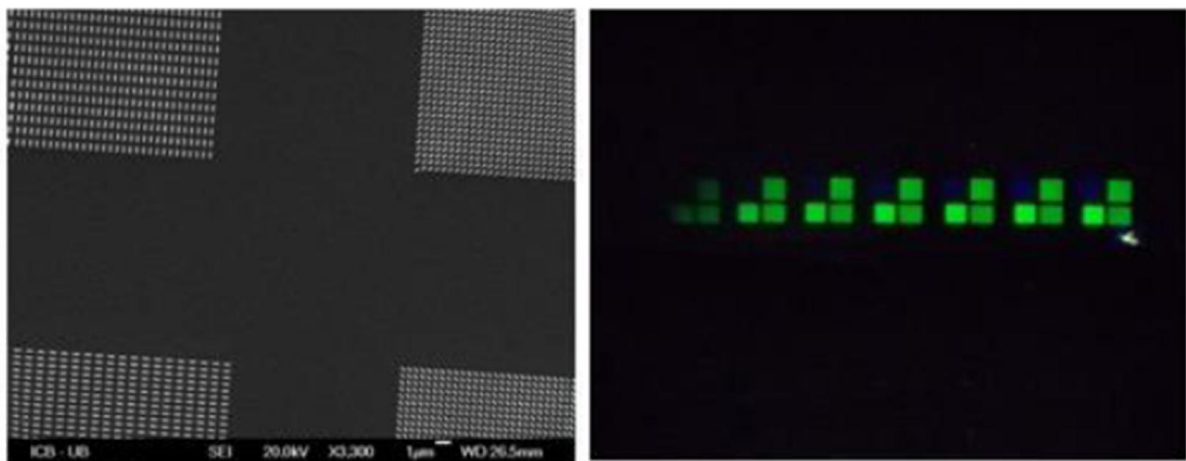


Figure 58: observation at the AFM of the networks realized

Observations of structures made under a microscope show several diffraction gratings in transmission and in variable pitch reflection.

There are three areas: the visible (400-800 nm), characterized by a weak absorption of the materials used to make the samples. In; the near-infrared plateau (800-1100nm), which corresponds to a low absorption of radiation, and therefore to high levels of reflectance and transmittance associated

with multiple scattering within the successive layers.

We report a comprehensive experimental study of optical and electrical properties of thin silver, germanium, and gold films in a wide range of film thicknesses (from 20 to 350 nm). Our experimental results are supported by theoretical calculations based on the measured morphology of the fabricated gold, silver, and germanium films. We demonstrate that the dielectric function of the metal is determined by its structural morphology, that Plasmon phenomena's as transmittance and reflectance depends to thickness, refractive, index, and angle on incidence of irradiation use.

Although the fabrication process can be absolutely the same for different films, the dielectric function can strongly depend on the film thickness. Our studies show that the imaginary part of the dielectric function of gold, which is responsible for optical losses, rapidly increases as the film thickness decreases for thicknesses below 80 nm. At the same time, we do not observe a noticeable dependence of optical constants on the film thickness for thicker samples. These findings establish design rules for thin-film plasmonic, optical and nanophotonic devices. Hence, investigation of the optical absorption, transmittance and reflectance of metal through interband and intraband electron transitions is an essential (**E**, **H**) input for a comprehensive understanding of the correlation between the metallic films structure and plasmonic/nanophotonic device intrinsic characteristics for the optical filters synthesis.

The purpose of the present study is therefore to deal with some of the questions remain und answered regarding the structural and optical properties of *thin* gold films. For this purpose, the high-quality gold films of various thicknesses (ranging from ~20 to 200 nm) were deposited on silicon substrate by use of conventional Lithography technique. Regarding the films thickness range (which we chose to work with), it is important to note that once the film thickness is less than 20 nm one can get island or highly roughened film surfaces and quantum confinement effects need to be considered. At the same time, the films with a thickness of more than 200 nm are guaranteed to behave as a bulk metal. Films were characterized by bispectrometer and atomic force microscopy (AFM) to study the structural morphology, by the four-point probe to determine the electrical properties (**E**, **H**) figure (48-j, 48-k, 48-l), (50-a and 50-b), to determine the optical constants in the spectral range from 300 to 1100 nm (figure 47 (a), (b), (c)).

The surface morphology and thickness of the thin Au-Ge-Ag or Ge-Ag-Au etc... Films were both investigated by tapping mode AFM and choose. The line scans have been performed for films of different thicknesses over the area with the largest difference between the heights of the step features. Several AFM scans of the same area (and at the same scanning parameters) were performed for each of the samples proving that Lithography is a powerful technique for preparing uniform films of controlled thickness. Thus, for example, Figures. 50 (a), (c), demonstrates a typical line-scan of the

thin Au-Ge-Ag or Ge-Ag-Au film, etc... surface revealing height-step of about d nm which is found to be close to the film thickness determined from the bispectrometer irradiance. The comparison between the results observation by AFM and computational simulations is shown in figures 48 (b), (d), and figures 52, 53, 54. These values are found to be in good agreement for all tests for the optical filter array synthesis in the range enter 300 nm to 1100 nm. In order to understand how the accuracy of the film thickness measurements affects the optical properties, one must theoretically studied the influence of uncertainty in the determined film thickness on the resulting damping factor γ .

We opted for the realization of least 3 series of 3 samples with different conditions of different deposits, configuration and different material in order to make a comparative study. The determination in the bibliographic and theoretical study (simulation) of the geometric parameters of the nanostructures, and their physical properties, allowed us to make new realizations of nanostructure samples of various geometric shapes and configurations presented in figures 54.

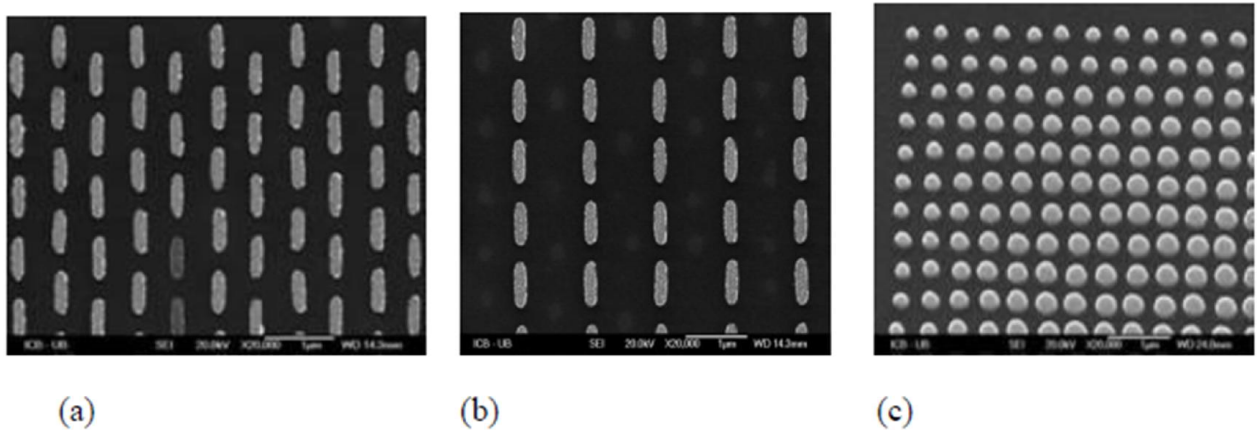


Figure 59: diagrams showing the different structures made

The analysis of the physical properties of these new samples, 55 (a), (b), (c), the observation, the characterization by AFM, by MEB, and by Raman spectroscopy through a stimulated study of the electrical properties enabled us to carry out a mapping of the composition of other samples made. The convincing results of the observations of these different samples confirmed our approach and provided concordances with the multispectral figure 47 (b), (d).

V.5.1.Design methodology

We have highlighted using the simulation results and the theoretical study carried out in the preceding chapters and paragraphs that we can design and synthesize filters by considering the properties of reflectances and transmittance of the chosen metamaterials

- **Reflectance filter**

In chapters 2.3, we have shown that when the structure has vertical symmetry, it is possible to obtain 100% of the energy reflected at resonance for a structure containing non-absorbent materials. In addition, to avoid losing energy in the other orders diffracted by the network, we will choose a

diffracting structure only one order. To minimize reflection outside the resonance, the equivalent structure must then be a good anti-reflection. To summarize, the characteristics of the structure are as follows:

- Symmetry with respect to a vertical axis (Oz).
- Subwavelength network.
- Materials without absorption.
- Good anti-reflection.

The first 3 characteristics make it possible to obtain a reflection R_{res} equal to 1 at the resonance. The rejection rate therefore only depends on the value of the anti-reflection with $\tau = \frac{1}{R_{res}}$.

- **Transmittance filter**

To obtain a real reflection zero and a transmission of 100% of the energy at resonance, the structure must, in this case, be symmetrical with respect to a horizontal axis (chapter 2.3). The reflection outside the resonance must be maximized; we will then use a structure behaving like a mirror.

The characteristics of the structure are as follows:

- Horizontal symmetry.
- Subwavelength network.
- Materials without absorption.
- Good mirror

- **Angular tolerance**

The angular tolerance of these filters is a very important element; in fact the incident beam is not a plane wave. For a filter, lit by an incident wave having an angular aperture larger than the tolerance of the filter, its spectral response will then be greatly degraded. We will note $\Delta\theta$ the angular tolerance of the filter and θ_f the angular divergence of the beam $\theta_f \cong \frac{\lambda}{d_w}$ being the waist of the bundle. To obtain the inequality $\Delta\theta > \theta_f$ and thus not to degrade the spectral response, we can increase the size of the beam, but the size of the filter to be produced will have to be larger than the size of the beam. When the inequality is verified, the low angular tolerance of these filters becomes interesting to obtain tunable filters according to the angle of incidence.

- **Indépendance à la polarisation**

A filter is independent of polarization when its spectral response, whose efficiency is close to unity, is the same regardless of the polarization of the incident wave. Intuitively, we can imagine independent structures with normal incidence polarization. On the other hand, for the oblique, or even strongly oblique, incidence, the design of structures independent of polarization will be much less

easy. We will first give a necessary condition to obtain independence from polarization then we will be interested in the two cases of illumination, in normal incidence then in oblique incidence as described in the previous chapters.

V.5.2. Synthesis methodology: Determination of stacking parameters

We are interested in this part in the methodology of synthesis of the reflectance and transmittance filters operating in oblique incidence and independent of polarization. we take into account the variations of the indices of the different metamaterials according to their thickness.

We are interested in this part in the methodology of synthesis of the reflectance and transmittance filters operating in oblique incidence and independent of polarization. we take into account the variations of the indices of the different metamaterials according to their thickness (figures).

The stack must be anti-reflective and support guided modes. We are looking for a stack with a very low reflectivity over a wide band around the expected operating point of the filter (angle of incidence and resonant wavelength), for all polarizations. Multilayer stacking reflectivity simulations make it possible to obtain the characteristics (thickness, index) of the layers. For the upper layer, which will contain the network, we take an equivalent index; this value is approximated because the filling rate is still subject to modification during the design.

We then seek the guided modes of this stack; they are characterized by their effective index n and by A , term allowing to quantify the capacity of the mode to be excited by an incident wave. Depending on the performance of the filter to be obtained, we can choose the mode to be excited.

Despite the advantages of holography for producing patterns on large surfaces, we had to choose electronic lithography which gives us the freedom to design different complex shapes of patterns (non regular hexagonal mesh, 2D double period pattern, etc.). In addition, the writing process is repeatable with an accuracy of less than 1 nm over the pattern period. But with this technique, the exposure times are long; we will therefore seek to design structures with low filling rate in order to reduce the exposure time and thus reduce the risk of drift of the settings of the electronic column during the sunstroke.

The figure below shows the simulations of the variations in the wavelength of the indices, the intensity of the electric field and the absorbance of each metamaterial used, namely Germanium, silver and gold.

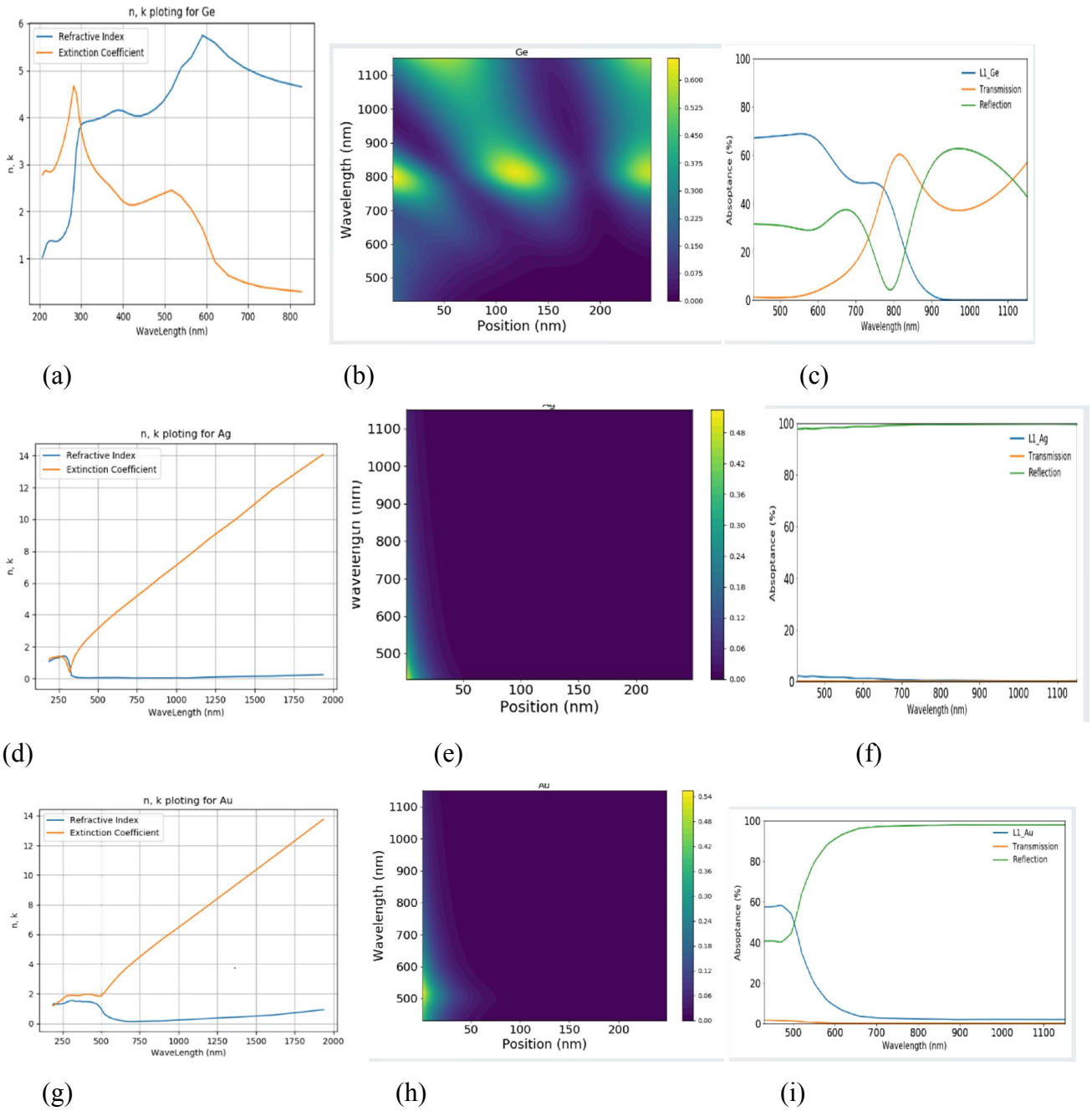


Figure 60: diagram showing the dispersion (a), the variation of the intensity of the electric field (b), the absorbance of germanium (c). Money case: (d), (e), (f); gold case: (g), (h), (i); highlighting, the colours of the reflected or transmitted radiation.

GENERAL CONCLUSION AND PERSPECTIVES

Nanoscale thin metal films are an inherent part of various nanophotonic and plasmonic applications [88, 89], such as high-sensitive sensors [90], plasmonic circuits [91], nanolasers [92], optical metamaterials and metasurfaces [93, 94], photonic hypercrystals [95], among others.

If we assume, as first approximation as we did on the theoretical study that a metallic thin layer is continuous, homogeneous, isotropic and limited by two plane and parallel faces can be characterized by three parameters: the thickness d , the refractive index n and the extinction index k , these two the latter can also constitute a complex index $n-jk$, as we have underlined in the paragraph on the theoretical bases of which depend the optical properties of the thin films which are the transmittance, the reflectance and absorption.

We have proposed, in the present work, to highlight these three properties, for very thin blades of silver, gold, and germanium, in the visible, the near infrared, knowing that the silver transparency band (3100 Å) is different from that of gold and germanium. By means of the results thus obtained we have tried to verify the theories described in the paragraphs of chapter V. we have finally obtained an order of magnitude of the maxima of the peaks of variations of the transmittances, and of the reflectance in the domains of the ultraviolet, the visible, and near infrared.

The results of computational simulations and AFM analysis show that the grain sizes of the Au-Ge-Ag or Ge-Ag-Au, etc...thin films increase with increasing film thickness from ~20 to 176 nm. We reported the real and imaginary parts of the dielectric function for the visible and NIR ranges and demonstrated that the optical losses increase significantly with the reduction of the film thickness lower than ~80 nm.

The experimental results (bispectrometer or monochromator observation) are not confirmed by theoretical investigations based on the measured morphology (AFM or MEB observations) of the fabricated sample films. This work proposes a non-absorption inorganic thin film color filter with superior color saturation characteristics. To produce red (R), green (G), and blue (B) color filters, samples of Au-Ge-Ag or (combination of 3) was prepared in three different thicknesses and sandwiched between two silver (Ag) reflective layers. Simulation results demonstrated the superior transmittance and color saturation of Au-Ge-Ag film over those of aluminum film. The degree to which the magnitude of the refractive index of Au-Ge-Ag influences the transmittance of the R, G, and B color filters is not significant; however, the peak wavelength of the red filter shifts approximately 20 nm. The ideal thicknesses of Au/Ge/Ag for color saturation and transmittance in R, G, and B color filters are 170 nm/350 nm/90 nm, 30 nm/131 nm/30 nm, and 30 nm/100 nm/30 nm, respectively figure 48 (b), (d). The proposed inorganic thin film color filter provides better color saturation and optical transmittance than organic photoresistance coating color filters.

In this work to achieve the goal, or to meet the specifications are organized in three steps: the first speaks of the theory and realization of a filter or network of multispectral color filters through nanostructure films. The second concerns the optical (visionics) multispectral characterization of Lithographic filter samples (nanostructure realization technique used IN the ICB laboratory). The third and last stage of the work is based on the comparison of experimental and theoretical modeling of the multispectral device. The realized structures have a size of 500 microns * 500 micros, the first aspect of these achievements is therefore to determine which materials and dimensions will be optimal to overcome the defects present in the current multispectral systems. The real problem is highlighted by the diagram below figure 61 above, which also highlights the current limitations of the process.

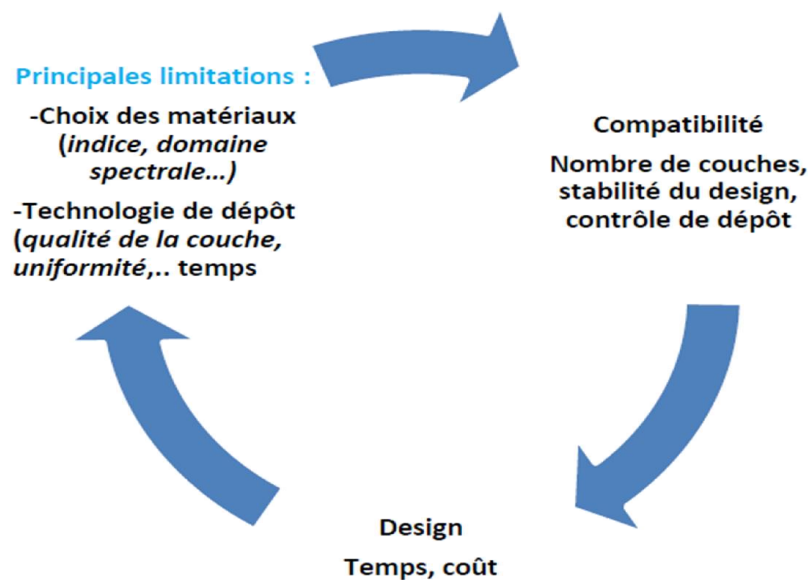


Figure 61: diagram highlighting the problem of manufacturing nanostructures.

One of the difficulties encountered in the course of this work is the study and the experimental characterization of the samples from the Bichromator present in the laboratory ImVIA, because this device is not calibrated, for the structure of the nanometric order, therefore calibration uncertainties range from 10-14 to 10-19. This insoluble problem due to lack of funding has been a significant drag for the continuation and confirmation of the results obtained during the simulated theoretical studies, and the physical observation at the MEB or AFM.

Finally, issues of the appliance of thin Au-Ag-Ge, Ge-Ag-Au, Ag-Au-Ge, etc... films for practical plasmonic devices and synthesis of optical filter array are discussed in the multilayer's thin films influence on the performance characteristics of the SPR biosensor, optical filter array. In particular, it is shown that the increase of average multilayer's thin film size from 14 to 59 nm results in the increase of SPR biosensor, electronic sensor, and optical multispectral devices.

With adequate financial means, an optical characterization system and a well-configured

experimental protocol (dedicated Nano-structure test bench) we could confirm the synthesis of diffraction grating, including multispectral filters from nanostructures.

In perspectives, the applications of this technology (nanotechnology) are numerous and hopeful in many fields of science. In color imaging and more generally multispectral or even hyperspectral is attracting more and more interest in image processing, electronics, medicine and biology.

Access to a finer analysis of the visible and IR spectrum allows for better tissue characterization for increased classification performance and provides vision beyond what is visible to the naked eye. Work shows promising results for the monitoring of skin pathologies, for example, in cell imaging or interventional surgery. Less ancient than terrestrial observation (remote sensing), this field of application opens up new perspectives and problems related to the living and often transparent nature of the observed materials.

BIBLIOGRAPHICAL REFERENCES

- [1] Richard Feynman prononça ce discours « *There's plenty of room at the bottom* » le 29 décembre 1959 au congrès annuel de l'American Physical Society au Caltech. On peut trouver ce texte sur la toile à l'adresse : <http://www.zyvex.com/nanotech/feynman.html>.
- [2] Un nanomètre (abréviation : nm) correspond à un milliardième de mètre, soit environ un dix-millième du diamètre d'un cheveu.
- [3] Bellon-Maurel V, Guizard C, Vigneau JL, Bertrand D. Camera for near infrared spectroscopy. In: Davies A.M. and Williams P (1996). Near Infrared Spectroscopy: the future waves. NIR publications, Chichester, UK,72-90.
- [4] Bertrand D, Robert P, Novales B, Devaux M. Chemometrics of multichannel imaging. In : Davies A.M.C and Williams P (1996). Near Infrared Spectroscopy: the future waves. NIR publications, Chichester, UK,72-90.
- [5] Guizard C, Bellon V, Sévila F. (1992). Vision artificielle dans les industries agro-alimentaires. Méthodes / Techniques / Choix. CEMAGREF-DICOVA, Antony.
- [6] Park B, Chen Y.R, Huffman R.W. Integration of visible / NIR spectroscopy and multispectral imaging for poultry carcass inspection. In Meyer GE, De Shazer JA (1994). Optics in Agriculture, Forestry, and Biological Processing, Proc SPIE 2345, Washington,162-171.
- [7] Robert P, Bertrand D, Devaux MF, Sire A (1992). Identification of chemical constituents by multivariate near infrared spectral imaging. Analytical Chemistry, 64:664-667.
- [8] Robert P, Devaux MF, Bertrand D (1991). Near Infrared video image analysis. Science des aliments, 11: 565-574.
- [9] Taylor SK, McClure WF. NIR imaging spectroscopy: measuring the distribution of chemical components. In: Iwamoto M, Kawano S (1989). The proceedings of the international near infrared spectroscopy conference. Koring publishing, Tokyo,393-404.
- [10] Treado PJ, Levin IW, Lewis EN (1992). Near-Infrared Acousto-optic filtered spectroscopic microscopy: a solid-state approach to chemical imaging. Applied Spectroscopy, 46(4) :553-559.
- [11] Paul Costa. <http://www.techniques-ingenieur.fr/base-documentaire/innovations-th10/innovations-en-materiaux-avances-42186210/introduction-aux-nanomateriaux-et-nanotechnologies-nm110/contexte-nm110niv10001.html>.
- [12] Lahmani M., Dupas C., Houdy P. - Nanosciences. - Belin éd.(2004).

- [13] Corriu P, Nozières P, Weisbuch C. Nanosciences et Nanotechnologies.- Académie des sciences et Académie des Technologies, Tec et Doc(2004).
- [14] The Royal Society & The Royal Academy of Engineering, « Nanoscience and nanotechnologies: opportunities and uncertainties », 2004 (), p.p5.
- [15] OECD, « Bibliometric Indicators of Nanoscience Research », *NESTI*, vol. 12, 2006, p.20p.
- [16] Samuel A.Wickline, MD; Gregory M. Lanza, MD, PhD. Nanotechnology for Molecular Imaging and Therapy.
- [17] Ronald N. Kostoff, Ray Koytcheff, Clifford GY. Lau. Structure of the Global Nanosciences and Nanotechnology Research Literature.
- [18] Mihail C. Roco, William Sims Bainbridge. “Societal Implications of Nanoscience and Nanotechnology” National Science Foundation. March2001.
- [19] Launay F. The Astronomer Jules Janssen: A Globe trotter of Celestial Physics. Springer; New York, NY, USA: 2011.
- [20] Pascal Cotte et Marcel Dupouy. CRISATEL high resolution multispectral system. *Proceedings of IS&T's PICS Conference*, pages 161-165, Rochester, 2003.(X)
- [21] Markku Hauta-Kasari, Kanae Miyazawa, Satoru Toyooka et Jussi Parkkinen. Spectral vision system for measuring color images. *Journal of the Optical Society of America A*, 16(10) : 2352-2362, 1999. (y)
- [22] Hiroaki Suguria, Tetsuya Kuno, Norihiro Watanabe, Narihiro Matoba, Junichiro Hayachi et Yoichi Miyake. Development of a multispectral camera system. *SPIE Proceedings*, volume 3965, pages 331- 339,2000.(z)
- [23] D. R. Smith, J. B. Pendry, and M. C. K. Wiltshire, “Metamaterials and negative refractive index,” *Science*, vol. 305, no. 5685, pp. 788–792, Aug.2004.
- [24]D. R. Smith, W. J. Padilla, D. C. Vier, S. C. Nemat-Nasser, and S. Schultz, “Composite medium with simultaneously negative permeability and permittivity,” *Phys. Rev. Lett.*, vol. 84, no. 18, pp. 4184– 4187, May 2000.
- [25] J. B. Pendry, “Negative refraction makes a perfect lens,” *Phys. Rev. Lett.*, vol. 85, pp. 3966– 3969, Oct. 2000.
- [26] N. Fang, H. Lee, C. Sun, and X. Zhang, “Sub-diffraction-limited optical imaging with a silver superlens,” *Science*, vol. 308, no. 5721, pp. 534–537, Apr.2005
- [27] S. P. Burgos, R. de Waele, A. Polman, and H. A. Atwater, “A single-layer wide-angle negative-index metamaterial at visible frequencies,” *Nature Mater.*, vol. 9, pp. 407–412, May2010.

- [28] N. Fang, D. J. Xi, J. Y. Xu, M. Ambati, W. Srituravanich, C. Sun, and X. Zhang, “Ultrasonic metamaterials with negative modulus,” *Nature Mater.*, vol. 5, pp. 452–456, Jun.2006.
- [29] D. Schurig, J. J. Mock, B. J. Justice, S. A. Cummer, J. B. Pendry, A. F. Starr, and D. R. Smith, “Metamaterial electromagnetic cloak at microwave frequencies
- [30] J.B.Pendry,D.Schurig,andD.R.Smith,“Controllingelectromagneticfields,”*Science*,vol.312, no. 5781, pp. 1780–1782, Jun.2006.
- [31] H. Tao, E. A. Kadlec, A. C. Strikwerda, K. B. Fan, W. J. Padilla, R. D. Averitt, E. A. Shaner, and X. Zhang, “Microwave and Terahertz wave sensing with metamaterials,” *Opt. Exp.*, vol. 19, no. 22, pp. 21620–21626, Oct. 2011.
- [32] C. Debus and P. H. Bolivar, “Frequency selective surfaces for high sensitivity terahertz sensing,” *Appl. Phys. Lett.*, vol. 91, no. 18, pp. 184102-1–184102-3, Oct.2007.
- [33] H.Tao, L.R. Chieffo, M.A. Brenckle ,S.M. Siebert, M.K. Liu, A.C. Strikwerda, K.B. Fan, D. L. Kaplan, X.Zhang, R.D. Averitt, and F.C. Omenetto, “Metamaterials on paper as a sensing platform,” *Adv. Mater.*, vol. 23, no. 28, pp. 3197–3201, Jul.2011.
- [34] Yeh P 1988 *Optical Waves in Layered Media* (New York: John Wiley andSons)
- [35] Hodgkinson I J and Wu Q h 1997 *Birefringent Thin Films and Polarizing Elements* (Singapore: World Scientific Publishing Co PteLtd)
- [36] Born M and Wolf E 2002 *Principles of Optics: Electromagnetic Theory of Propagation, Interference and Diffraction of Light* ed 7 (New York: Cambridge UniversityPress)
- [37]D. Yu. Fedyanin, A. V. Krasavin, A. V. Arsenin, and A. V. Zayats, “Surface plasmon polariton amplification up on electrical injection in highly integrated plasmonic circuits,”*NanoLett.***12**(5),2459– 2463 (2012).
- [38] Moharam et al [83], *Journal of the Optical Society of America (JOSA)*, A12, n5, pp1068-1076, 1995
- [39] Anis Zribi, Jeffrey Fortin. « Fonctionnal Thin Films and Nanostructures for Sensors: Synthesis, Physics, and applications”
- [40] Moharam et al., *JOSA*, A12, n5, pp1077-1086, 1995
- [41] Abelès F 1950 Recherches sur la propagation des ondes électromagnétiques sinusoïdales dans les milieux stratifiés. Applications aux couches minces. I *Annales de Physique, 12th Séries* 5596–640
- [42] Abelès F 1950 Recherches sur la propagation des ondes électromagnétiques sinusoïdales dans les milieux stratifiés. Applications aux couches minces. II *Annales de Physique, 12th Séries* 5706–784
- [43] Joachim Sukmanowski, Etienne Moulin, Helmut Stiebig, Karl Andert, François-Xavier Royer

- [44] Stearns D.G., *J. Appl. Phys.*, 65, N°2, (1989), pp. 491-506.
- [45] D. Yu. Fedyanin, A. V. Krasavin, A. V. Arsenin, and A. V. Zayats, “Surface plasmon polariton amplification up on electrical injection in highly integrated plasmonic circuits,” *NanoLett.* **12**(5), 2459–2463 (2012).
- [46] Bartlett PN, Baumberg JJ, Coyle S, Abdelsalam ME (2004) Optical properties of nanostructured metal films. *Faraday Discuss.*, 125 : 117 – 132.
- [47] Biswas A, Aktas OC, Schürmann U, Saeed U, Zaporojtchenko V, Faupel F, Strunskus T (2004) Tunable multiple plasmon resonance wavelengths response from multicomponent polymermetal nanocomposite systems. *Appl. Phys. Lett.*, 84 : 2655 – 2657.
- [48] Biswas A, Marton Z, Kanzow J, Kruse J, Zaporojtchenko V, Faupel F, Strunskus T (2003) Controlled generation of Ni nanoparticles in the capping layers of Teflon AF by vapor-phase tandem evaporation. *Nano Lett.*, 3 : 69 – 73.
- [49] Caruso R.A, Antonietti M (2001) Sol-gel nanocoating: An approach to the preparation of structured materials. *Chem. Mater.*, 13 : 3272 – 3282.
- [50] Anis Zribi, Jeffrey Fortin. « Fonctionnal Thin Films and Nanostructures for Sensors: Synthesis, Physics, and applications ».
- [51] Horst Hahn, Mohsen Pouryazdan, Askar Kilmametov, Julia Ivanisenko, Sre Harsha.N. Mechanical synthesis and mechanical properties of nanomaterials”.
- [52] Robbie, K., Sit, J.C, and Brett, M.J. (1998). Advanced techniques for glancing angle deposition. American Vacuum Society, 16(3): 1115-1122.
- [53] Smith, D. O. (1959). *Appl. Phys.*, 30:264
- [54] Knorr, T. G. and Hoffman, R. W. (1959). *Physical Review*, 113:1039.
- [55] Liu, F. (1999). The growth of nanoscale structured iron films by glancing angle deposition. *Journal of applied physics*, 85(8)
- [56] Dario G et al. (2005) First microprocessors printed with immersion lithography. *Microlithography World*, 14: 4, 6, 18
- [57] Baek IB et al. (2005) Electron beam lithography patterning of sub-10 nm line using hydrogen silsesquioxane for nanoscale device applications. *Journal of Vacuum Science and Technology*
- [58] Gamo K, Namba S (1984) Ion beam lithography. *Ultra microscopy*, 15: 261 –269.
- [59] Dhaliwal R Setal. (2001) PREVAIL–Electron projection technology approach for next-generation lithography. *IBM Journal of Research and Development*, 45: 615 –636.
- [60] Doering H-J et al. (2005) Proof-of-concept tool development for projection mask-less lithography

- (PML2). Progress in Biomedical Optics and Imaging – Proceedings of SPIE, Emerging Lithographic Technologies IX, 5751: 355 – 365.
- [61] Eguchi H et al. (2005) Image placement of large window-size membrane for EPL and LEEPL mask. Proceedings of SPIE – The International Society for Optical Engineering, Photomask and Next- Generation Lithography Mask Technology XII, 5853: 910 –920.
- [62] Kasahara H et al. (2005) Performances by the electron optical system of low energy electron beam proximity projection lithography tool with a large scanning field. Journal of Vacuum Science and Technology B: Microelectronics and Nanometer Structures, 23: 2754 –2757.
- [63] Quate CF (1997) Scanning probes as a lithography tool for nanostructures. Surface Science, 386: 259 – 264.
- [64] Ginger, D. S.; Zhang, H.; Mirkin, C. A. Angew. Chem., Int. Ed.2004, 43, 30.
- [65] Wouters, D.; Schubert, U. S. Angew. Chem., Int. Ed. 2004, 43,2480.
- [66] Hong, S.; Mirkin, C. A. Science 2000, 288,1808
- [67] Hong, S.; Zhu, J.; Mirkin, C. A. Science 1999, 286,523
- [68] Ryu, K. S.; Wang, X.; Shaikh, K.; Bullen, D.; Goluch, E.; Zou, J.; Liu, C.; Mirkin, C. A. Appl. Phys. Lett. 2004, 85,136.
- [69] Aizenberg, J.; Black, A. J.; Whitesides, G. M. Nature 1998, 394,868.
- [70] Pfeiffer,L.;West,K.W.;Stormer,H.L.;Eisenstein,J.P.;Baldwin,K.W.;Gershoni,D.;Spector, J. Appl. Phys. Lett. 1990,
- [71] Toh, K. K. H.; Dao, G.; Singh, R.; Gaw, H. Proc. SPIE-Int. Soc. Opt. Eng. 1991, 1496,27.
- [72] Black, A. J.; Paul, K. E.; Aizenberg, J.; Whitesides, G. M. J. Am. Chem. Soc. 1999, 121,8356
- [73]Rogers, J. A.; Paul, K. E.; Jackman, R. J.; Whitesides, G. M. Appl. Phys. Lett. 1997, 70,2658.
- [74] Fasol, G. Science 1998, 280, 545.
- [75] Melosh,N.A. ;Boukai,A.; Diana,F.; Gerardot,B.; Badolato,A.; Petroff, P.M.; Heath, J.R. Science 2003, 300,112.
- [76] Lehn, J. M. Angew. Chem., Int. Ed. Engl. 1990, 29,1304.
- [77] Sun, S. H.; Murray, C. B.; Weller, D.; Folks, L.; Moser, A. Science 2000, 287,1989.
- [78] Rogers,J.A.; Baldwin,K.; Bao, Z.; Dodabalapur, A.; Raju, V.R.; Ewing, J.; Amundson, K.Mater. Res. Soc. Symp. Proc. 2001, 660, JJ71/1.
- [79] Srinivasan, U.; Liepmann, D.; Howe, R. J. Microelectromech. Sys. 2001, 10,17.
- [80] Srinivasan,U.;Helmbrecht,M.;Rembe,C.;Muller,R.;Howe,R.IEEEJ.Sel.Top.Quantum2002, 8, 4.
- [81] Snyder, E.; Chideme, J.; Craig, G. Jpn. J. Appl. Phys. 2002, 41,4366.
- [82] Hodgkinson I J and Wu Q h 1997 *Birefringent Thin Films and Polarizing Elements* (Singapore:

World Scientific Publishing Co PteLtd)

[83] Born M and Wolf E 2002 *Principles of Optics: Electromagnetic Theory of Propagation, Interference and Diffraction of Light* ed 7 (New York: Cambridge University Press)

[84] Moharam et al [83], Journal of the Optical Society of America (JOSA), A12, n5, pp1068-1076, 1995

[85] Moharam et al., JOSA, A12, n5, pp1077-1086, 1995

[86] Stearns D.G., *J. Appl. Phys.*, 65, N°2, (1989), pp. 491-506.

[87] R. Lu, Q. Hong, Z. Ge, and S. T. Wu, *Opt. Express* 14, 6243(2006).

[88] S. A. Maier, *Plasmonics: Fundamentals and Applications* (Springer,2007).

[89] V. Bochenkov, J. Baumberg, M. Noginov, F. Benz, H. Aldewachi, S. Schmid, V. Podolskiy, J. Aizpurua, K. Lin, T.Ebbesen, A.A.Kornyshev, J. Hutchison, K. Matczyszyn, S. Kumar, B. deNijs, F. Rodríguez Fortuño, J. T. Hugall, P. de Roque, N. van Hulst, S. Kotni, O. Martin, F. J. García deAbajo, M. Flatté, A. Mount, M. Moskovits, P. Ginzburg, D. Zueco, A. Zayats, S.-H. Oh, Y. Chen, D.Richards, A. Belardini, and P. Narang, “Applications of plasmonics: general discussion,” *Faraday Discuss.* **178**, 435–466 (2015).

[90] B. Špačková, P. Wrobel, M. Bocková, and J. Homola, “Optical biosensors based on plasmonic nanostructures: a review,” *Proc. IEEE* **104**(12), 2380–2408(2016).

[91] Y.FangandM.Sun, “Nanoplasmonic waveguides: towards applications in integrated nanophotonic circuits,” *Light Sci. Appl.* **4**(6), e294(2015).

[92] S. Gwo and C.-K. Shih, “Semiconductor plasmonic nanolasers: current status and perspectives,” *Rep. Prog. Phys.* **79**(8), 086501(2016).

[93] S. Palomba, S. Zhang, Y. Park, G. Bartal, X. Yin, and X. Zhang, “Optical negative refraction by four-wave mixing in thin metallic nanostructures,” *Nat. Mater.* **11**(1), 34–38(2011).

[94] A. Pors, M. G. Nielsen, and S. I. Bozhevolnyi, “Analog computing using reflective plasmonic metasurfaces,” *Nano Lett.* **15**(1), 791–797(2015).

[95] T.Galfsky, J. Gu, E. E. Narimanov, and V. M. Menon, “Photonic hypercrystals for control of light-matter interactions,” *Proc. Natl. Acad. Sci. U.S.A.* **114**(20), 5125–5129(2017).

[96] Optical characterization parameters by study and comparison of subwavelength patterns for color filtering and multispectral purpose, J. Matanga, Y. Lacroute, P. Gouton, E. Bourillot, *Sensors, Cameras, and Systems for Industrial/Scientific. Applications XIV, Electronic Imaging Conference*, vol 8659-30, February

[97] Method for the optimal approximation of the spectral response of multicomponent image, J. Matanga, P. Gouton, E. Bourillot, S. Journaux, P. Ele, *Electronic Imaging* 2019 (9), 371-1-371-9.

[98] A-L. Fehrembach: Réseaux résonnants à Bande Interdite Photonique, nouveaux filtres pour le D. W. D. M. 2006.

- [99] S.C. Lin, Y.L. Lee, C.H. Chang, Y.J. Shen... - Applied physics ..., 2007 - aip.scitation.org: Quantum-dot-sensitized solar cells: Assembly of CdS-quantum-dots coupling techniques of self-assembled monolayer and chemical bath deposition
- [100] C Pagnoux, A Mahr, P Cohen, L Guillevin - Medicine, 2005: Presentation and outcome of gastrointestinal involvement in systemic necrotizing vasculitides: analysis of 62 patients with polyarteritis nodosa, microscopic, journals.lww.com.
- [101] G. Dreyfus: Handwritten Digit Recognition by neural Network with Single-Layer Training, IEEE Transactions on Neural Network, vol 3 No 6, 1992.
- [102] V. Vapnik: Local Learning Algorithm, Neural Computation 4, 888-900, 1992.
- [103] R. Robert, J. Sommeria - Journal of Fluid Mechanics, 1991 - cambridge.org: Statistical equilibrium states for two-dimensional flows
- [104] T.G Park - Biomaterials, 1995 - Elsevier: Degradation of poly (lactic-co-glycolic acid) microspheres: effect of copolymer composition
- [105] P.J. Treado, I.W Levin, E.N. Lewis - Applied spectroscopy, 1992 - osapublishing.org: High-fidelity Raman imaging spectrometry: a rapid method using an acousto-optic tuneable filter